First principle kinetic study of butene cracking on H-ZSM-5

Pieter Cnudde

Supervisor: Prof. dr. ir. Veronique Van Speybroeck
Counsellors: Jeroen Van der Mynsbrugge, Kristof De Wispelaere

Master's dissertation submitted in order to obtain the academic degree of
Master of Science in Chemical Engineering

Department of Applied Physics
Chairman: Prof. dr. ir. Christophe Leys
Faculty of Engineering and Architecture
Academic year 2013-2014

UNIVERSITEIT GENT

Dit onderzoekswerk werd uitgevoerd in het Centrum voor Moleculaire Modellering.

Dankwoord

Terwijl de zon ondergaat en de laatste uren voor de deadline wegtikken, pen ik de laatste zinnen van deze thesis neer. Het tot stand brengen van dit eindwerk was uiteraard niet mogelijk geweest zonder de harde inspanningen van verschillende personen. Met deze laatste woorden wil ik hen van harte bedanken, omdat zij het mogelijk hebben gemaakt mijn studententijd met deze bijzonder leerrijke (en soms toch ook wel aangename) thesisperiode af te sluiten.

Vooreerst richt ik een woord van dank aan mijn promotor, prof. dr. ir. Veronique Van Speybroeck omdat u mij de kans gegeven hebt dit onderzoek uit te voeren binnen het CMM (Centrum voor Moleculaire Modellering). Ik wil u ook bedanken om mij de mogelijkheid te bieden als thesisstudent mijn resultaten te kunnen voorstellen met een posterpresentatie tijdens de XV^{th} Netherland's Catalysis and Chemistry Conference. Tot slot wens ik u, samen met prof. em. dr. Michel Waroquier en prof. dr. ir. Karen Hemelsoet te bedanken om mij de kans te bieden volgend academiejaar een doctoraat te beginnen alsook voor de vele hulp bij het opstellen van mijn FWO-aanvraag.

Mijn grootste dank gaat uit naar Jeroen, Kristof en Karen, de begeleiders van mijn thesis, die mij met raad en daad het hele jaar hebben bijgestaan. Enkel dankzij jullie ideeën, opmerkingen en vooral veel enthousiasme is dit werk tot een goed einde gebracht. Jullie stonden steeds klaar om al mijn vragen te beantwoorden en mijn problemen op te lossen. Bedankt voor de vele uren die jullie in deze thesis geïnvesteerd hebben. Ik wil ook mijn dank richten aan Karen, Kristof, Thomas, Sam, Julianna en Kevin voor de leuke avonden tijdens de NCCC conferentie.

Voor het aangename gezelschap en het opvrolijken van de vele werkuren op het labo, wens ik mijn medethesisstudenten Pieter, Ruben, Steven, Sven, Michiel en in het bijzonder mijn bureau- en klasgenoten Thomas en Tom te bedanken. Zonder jullie zou de sfeer nooit zo goed zijn geweest!

Ik wil ook mijn vrienden en medestudenten bedanken voor de aangename lunchpauzes, de legendarische chemieweekendjes, de ontspannende vakanties en nog zo veel meer. Bedankt voor alle toffe momenten die we samen beleefd hebben en die mijn studenperiode tot de mooiste tijd van mijn leven hebben gemaakt.

Tot slot richt ik mijn dank aan mijn familie. Hoewel ze van deze thesis wellicht enkel dit voorwoord ten volle zullen begrijpen, hebben ze toch steeds met mij meegeleefd tijdens mijn studies. In het bijzonder dank ik mijn ouders die mij alle kansen gegeven hebben en mij altijd door dik en dun hebben gesteund. Voor jullie onvoorwaardelijke steun en liefde, wil ik jullie nog eens speciaal in de bloemetjes zetten.

Bedankt!

Ab initio studie naar de kinetiek van buteenkraking in H-ZSM-5

Pieter Cnudde

Promotor: prof. dr. ir. Veronique Van Speybroeck
Begeleiders: dr. ir. Jeroen Van der Mynsbrugge, ir. Kristof De Wispelaere

Masterproef ingediend tot het behalen van de academische graad van
Master of Science in Chemical Engineering
Academiejaar 2013–2014

Centrum voor Moleculaire Modellering
Faculteit Ingenieurswetenschappen en Architectuur – Universiteit Gent

Samenvatting

Katalytisch kraken van buteen in zure zeolieten verloopt via een carbeniumionmechanisme, waarbij een grote variatie aan organische species kan gevormd worden in de zeolietporiën. Op basis van experimentele waarnemingen werd een gedetailleerd reactienetwerk voorgesteld in de literatuur. In deze studie worden de reactiepaden met vermoedelijk de grootste bijdrage tot de productie van lichte olefines in H-ZSM-5 onderzocht, nl. monomoleculair en bimoleculair kraken, met behulp van statische clusterberekeningen en moleculaire dynamica simulaties.

Trefwoorden: katalytisch kraken, moleculaire modellering, alkenen, carbeniumionen, zeolieten

Ab initio studie naar de kinetiek van buteenkraking in H-ZSM-5

Pieter Cnudde

Promotor: prof. dr. ir. Veronique Van Speybroeck
Begeleiders: dr. ir. Jeroen Van der Mynsbrugge, ir. Kristof De Wispelaere

Abstract— **Katalytisch kraken van buteen in zure zeolieten verloopt via een carbeniumionmechanisme, waarbij een grote variatie aan organische species kan gevormd worden in de zeolietporiën. Op basis van experimentele waarnemingen werd een gedetailleerd reactienetwerk voorgesteld in de literatuur. In deze studie worden de reactiepaden met vermoedelijk de grootste bijdrage tot de productie van lichte olefins in H-ZSM-5 onderzocht, nl. monomoleculair en bimoleculair kraken, met behulp van statische clusterberekeningen en moleculaire dynamica simulaties.**

Keywords—**katalytisch kraken, moleculaire modellering, alkenen, carbeniumionen, zeolieten**

I. Inleiding

TOT op heden vormen etheen en propeen de belangrijkste basischemicaliën met een jaarlijks stijgende vraag. De belangrijkste grondstoffen voor de productie van deze lichte olefines zijn afgeleiden van ruwe aardolie en aardgas. Traditionele productieprocessen van etheen en propeen zijn stoomkraken en katalytisch kraken. Twee recente evoluties hebben echter een belangrijke impact op de olefine-industrie. Ten eerste is de interesse in nieuwe, op hernieuwbare grondstoffen gebaseerde technologieën aangewakkerd door alarmerende berichten rond de krimpende oliereserves. [1] Een van de meest veelbelovende alternatieven voor productie van lichte olefines is het *methanol-to-olefins* (MTO) proces. Ten tweede is er een onevenwicht ontstaan tussen vraag en aanbod van propeen. De oorzaak hiervan kan gezocht worden in de ontginning van schaliegas in de U.S.A. en de bouw van grote ethaankrakers in het Midden-Oosten. Om in de toekomst aan de stijgende propeenvraag te kunnen voldoen, zullen verschillende *on-purpose* technologieën zoals metathese of kraken van olefines economisch interessant worden. [2]

Alkeenkraking in zure zeolieten vormt een cruciale stap in zowel katalytisch kraken, het MTO-proces als het proces van olefinekraking op zich. In deze thesis wordt de kraking van n-buteen in de industrieel relevante H-ZSM-5-katalysator onderzocht. In de vakliteratuur werd een kinetisch model voorgesteld voor buteenkraking op basis van experimentele studies (zie Figuur 1) [3], [4] Een buteenmolecule kan een β - scissie ondergaan naar twee etheenspecies via de zogenaamde monomoleculaire krakingsroute, isomeriseren naar isobuteen of dimeriseren naar een C_8 molecule. Deze laatste kan dan kraken via een zogenaamde bimoleculaire krakingsroute, isomeriseren of verder oligomeriseren indien de poriën voldoende ruim zijn.

De meeste studies over dit onderwerp gaan uit van een carbenium ion mechanisme, [5], [6] hoewel er nog heel wat discussie bestaat omtrent de precieze aard van de (geprotoneerde)

P. Cnudde is onderzoeker aan het Centrum voor Moleculaire Modellering, Universiteit Gent (UGent), België. E-mail: Pieter.Cnudde@UGent.be

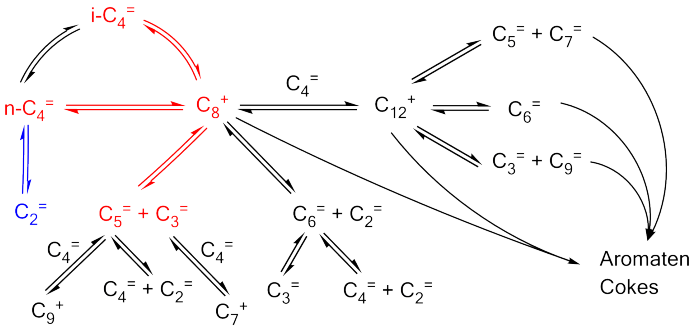

Fig. 1. Reactienetwerk voor buteenkraking [3]

intermediairen. De vraag blijft of carbokationen de werkelijke tussentijds gevormde species zijn en voldoende persistent zijn in de zeolietporiën of dat roostergebonden alkoxiden de meest stabiele intermediairen vormen. De korte levensduur van kleine alkylcarbeniumionen maakt experimentele waarneming moeilijk. Moleculaire modellering kan aangewend worden om opheldering te bieden in deze discussie. Verschillende theoretische studies zijn gewijd aan de protonering van isobuteen en de vorming van t-butylkationen. [7], [8] Er werd vastgesteld dat de stabiliteit van carbeniumionen in hoofdzaak beïnvloed wordt door twee factoren die beide afhankelijk zijn van de zeolietdimensies: enerzijds stabiliserende elektronische effecten en destabiliserende sterische limitaties anderzijds. Voor H-ZSM-5 bleek het t-butylkation het meest stabiele species te zijn vanaf 500 K. [7]

Het kraken van olefines bestaat uit een complex geheel van reacties. Een aanvaardbare veronderstelling is dat isomerisaties op een kleinere tijdschaal plaatsvinden dan β - scissies. [9] Bijgevolg zal een grote variatie aan butyl-, octyl- (en dodecyl)kation isomeren aanwezig zijn in de zeolietporiën. Moleculaire modellering kan assisteren in het ontrafelen van de meest waarschijnlijke reactiepaden. Lesthaeghe et al. bestudeerden de kraking van n-alkenen in de context van het MTO-proces. [10] Mazar et al. onderzochten β - scissies van verschillende hexyl en octyl kationen. [11] Enkele interessante bevindingen zijn uit deze studies naar voren gekomen: Ten eerste blijkt de kraking naar propeen sneller te zijn dan naar etheen. Ook vond men dat de barrière voor kraking afneemt met toenemende koolstofgetallen. Tot slot rapporteerde men dat het type kationtransitie een belangrijke invloed heeft op de activeringsenergie.

In dit onderzoek worden verschillende monomoleculaire en bimoleculaire krakingspaden geanalyseerd (respectievelijk in blauw en rood aangeduid op Figuur 1). Een kinetische en thermodynamische analyse wordt uitgevoerd om te bepalen welke

de belangrijkste reactiepaden voor buteenkraking zijn. Op basis van bovenstaande observaties lijkt het aanvaardbaar om enkel scissies naar propeen en penteen of naar butenen in aanmerking te nemen. Verder wordt er een onderscheid gemaakt tussen secundaire en tertiare kationtransities. Daarnaast wordt het gedrag van een 2-butylkation en verschillende octylkationen onderzocht met behulp van ab initio moleculaire dynamica simulaties. Isomeren met een verschillende vertakkingsgraad worden bestuurd om het kort- of langlevend karakter van carbeniumionen te verifiëren. Er wordt ook gepoogd een link te leggen met de verwachte productdistributie voor buteenkraking.

II. Theoretische methoden

Om een onderscheid te kunnen maken tussen de verschillende reactiepaden worden enkele elementaire β - scissie stappen gemodelleerd met statische berekeningen op een 46T-cluster model van H-ZSM-5. De IRC methode wordt toegepast om de reactant- en productminima op het potentiële energieoppervlak te lokaliseren. Alle geometrieën zijn geoptimaliseerd met het computationeel efficiënte 8T:46T ONIOM(B3LYP/6-31+g(d,p):pm3) schema. Een energieverfijning op het ωB97X-D niveau wordt toegepast op de volledige 46T-cluster. Kinetische coëfficiënten worden bepaald met transitietoestandstheorie. Alle berekeningen zijn uitgevoerd met het softwarepakket Gaussian09.

Om inzicht te verwerven in het gedrag van de intermediaire species in de zeolietkanalen worden ab initio moleculaire dynamica (MD) simulaties uitgevoerd op een periodieke H-ZSM-5 structuur met de revPBE functionaal aangevuld met Grimme D3 dispersiecorrecties, gecombineerd met de DZVP-GTH basisset. Statistische sampling (met tijdsstappen van 0.5 fs) vindt plaats in het NPT ensemble met behulp van de CSVR thermostaat op 560 °C en op 1 bar druk. Alle simulaties worden uitgevoerd met het softwarepakket CP2K.

III. Resultaten en Discussie

Als eerste wordt het monomoleculaire krakingspad onderzocht. Binnen deze klasse bestaat slechts één mogelijke β - scissie reactie, met name kraking van een 1-butylkation in etheen en een ethylkation. Het ethylkation, dat gevormd wordt in de transitietoestand, is een zeer onstabiel species, waardoor het kleine kationfragment tijdens de productoptimalisatie aan een zuurstof van het zeolietrooster bindt om zo een stabiel ethoxide te vormen. De intrinsieke vrije energiebarrière bedraagt 79.7 kJ/mol. Het 1-butylkation, de reactanttoestand, blijkt echter onstabiel te zijn aangezien een barrièreloze transitie naar het 2-butylkation plaatsvindt tijdens de reactantoptimalisatie. Hoewel statische berekeningen aantonen dat het 2-butyl kation als stabiel minimum op het potentiële energieoppervlak bestaat, wijzen MD-simulaties uit dat dit ion zeer kortlevend is en enkel gedurende 1 à 3 ps kan bestaan in geprotoneerde toestand. Bovenstaande beschouwingen geven aan dat de monomoleculaire route niet de meest waarschijnlijke zal zijn.

Ten tweede wordt het bimoleculair krakingspad beschouwd. Twee representatieve reacties (een met propeen en een met buteen als product) van zowel de tertiaire als secundaire kationtransities worden onderzocht met statische berekeningen. De vrije energiebarrières zijn weergegeven in Figuur 2.

In de transitietoestandsgeometrie wordt de $C-C$-binding in β-positie verlengd, gebroken en verschuift de positieve lading naar de β-C positie. Als een secundair of primair ion gevormd wordt, vindt een herorganisatie naar een stabiel alkoxide plaats tijdens de productoptimalisatie. Als er echter een tertiair ion gevormd wordt als product, bindt dit niet aan een roosterzuurstof, maar blijft het als 'vrij' ion bestaan. Een tertiair carbeniumion is dus een lokaal minimum op het potentiële energieoppervlak. Tot slot kan vermeld worden dat voor volumineuze reactant- en productspecies zoals secundaire - tertiaire transities, het 46T-clustermodel de belangrijke interacties niet meer accuraat kan beschrijven.

Drie tendensen kunnen waargenomen worden in Figuur 2. Ten eerste volgen de barrières van reacties met een tertiair of secundair reactant een dalende trend volgens primaire $>$ secundaire $>$ tertiaire producten. Dit is een weerspiegeling van de volgorde van stabiliteit van carbenium ionen in de transitietoestand. Ten tweede volgen de barrières van reacties met een primair of secundair product een dalende trend volgens tertiaire $>$ secundaire reactanten, wat kan toegeschreven worden aan het grotere verschil in stabilisatie van tertiaire ten opzichte van secundaire reactanten. Ten derde zijn de barrières voor kraking naar C_4 species meestal hoger dan naar C_3 en C_5 species, wat in overeenstemming is met de verwachte productopbrengst.

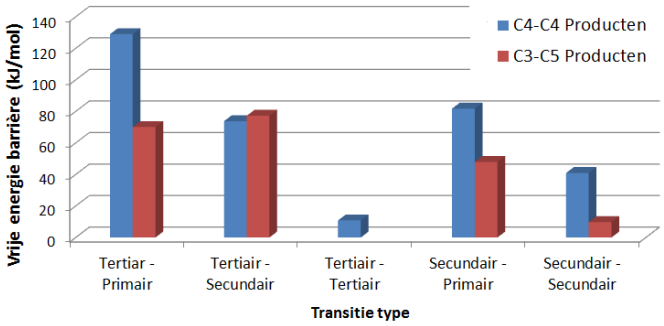

Fig. 2. Vrije energiebarrières (in kJ/mol) bij 560 °C voor β - scissie naar twee C_4 species (blauw) en naar een C_3 en C_5 species (rood), gegroepeerd volgens het type van kationtransitie (LOT : ωB97X-D/6-31+g(d,p)//ONIOM(B3LYP/6-31+g(d,p):pm3))

Om te bepalen welke reactiestappen de belangrijkste bijdrage tot de productopbrengst zullen leveren is intrinsieke kinetiek één belangrijk aspect. Een tweede aspect is echter de mogelijkheid tot vorming van de reactantmoleculen en de concentratie van deze species in de zeolietkanalen. Om inzicht te krijgen in dit tweede aspect worden MD-simulaties uitgevoerd.

Ten eerste tonen MD-simulaties aan dat octylcarbeniumionen wel stabiele en langlevende intermediairen zijn. Transities tussen de geprotoneerde kationtoestand en de gedeprotoneerde alkeentoestand worden gesampled. De dubbele binding van het alkeen interageert met de zure roosterwaterstof door vorming van een π - complex. Verder worden hydrideshifts met lage activeringsenergieën waargenomen. Methylshifts blijken een te hoge barrière te hebben om gesampled te worden. Een algemene trend in alle simulaties is dat geen isomerisaties naar primaire carbeniumionen optreden, wat bevestigt dat deze inderdaad minder stabiel zijn dan secundaire of tertiare kationen in de zeolietkanalen en het dus gerechtvaardigd was enkel de kinetiek van secundaire en tertiaire transities te onderzoeken.

De verschillen tussen een lineaire keten en één met drie vertakkingen zijn opvallend. Het lineaire 2-octylkation ondervindt een grote mobiliteit in de zeolietkanalen, wat de keten toelaat

zich te herschikken in specifieke configuraties. Drie verschillende hydrideshifts werden geobserveerd: een 1,2-hydrideshift tussen naburige koolstofatomen, een 1,3-hydrideshift tussen op één na naburige atomen en een 1,5-hydrideshift (zie Figuur 3), die het opvouwen van de keten vereist zodat de protontransfer over een 6-ringtransitietoestand kan plaatsvinden.

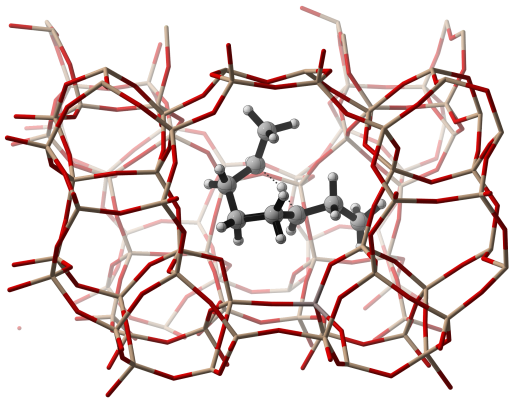

Fig. 3. Snapshot van een 1,5-hydrideshift in een lineaire octylketen in H-ZSM-5 tijdens een MD-simulatie, gezien doorheen het sinusoïdaal kanaal

Op regelmatige tijdstippen vindt een hydrideshift plaats en verplaatst de positieve lading zich doorheen de keten - van de tweede tot de zevende positie (zie Figuur 4). Alhoewel men weinig verschil in stabiliteit tussen de verschillende carbeniumionen verwacht, lijkt een toestand waarin de positieve lading zich op de centrale koolstofatomen (4-octyl) bevindt het meest stabiel te zijn, gevolgd door de 3-octyl- en 2-octylkationen. De positieve lading verblijft dan ook het grootste deel van de tijd op de centrale atoomposities, 4 en 5, die gekenmerkt zijn door een grotere hyperconjugatie en inductieve stabilisatie.

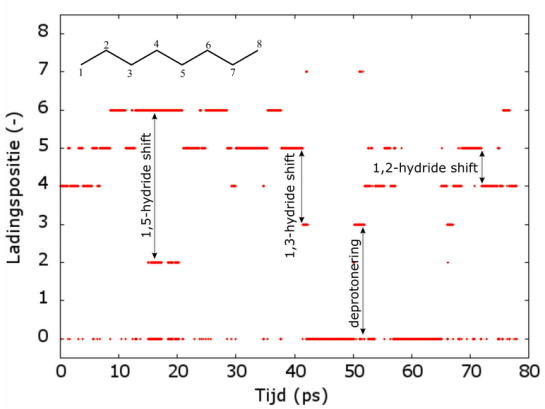

Fig. 4. Evolutie van de positie van de positieve lading in een MD-simulatie van een lineaire octylketen (koolstofpositie 1 t.e.m. 8; 0 is ofwel een protontransfer tussen koolstofatomen onderling, een protontransfer naar het zeolietrooster of een gedeprotoneerde toestand)

Het 2,4,4-trimethyl-2-pentylcarbeniumion daarentegen heeft een lagere mobiliteit, wat kan verklaard worden door de beperkte poriegrootte van het H-ZSM-5-zeoliet. De enige isomerisatie die plaatsvindt tijdens de simulatie is een 1,2-hydrideshift naar het secundaire 2,4,4-trimethyl-3-pentylcarbeniumion. Dit ion wordt echter slechts gedurende 0.2 % van de totale simulatietijd gesampled.

IV. Conclusie

Bimoleculaire kraking van buteen biedt een meer realistische route voor de productie van lichte olefines dan de eerder hoog geactiveerde monomoleculaire kraking. Door dimerisatie kunnen verschillende C_8-isomeren gevormd worden die vervolgens kraken in kleinere olefines. Statische berekeningen hebben aangetoond dat kraken van secundaire carbeniumionen typisch lager geactiveerd is. Uit MD-simulaties kon besloten worden dat een grote fractie van de C_8-isomeren zal bestaan uit tertiaire kationen, al heeft kraking van deze species vaak een hoge activeringsenergie. Beide resultaten zijn in overeenstemming met elkaar: door hun hogere stabiliteit kan men verwachten dat tertiaire ionen een hogere concentratie zullen hebben. Op voorwaarde dat enkel lineaire kationen zouden voorkomen in de poriën, kan men de kinetische parameters linken aan de kationdistributie uit MD-simulaties om de reactiesnelheden van verschillende krakingsstappen in te schatten. Zo werd vastgesteld dat de productiesnelheid van propeen inderdaad hoger ligt dan die van etheen of buteen. Aangezien ook vertakte species in de zeolietporiën kunnen bestaan, dient de precieze samenstelling van C_8-species gekend te zijn om de resultaten te kunnen doortrekken naar het globale buteenkrakingsproces. De combinatie van accurate statische berekeningen en statistische significante moleculaire dynamica simulaties kan een krachtige tool vormen voor de analyse van de verschillende reactieklassen in de nabije toekomst.

References

[1] P. N. R. Vennestrøm, C. M. Osmundsen, C. H. Christensen, and Esben Taarning, "Beyond petrochemicals: The renewable chemicals industry," *Angewandte Chemie International Edition*, vol. 50, no. 45, pp. 10502–10509, 2011.

[2] Michael J. Tallman and Curtis N. Eng, "Catalytic routes to olefins," *AIChE Paper 219c*.

[3] Xianghai Meng, Chunming Xu, Li Li, and Jinsen Gao, "Kinetic study of catalytic pyrolysis of C_4 hydrocarbons on a modified ZSM-5 zeolite catalyst," *Energy & Fuels*, vol. 24, no. 12, pp. 6233–6238, 2010.

[4] Xiangxue Zhu, Shenglin Liu, Yueqin Song, Sujuan Xie, and Longya Xu, "Catalytic cracking of 1-butene to propene and ethene on MCM-22 zeolite," *Applied Catalysis A: General*, vol. 290, no. 12, pp. 191–199, 2005.

[5] J.S. Buchanan, J.G. Santiesteban, and W.O. Haag, "Mechanistic considerations in acid-catalyzed cracking of olefins," *Journal of Catalysis*, vol. 158, no. 1, pp. 279–287, 1996.

[6] Yury V. Kissin, "Chemical mechanisms of catalytic cracking over solid acidic catalysts: Alkanes and alkenes," *Catalysis Reviews*, vol. 43, no. 1-2, pp. 85–146, 2001.

[7] Cuong M. Nguyen, Bart A. De Moor, Marie-Françoise Reyniers, and Guy B. Marin, "Isobutene protonation in H-FAU, H-MOR, H-ZSM-5, and H-ZSM-22," *The Journal of Physical Chemistry C*, vol. 116, no. 34, pp. 18236–18249, 2012.

[8] Christian Tuma and Joachim Sauer, "Protonated isobutene in zeolites: tert-butyl cation or alkoxide?," *Angewandte Chemie*, vol. 117, no. 30, pp. 48474849, 2005.

[9] M. Guisnet, P. Andy, N. S. Gnep, E. Benazzi, and C. Travers, "Skeletal isomerization of n-butenes: I. mechanism of n-butene transformation on a nondeactivated H-Ferrierite catalyst," *Journal of Catalysis*, vol. 158, no. 2, pp. 551–560, 1996.

[10] David Lesthaeghe, Jeroen Van der Mynsbrugge, Matthias Vandichel, Michel Waroquier, and Veronique Van Speybroeck, "Full theoretical cycle for both ethene and propene formation during methanol-to-olefin conversion in H-ZSM-5," *ChemCatChem*, vol. 3, no. 1, pp. 208212, 2011.

[11] Mark N. Mazar, Saleh Al-Hashimi, Matteo Cococcioni, and Aditya Bhan, "β-scission of olefins on acidic zeolites: A periodic PBE-D study in H-ZSM-5," *The Journal of Physical Chemistry C*, vol. 117, no. 45, pp. 23609–23620, 2013.

Dankbetuigingen—*De gebruikte computationele infrastructuur (Stevin Supercomputer Infrastructuur) en diensten in deze thesis werden voorzien door het VSC (Vlaams Supercomputer Centrum), gefinancierd door Universiteit Gent, de Hercules Stichting en de Vlaamse Overheid - departement EWI.*

First principle kinetic study of butene cracking on H-ZSM-5

Pieter Cnudde

Supervisor: prof. dr. ir. Veronique Van Speybroeck
Counsellors: dr. ir. Jeroen Van der Mynsbrugge, ir. Kristof De Wispelaere

Abstract—**Catalytic butene cracking on acidic zeolites proceeds through a carbenium ion mechanism, in which a pool of different organic species is formed inside the zeolite pores. Experimental observations have led to the proposal of a detailed reaction network. In this study, the pathways that are expected to contribute most to the light olefin yield in H-ZSM-5, i.e., monomolecular and bimolecular cracking, are investigated through static cluster calculations and molecular dynamics simulations.**

Keywords— **catalytic cracking, molecular modeling, alkenes, carbocations, zeolites**

I. Introduction

ETHENE and propene remain to date the most important base chemicals with rapidly increasing demand, driven by the growing polymer industry. Light olefin production is mainly based on crude oil and natural gas derivatives. Traditional ethene and propene production ways are through steam pyrolysis and catalytic cracking. However, two recent trends have seriously impacted the light olefin economy. Over the past decades, a rising interest in new technologies based on alternative feedstocks has emerged, fueled by the warnings of shrinking oil reserves.[1] One of the most promising alternatives for light olefin production is the methanol-to-olefins (MTO) process. Secondly, due to the expanding shale gas business in the USA and the large ethane crackers in the Middle East, an imbalance between propene demand and supply has developed. To meet the propene demand, several on-purpose technologies, such as metathesis and olefin cracking processes will become economically interesting in the near future. [2]

Alkene cracking on acidic zeolite catalysts plays a crucial role both in fluid catalytic cracking (FCC), MTO and olefin cracking processes. In this study, n-butene cracking on the industrially important H-ZSM-5 catalyst is investigated. Based on experimental observations, a kinetic model has been proposed in literature (see Figure 1). [3], [4] A single n-butene molecule can either undergo immediate β - scission to two ethene species, so-called monomolecular cracking, isomerize to isobutene or dimerize to an octene molecule. The latter may again crack, so-called bimolecular cracking, isomerize or oligomerize if allowed by the pore dimensions.

Most studies on this subject are based on a carbenium ion reaction mechanism. [5], [6] However, there is still a lot of discussion regarding the exact nature of the (protonated) intermediates. The question remains if carbocations are the true intermediate species and remain long-lived in the zeolite pores or if the reaction intermediates are stable framework bound alkoxides, which can only crack upon a sporadic desorption. Due to the short-livingness of simple alkyl carbenium ions, experimental observation is difficult. Molecular modeling can be applied to elucidate this issue. Several studies have focused on the protonation of isobutene and the formation of a t-butyl cation. [7], [8] Carbenium ion stability was found to depend mainly on two factors: stabilizing electronic effects on the one hand and destabilizing steric constraints on the other hand, both depending on the zeolite pore dimensions. For H-ZSM-5, it was suggested that due to the large entropy loss upon alkoxide formation, the t-butyl cation is the most stable species at temperatures of 500 K or higher.[7]

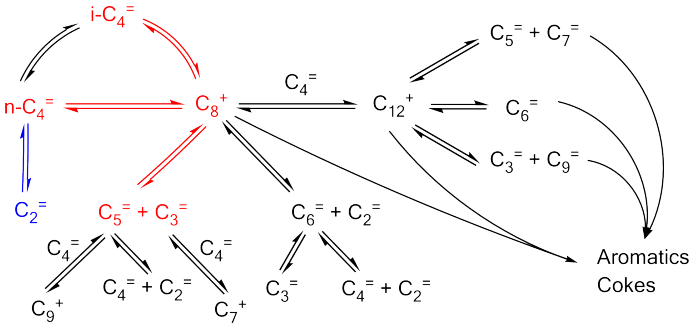

Fig. 1. Kinetic model of butene cracking [3]

An olefin cracking process consists of a complex network of reactions. It can safely be assumed that isomerizations take place at a much higher rate than β - scissions. [9] Consequently, a whole range of butyl, octyl (and dodecyl) carbenium ions are present as cracking reactants in the zeolite pores, complicating an experimental determination of the precise reaction mechanism. Molecular modeling can assist to distinguish between different feasible reaction pathways. Lesthaeghe et al. studied cracking of n-butene, n-pentene and n-hexene in the context of the MTO process. [10] Mazar et al. studied β - scission reactions on different hexyl and octyl cations. [11] Some interesting trends have been observed. First, reaction rates for cracking towards propene are higher than those for cracking towards ethene. Secondly, cracking barriers were found to decrease with increasing carbon numbers. Thirdly, the type of cationic transition has been established to play a crucial role in the activation barriers.

In this thesis research, different monomolecular and bimolecular cracking pathways are investigated (indicated in blue and red respectively in Figure 1). A kinetic and thermodynamic analysis is carried out to determine feasible reaction routes for butene cracking. Based on the aforementioned observations, only octyl carbenium ion β - scissions towards propene and pentene or towards butenes are studied. Furthermore, a distinction

P. Cnudde is with the Center for Molecular Modeling, Ghent University (UGent), Ghent, Belgium. E-mail: Pieter.Cnudde@UGent.be

is made between secondary and tertiary cationic transitions. Additionally, the behavior of a 2-butyl cation and several octyl carbenium ion species is investigated with ab initio molecular dynamics simulations. Isomers with different branching degrees are studied to verify the lifetime of tertiary versus secondary carbenium ions. The link between these observations and the expected product distribution of butene cracking is examined.

II. Theoretical Methods

To discriminate between different reaction pathways, several β - scission elementary steps are modeled using static calculations on a 46T-cluster model of H-ZSM-5. The IRC approach is applied to find the reactant and product minima on the potential energy surface. For computational efficiency, all geometries have been optimized with the QM/QM 8T:46T ONIOM(B3LYP/6-31+g(d,p):pm3) scheme. Despite the accurate description of reaction geometries, ONIOM energies have proven to be less reliable. Therefore, a single point energy calculation at the ωB97X-D level of theory has been performed on the entire 46T-cluster. Transition state theory allows to determine kinetic coefficients from these final results. The Gaussian09 package has been employed for static calculations.

To observe the behavior of the intermediate species in the zeolite channels, ab initio molecular dynamics (MD) simulations have been carried out on a periodically extended H-ZSM-5 unit cell with the revPBE functional with additional Grimme D3 dispersion corrections, combined with the DZVP-GTH basis set. Statistical sampling occurs in the NPT ensemble with the CSVR thermostat, set at a temperature of 560 °C and a pressure set at 1 bar. A sampling period of 0.5 fs has been selected. The CP2K package has been used for molecular dynamics simulations.

III. Results and Discussion

First, the monomolecular cracking pathway is studied. Only a single feasible β - scission possibility can be written down, i.e. cracking of a 1-butyl cation into ethylene and an ethyl cation. The ethyl cation, formed in the transition state, is a very unstable species, hence the small ethyl cationic fragment binds to a framework oxygen, forming a stable ethoxide species. The intrinsic free energy barrier amounts to 79.7 kJ/mol. However, the 1-butyl cationic reactant state appears to be a very unstable species since a barrierless transition to the more stable 2-butyl cation occurs during reactant optimization. Although static calculations indicate that the secondary butyl carbenium ion is a local minimum on the potential energy surface, three independent MD simulations on this cation have shown that between 1 and 3 ps, the carbenium ion deprotonates to the framework, indicating that butyl carbenium ions will have a rather short lifetime. These results thus indicate that monomolecular cracking is probably not the most feasible pathway.

Secondly, the bimolecular cracking pathway is investigated. From both the tertiary and secondary cation transition classes, two representative reactions (one reaction yielding propene and one yielding butene) have been investigated with static calculations. The resulting free energy barriers are shown in Figure 2.

In the transition state geometry, the $C-C$ bond in β position is elongated, broken, and the positive charge has shifted to the β -C position. If a secondary or primary carbenium is formed as product, it will spontaneously rearrange to an alkoxide during product optimization. However, for a tertiary ionic product fragment, product optimization does not yield a tertiary alkoxide but a 'free' carbenium ion, confirming the premise that tertiary carbenium ions are stable local minima on the potential energy surface. Finally, it should be noted that for bulky reactant and product species (e.g. secondary - tertiary transitions), the small 46T-cluster model reaches its limits and is no longer sufficient to accurately describe the interactions with the large adsorbates.

Three general trends are recognized from Figure 2. First, starting from either a tertiary or secondary reactant, the barriers follow a decreasing trend in the order: primary $>$ secondary $>$ tertiary products, which is a reflection of the carbenium ion stability order in the transition state. Secondly, forming either primary or secondary products, the barriers follow a decreasing trend in the order: tertiary $>$ secondary reactants, which may be attributed to a larger difference in stabilization, starting from a tertiary reactant compared to a secondary reactant. Thirdly, the barriers for cracking towards C_4 species are typically higher than towards C_3 and C_5 species, in agreement with expected product distributions.

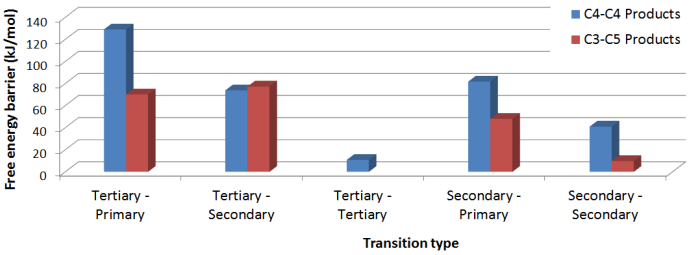

Fig. 2. Free energy barriers (in kJ/mol) at 560 °C for β - scissions towards two C_4 species (blue) and towards a C_3 and C_5 species (red), grouped by transition type (LOT : ωB97X-D/6-31+g(d,p)//ONIOM(B3LYP/6-31+g(d,p):pm3))

Intrinsic reaction kinetics are only one aspect in the determination of feasible reaction paths. A second aspect is the question if the required reactant species can be formed inside the zeolite channels and what the concentration of these species will be. To address this issue, MD simulations are applied.

First, molecular dynamics simulations demonstrate that octyl carbenium ions indeed appear to be stable, long-lived intermediates. Transitions between the protonated cationic states and the deprotonated alkene states are sampled. The double bond of the latter interacts with the acidic framework hydrogen by forming a π -complex. Secondly, during the simulations, hydride shifts with low activation barriers are observed. The backbone configuration of the chain however remains unaltered, since the activation energy of methyl shifts appears to be too high for an adequate sampling. As a general trend, no primary carbenium ions are observed during the simulations, confirming that these cations are indeed more unstable than secondary and tertiary cations and will hence barely be present in the zeolite channels. These MD simulations justify the choice to only investigate secondary and tertiary transitions with static calculations.

Large differences are observed between the dynamic behavior of the linear chain and the triple branched chain. The linear 2-octyl carbenium ion has the highest mobility in the zeolite channels, allowing the chain to rearrange into specific configurations. Three different hydride shifts are observed: a 1,2-hydride shift between neighboring carbon atoms, a 1,3-hydride shift requir-

ing an optimal trans configuration of the chain and a 1,5-hydride shift (shown in Figure 3) requiring a folding of the chain, so the proton transfer occurs over a 6-ring transition state.

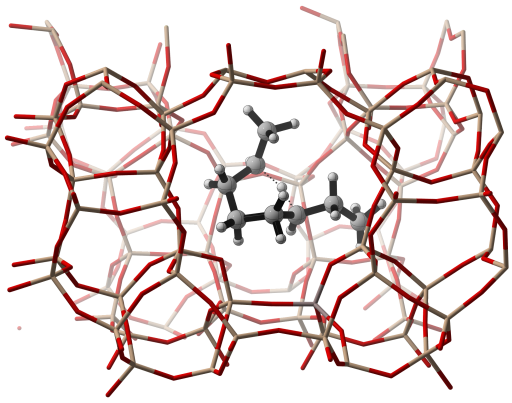

Fig. 3. Snapshot of a 1,5-hydride shift from a linear octyl chain MD simulation in H-ZSM-5, seen along the sinusoidal channel

Frequent hydride shifts take place, so the positive charge moves along the chain - from the second to the seventh position - during the simulation (see Figure 4). Although little difference in stability between different secondary carbenium ions can be expected, the positive charge is most located at the central carbon atoms (position 4 and 5), followed by position 3 and 6, while the charge barely resides on carbon atom 2 and 7. Clearly, a 4-octyl cation is more stable than a 3-octyl cation, which is more stable than a 2-octyl cation. This trend is explained by increased inductive and hyperconjugative stabilization for the central carbon atoms.

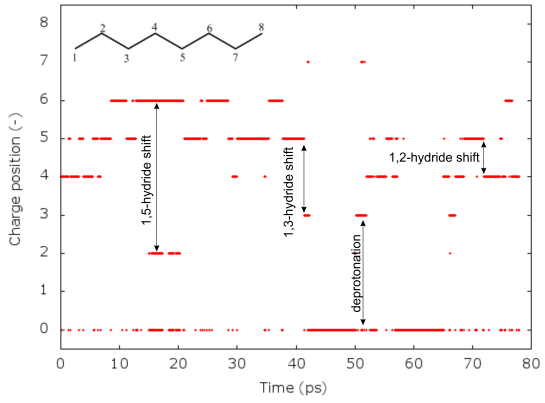

Fig. 4. Evolution of the positive charge position in a linear octyl chain (carbon number 1 to 8; 0 is either a proton transfer between different carbon atoms, a proton transfer to the zeolite framework or a deprotonated state)

The 2,4,4-trimethyl-2-pentyl carbenium ion in contrast, has a much lower mobility, which may be explained by the confinement effect of the H-ZSM-5 zeolite pores. The only observed isomerization is a 1,2-hydride shift to the secondary 2,4,4-trimethyl-3-pentyl carbenium ion. The secondary isomer is only sampled during 0.2 % of the total simulation run.

IV. Conclusion

Bimolecular cracking of butene offers a viable alternative to the rather high-barrier monomolecular cracking route for light olefin production. Several C_8 isomers can be formed upon dimerization, which can subsequently undergo cracking. Static calculations have shown that cracking of secondary carbenium ions generally have lower activation energies. MD simulations have demonstrated that a large fraction of the cationic species in the organic pool will probably be formed by tertiary cations. However due to their high stability, activation barriers can be rather high. Both results are in agreement since the secondary carbenium ions are less stable than tertiary carbenium ions and will hence be less present. Assuming only linear carbenium ions would exist inside the zeolite pores, the kinetic parameters from static calculations can be combined with the cation distribution from MD simulations to estimate actual reaction rates. Comparing the relative cracking rates, it is found that the propene production rate is indeed higher than the butene or ethene production rate. However, since not only linear species will be present, the exact distribution of the C_8 isomer species should be known to obtain results for the global cracking process. Calculation of actual reaction rates from the molar fractions of different isomers, obtained from molecular dynamics simulation, together with accurate rate coefficients from static calculations can be a powerful tool for determining the most important reactions or reaction classes in the butene cracking process in the near future.

References

[1] P. N. R. Vennestrøm, C. M. Osmundsen, C. H. Christensen, and Esben Taarning, "Beyond petrochemicals: The renewable chemicals industry," *Angewandte Chemie International Edition*, vol. 50, no. 45, pp. 10502–10509, 2011.

[2] Michael J. Tallman and Curtis N. Eng, "Catalytic routes to olefins," *AIChE Paper 219c*.

[3] Xianghai Meng, Chunming Xu, Li Li, and Jinsen Gao, "Kinetic study of catalytic pyrolysis of C_4 hydrocarbons on a modified ZSM-5 zeolite catalyst," *Energy & Fuels*, vol. 24, no. 12, pp. 6233–6238, 2010.

[4] Xiangxue Zhu, Shenglin Liu, Yueqin Song, Sujuan Xie, and Longya Xu, "Catalytic cracking of 1-butene to propene and ethene on MCM-22 zeolite," *Applied Catalysis A: General*, vol. 290, no. 12, pp. 191–199, 2005.

[5] J.S. Buchanan, J.G. Santiesteban, and W.O. Haag, "Mechanistic considerations in acid-catalyzed cracking of olefins," *Journal of Catalysis*, vol. 158, no. 1, pp. 279–287, 1996.

[6] Yury V. Kissin, "Chemical mechanisms of catalytic cracking over solid acidic catalysts: Alkanes and alkenes," *Catalysis Reviews*, vol. 43, no. 1-2, pp. 85–146, 2001.

[7] Cuong M. Nguyen, Bart A. De Moor, Marie-Françoise Reyniers, and Guy B. Marin, "Isobutene protonation in H-FAU, H-MOR, H-ZSM-5, and H-ZSM-22," *The Journal of Physical Chemistry C*, vol. 116, no. 34, pp. 18236–18249, 2012.

[8] Christian Tuma and Joachim Sauer, "Protonated isobutene in zeolites: tert-butyl cation or alkoxide?," *Angewandte Chemie*, vol. 117, no. 30, pp. 48474849, 2005.

[9] M. Guisnet, P. Andy, N. S. Gnep, E. Benazzi, and C. Travers, "Skeletal isomerization of n-butenes: I. mechanism of n-butene transformation on a nondeactivated H-Ferrierite catalyst," *Journal of Catalysis*, vol. 158, no. 2, pp. 551–560, 1996.

[10] David Lesthaeghe, Jeroen Van der Mynsbrugge, Matthias Vandichel, Michel Waroquier, and Veronique Van Speybroeck, "Full theoretical cycle for both ethene and propene formation during methanol-to-olefin conversion in H-ZSM-5," *ChemCatChem*, vol. 3, no. 1, pp. 208212, 2011.

[11] Mark N. Mazar, Saleh Al-Hashimi, Matteo Cococcioni, and Aditya Bhan, "β-scission of olefins on acidic zeolites: A periodic PBE-D study in H-ZSM-5," *The Journal of Physical Chemistry C*, vol. 117, no. 45, pp. 23609–23620, 2013.

Acknowledgements—*The computational resources (Stevin Supercomputer Infrastructure) and services used in this work were provided by the VSC (Flemish Supercomputer Center), funded by Ghent University, the Hercules Foundation and the Flemish Government - department EWI.*

Contents

List of abbreviations

CHA	Chabazite
DFT	Density functional theory
DME	Dimethylether
FCC	Fluid catalytic cracking
HF	Hartree-Fock
HL	High level of theory region
HS-FCC	High severity fluid catalytic cracking
I	Inner Region
IRC	Intrinsic reaction coordinate
LL	Low level of theory region
LOT	Level of theory
MD	Molecular dynamics
MM	Molecular mechanics
MNDO	Modified Neglect of Diatomic Overlap
MP	Møller- Plesset perturbation method
MTG	Methanol-to-gasoline
MTH	Methanol-to-hydrocarbons
MTO	Methanol-to-olefins
MTP	Methanol-to-propene
O	Outer Region
OCP	Olefin Cracking Process
ONIOM	Our own N-layered Integrated molecular Orbital and molecular Mechanics
P/E	Propene to ethene production ratio
PA	Proton affinity
PCP	Protonated cyclopropane
PES	Potential energy surface
PHVA	Partial Hessian Vibrational Analysis
PM3	Parametric Method 3
QM	Quantum mechanics
R/P	Reserves to production ratio
SAPO	Silicoaluminophosphate

TOS	Time on stream
TS	Transition state
TST	Transition state theory
WHSV	Weight hourly space velocity
ZPE	Zero-point energy

List of symbols

$\ddagger$		Transition state
$\Delta E^{\ddagger}$	kJ mol^{-1}	Electronic reaction barrier
ΔE_r	kJ mol^{-1}	Electronic reaction energy
$\Delta G^{\ddagger}$	kJ mol^{-1}	Free energy barrier
ΔG_r	kJ mol^{-1}	Reaction free energy
ΔH	kJ mol^{-1}	Enthalpy difference
$\Delta H^{\ddagger}$	kJ mol^{-1}	Enthalpic barrier
ΔH_r	kJ mol^{-1}	Reaction enthalpy
ΔS	J $mol^{-1}K^{-1}$	Entropy difference
$\Delta S^{\ddagger}$	J $mol^{-1}K^{-1}$	Entropy barrier
ΔS_r	J $mol^{-1}K^{-1}$	Reaction entropy
Δt	s	Sampling period
ν	s^{-1}	Vibrational frequency
σ		Symmetry number of a molecule
ψ_{el}		Electronic wave function
A	s^{-1}	Pre-exponential factor
c_R	mol m^{-3}	Reactant concentration
E_a	kJ mol^{-1}	Activation energy
$\bar{F}$	N	Force vector
$\hat{H}_{el}$		Electronic Hamiltonian
I_X,I_Y,I_Z	kg m^2	Moments of inertia of a rigid molecule
h	J s	Planck's constant
k_{fwd}	s^{-1}	Intrinsic forward rate coefficient
k_{bwd}	s^{-1}	Intrinsic backward rate coefficient
k_B	J K^{-1}	Boltzmann's constant
k(T)	s^{-1}	Temperature dependent rate coefficient
N		Number of atoms
m	Da	Atomic mass
P		Product
P_i		Probability of state i

Q	m^{-3}	Global partition function
$q_{\ddagger}$	m^{-3}	Partition function of the transition state
q_R		Reactant partition function
q_el		Electronic partition function
q_rot		Rotational partition function
q_trans		Translational partition function
q_vib		Vibrational partition function
$\bar{R}$	m	Position vector
R	J mol^{-1} K^{-1}	Universal gas constant
R		Reactant
r	mol m^{-3} s^{-1}	Reaction rate per unit volume
T	K	Temperature
U , V	kJ mol^{-1}	Potential energy
$\bar{v}$	m s^{-1}	Velocity vector
$-_{int}$		Property of the intrinsic reaction
$-_{chem}$		Property of the reaction with a chemisorbed reactant state
$-_{phys}$		Property of the reaction with a physisorbed reactant state

A single dream is more powerful than a thousand realities.

- John Ronald Reuel Tolkien -

Chapter 1

Introduction

1.1 Light olefin production

Ethene and propene are the two most important commodity chemicals with rapidly growing global demand. Many chemical products are based on light olefins and their derivatives. The largest part of these olefins is consumed by the polymer industry for polyethene, polypropene or copolymers production. Additionally, ethene is used for the production of ethylene oxide, ethylene glycol, ethylbenzene, styrene, while other propene markets include the production of propylene oxide, acrylonitrile, acrolein and cumene. Ethene and propene demand keeps increasing annually, mainly due to the growth of the polymer industry, which is driven by the expanding economies of the BRIC countries and the growing world population. [1]

One of the most important classic ways to produce light olefins is steam cracking, a high-temperature pyrolysis in the presence of dilution steam. Feedstock can vary from ethane over naphtha to heavy gas oil fractions. Ethane pyrolysis yields mostly ethene and ethane. The latter can be recycled to the furnace inlet. Naphtha pyrolysis yields mostly ethene, propene, butenes, methane, ethane, propane, butanes, BTX′s and pyrolysis gasoline. For a long time, propene was overshadowed by its homologue ethene, and considered a byproduct of ethene production. [1]

A second traditional way to produce light olefins is fluid catalytic cracking (FCC). Catalytic pyrolysis of atmospheric gas oil is carried out over an acid catalyst in refineries to produce gasoline. Considerable amounts of propene (and ethene) are formed as side products. The main advantages compared to steam pyrolysis are the lower operating temperature and energy consumption, the higher yields of C_3 - C_4 and lower yields of C_1 - C_2 hydrocarbons. [1]

To date, light olefin production (ethene and propene) is based on crude oil or natural gas

derivates. However, the depletion of oil reserves and the search for viable alternatives has been a hot issue in recent years. The exact moment when oil reserves will run out is very difficult to predict due to the economic cycles. The reserves to production ratio (R/P ratio) is a justified estimate for the number of years left until the fossil fuel sources are depleted. The estimated oil and natural gas reserves per region are plotted in Figure 1.1.[2] Currently, oil reserves are estimated to last for 53 years of global production. Natural gas reserves, which seem an interesting short term alternative since the discovery and exploitation of shale gas are estimated to last for 56 years of global production.[2]

Figure 1.1: World proven oil (left) and natural gas (right) reserves expressed as reserves-to-production ratio at the end of 2012[2]

The price evolution of crude oil is shown in Figure 1.2. The rising trend of crude oil prices indicates that sooner or later the market of renewable chemicals will become an economically interesting alternative for the fossil fuel based chemicals. A second aspect that could trigger the search for alternative technologies is global warming. Traditional ethene and propene production results in significant amounts of CO_2 emissions. Unlike fossil fuel based products, biomass chemicals are almost CO_2 neutral.[3]

The price evolution of natural gas over the past decades is shown in Figure 1.3. In contrast to the oil price, the natural gas price follows a decreasing or stabilizing trend over the last years due to the recent shale gas recovery, in particular in the USA.[2]

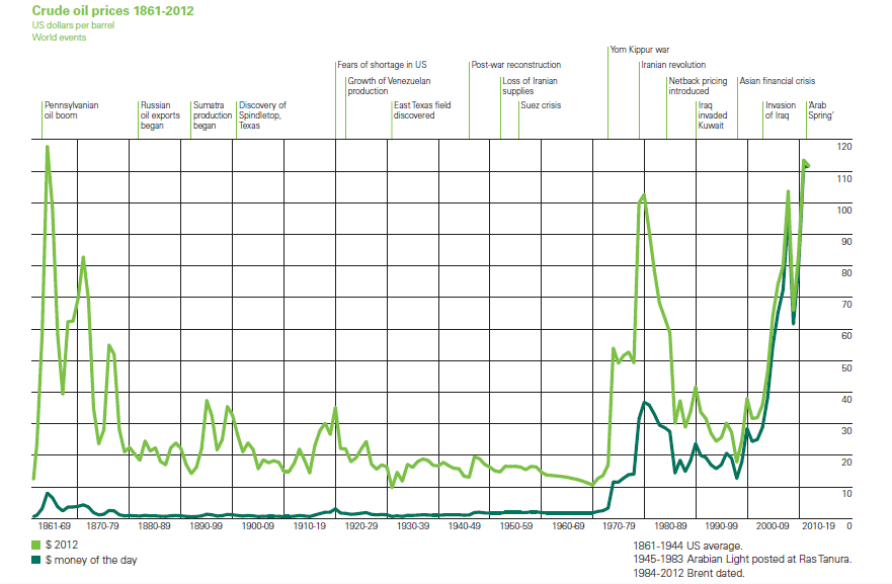

Figure 1.2: Evolution of the crude oil prices from 1861 to 2012 [2]

Figure 1.3: Evolution of the natural gas prices per region from 1995 to 2012 [2]

Shale gas is a promising short-term alternative for the decreasing oil reserves and the accompanying rise in energy cost. On the one hand, the dependency on natural gas or oil import from geopolitical instable regions can be reduced, while on the other hand, it gives a boost to the local industry. The USA has recently changed to an economy with a larger export of natural gas than import. [4] The exploitation of shale gas has set the search for renewable chemicals a large step backwards. [5] However, experts suggest that the shale gas advantage will fade out over the next decades, as the increasing demand for natural

gas, especially steered by the rising electricity demand, together with the depletion of the easy accessible gas reserves, will render the shale gas recovery less economically attractive. Nevertheless, a lot of uncertainty remains in these predictions.[4,5]

Due to the booming shale gas business in the USA[6] and the large ethane crackers in the Middle East,[7,8] ethene prices have dropped, while propene prices have risen because of the resulting unbalance between ethene and propene on the market. Figure 1.4 depicts the evolution of the propene to ethene price ratio. Due to the shift of naphtha cracking to ethane cracking, the propene supply has decreased while the demand still increases. This discrepancy has caused the propene to ethene price ratio to increase to about 1.5 at present.[5]

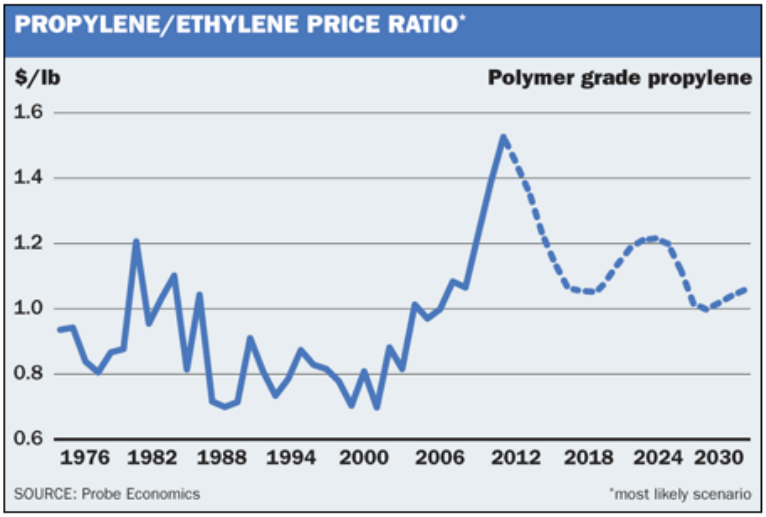

Figure 1.4: Evolution of the propene to ethene price ratio from 1976 to 2030[5]

Although steam cracking will remain the main production route for propene, the propene to ethene production ratio (P/E ratio) is not flexible enough to meet future market demands. Several on-purpose propene production technologies will become economically interesting, e.g. dehydrogenation of propane, methanol-to-olefins (MTO), metathesis of ethene and 2-butene, HS-FCC or cracking of olefins.[9,10] In Figure 1.5, the contribution of these production routes to the total propene production is shown. Also for ethene, several promising alternative production pathways may become interesting in the future,e.g., (bio-)ethanol dehydration, oxidative coupling of methane.[1]

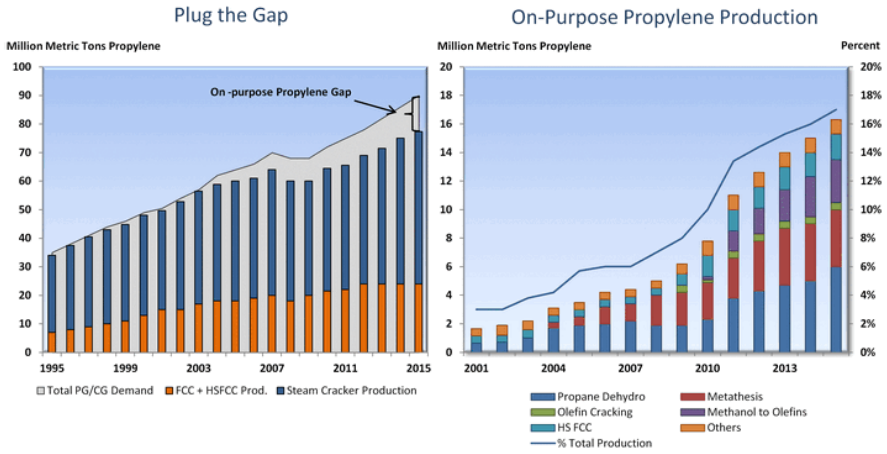

Figure 1.5: Evolution of the propylene production (left) and contribution of on-purpose propylene production technologies to the total production (right) from 1995 to 2015) [10]

1.2 Role of olefin catalytic cracking in industrial processes

In many of the on-purpose propene and ethene technologies, olefin cracking plays a crucial role. These processes are typically carried out over an acidic zeolite catalyst. In this section, an overview of the most important examples is given.

1.2.1 Fluid catalytic cracking

Fluid catalytic cracking (FCC) is one of the most important processes in a refinery. High molecular weight petroleum fractions, like vacuum gas oils or atmospheric gas oils are converted into gasoline and olefins via isomerization and cracking reactions. Next to ethene and propene, the C_4 cut is also an important fraction, which is typically converted in alkylation units to produce high octane number gasoline additives. Most olefins are produced through catalytic cracking via a carbenium ion mechanism, although a small fraction is produced via thermal cracking.

Typical process conditions are 500 - 550°C, a contact time of a few seconds and a catalyst to oil weight ratio of 4 - 9.[11] In contrast with steam cracking, the effect of different feedstocks on the light olefin yield is less pronounced in catalytic cracking and the P/E ratio depends on the catalyst properties, e.g., acid site density, acid strength. and operating conditions. Conventional FCC light olefin yields are lower than 10% with an ethene yield of only a few percentages.[1,11]

The FCC process uses a shape-selective zeolite catalyst, mostly a stabilized H-Y zeolite. Addition of H-ZSM-5 to the catalyst has proven to increase the selectivity for light olefins because this zeolite minimizes hydrogen transfer reactions and promotes isomerization

and cracking of C_{5+} species, hereby effectively increasing light olefin yields. Olefin cracking is an important link in the complex reaction network of FCC processes. [11,12]

The process is typically performed in a riser reactor system (see Figure 1.6) with continuous catalyst regeneration. The feed and the fresh catalyst enter at the bottom of the reactor and rise to the top, while catalytic reactions occur in the vapor phase. After exiting the riser, the catalyst is separated from the product vapor in the reactor vessel. The deactivated catalyst is sent to a regenerator where coke is combusted with air. This regenerator restores the catalytic activity and also supplies heat to the reactor. [13]

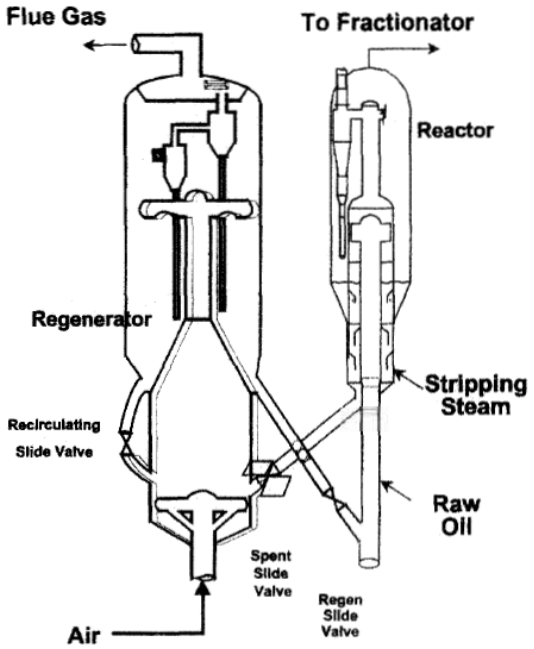

Figure 1.6: Sketch of the UOP fluid catalytic cracking riser reactor model [13]

Recently, a new process was developed to attain a higher light olefin yield: High Severity Fluid Catalytic Cracking (HS-FCC). [14] Compared to conventional FCC, the HS-FCC process is typically performed under more severe operating conditions with temperatures ranging from 550 - 650°C, contact times less than 1 second and a catalyst/oil weight ratio of 20 - 40 in a down flow fluid-solid reaction system. These conditions allow obtaining a high selectivity for olefins by reducing the importance of olefin consuming secondary reactions, while maintaining a high conversion. A catalyst with low acid site density should be selected to minimize hydrogen transfer reactions and maximize the olefin yield. Combined light olefin yields of 30 - 40 wt% have been demonstrated. [14]

1.2.2 Methanol-to-olefins

The methanol-to-olefins (MTO) process is an emerging technology to produce light olefins. Methanol is a potential low-cost feedstock for the formation of methylesters, aceton, formaldehyde and olefins. It can be produced from synthesis gas (syngas), a mixture of CO and H_2 that can in turn be synthesized from fossil fuel based resources, e.g., through coal gasification, steam reforming of natural gas, or from renewable resources through biomass gasification.[1] Biomass has the big disadvantage that the harvest is often season dependent and that crop cultivation requires large arable lands. Furthermore, biomass cultivation occurs in competition with food production. This ethical question can be solved if biomass of the second generation is used, i.e. lignocellulosic non-edible biomass.

Methanol to hydrocarbons conversion was discovered in the early '70s. Mobil researchers developed a methanol-to-gasoline (MTG) process based on a H-ZSM-5 catalyst.[15] This catalyst shows a relatively low selectivity for ethylene and paraffins, but a high propylene and C_{4+} selectivity. Methanol is catalytically dehydrated and partially converted to ethene, propene and a large fraction C_{4+} hydrocarbons. The MTG process is carried out on a fixed bed reactor system with intermittent regeneration. Adapting the process conditions can significantly increase the selectivity for ethene and propene. The relatively high yield of C_{4+} species however, remains an important disadvantage of this technology for light olefin production.[15–17]

UOP/Hydro developed a MTO process based on a H-SAPO-34 catalyst.[18] This process is carried out on a fluidized bed reactor (riser type reactor) with a regenerator system to remove the accumulated coke formed inside the catalyst pores. The MTO reactor operates at relatively low pressure 1 - 3 barg and at temperatures typically between 400°C and 550°C. Figure 1.7 compares the product composition between the two different catalysts.[19] Due to the small pore size of H-SAPO-34, diffusion of large and branched products is restricted, resulting in high selectivities for ethene and propene and smaller C_{4+} selectivity. Aromatics can be formed, but will be trapped in the cages. In contrast, on H-ZSM-5 larger molecules, all the way up to aromatics, can be produced and can exit the catalyst pores.[18,19]

In parallel, Lurgi developed a variant based on the H-ZSM-5 route with particular focus on maximizing the propylene yields, the methanol-to propylene (MTP) process.[20] Undesired products such as primary olefins, ethene and butenes are recycled to the reactor. This olefin recycle also serves as a heat sink for the exothermic reactions. Recycled process condensate water serves as a diluting agent and increases the selectivity towards olefins.[17,20]

Figure 1.8 shows a process flow diagram of the reaction and separation section of an

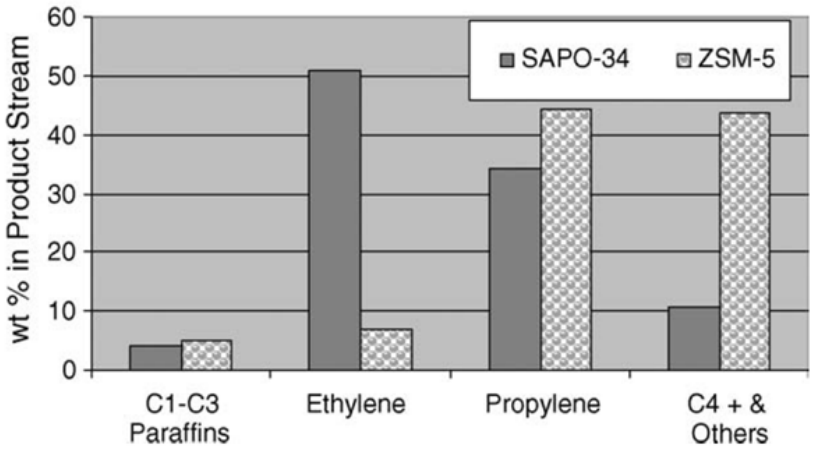

Figure 1.7: Comparison of the MTO product composition with a ZSM-5 or a SAPO-34 catalyst [19]

industrial unit. For every mole of methanol converted, one mole of water is generated. A portion of the unconverted methanol leaves the reactor as dimethylether (DME). To purify the reactor effluent from these byproducts, an oxygenate removal section needs to be implemented. By adjusting the amount of heat input into the feed, the reactor temperature can be tuned and hence a desired P/E ratio, typically ranging from 0.9 to 1.5, can be attained. [18]

The exact mechanism governing the MTO process has been one of the most controversial in heterogeneous catalysis. Today, it is generally accepted that a pool of hydrocarbons must be present in the zeolite pores to act as a cocatalyst. These species repeatedly undergo methylation and subsequent light olefin eliminiation, thus closing the catalytic cycle. [21] The precise reaction mechanism depends on the zeolite framework. In H-SAPO-34, polymethylbenzene species were found to be the basis of the hydrocarbon pool. In H-ZSM-5, however, a dual cycle concept was developed in which both aromatics and alkenes play a role as cocatalysts. [22,23] The aromatic polymethylbenzene cycle yields mostly ethene, while the alkene cycle (shown in Figure 1.9) yields mostly propene and higher alkenes. Both cycles are interconnected: propene can also be produced from the aromatics cycle and alkenes can undergo oligomerization and cyclization to aromatics. Thorough insight in these cycles is necessary to be able to tune the P/E ratio. [17,24]

Alkene cracking plays a crucial role in the alkene cycle as illustrated in Figure 1.9. Once a sufficiently long carbon chain is formed through subsequent methylations (going from propene over butene, pentene to hexene), cracking reactions result in the for-

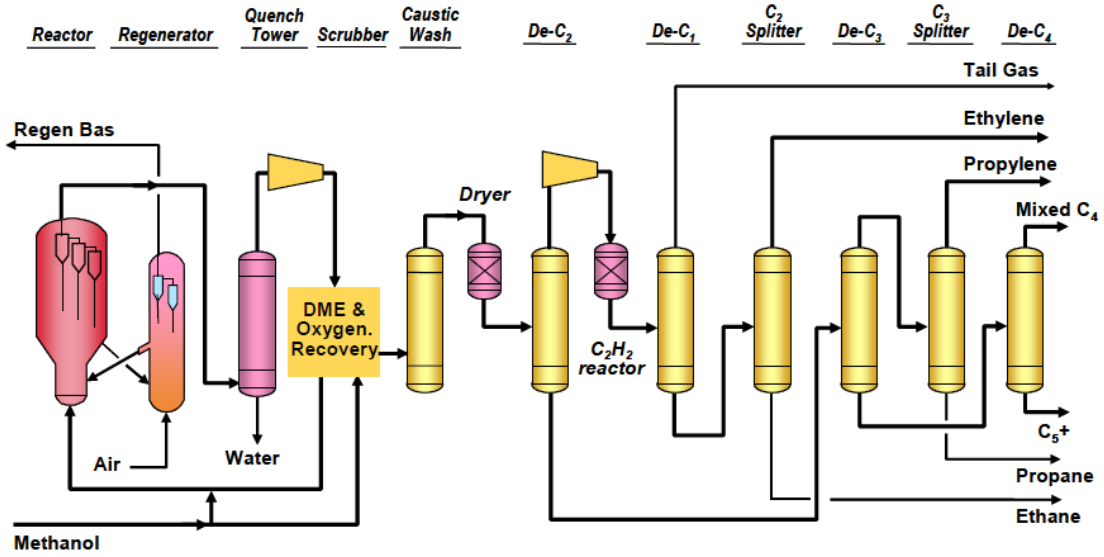

Figure 1.8: Flow diagram of a MTO reaction and separation section [18]

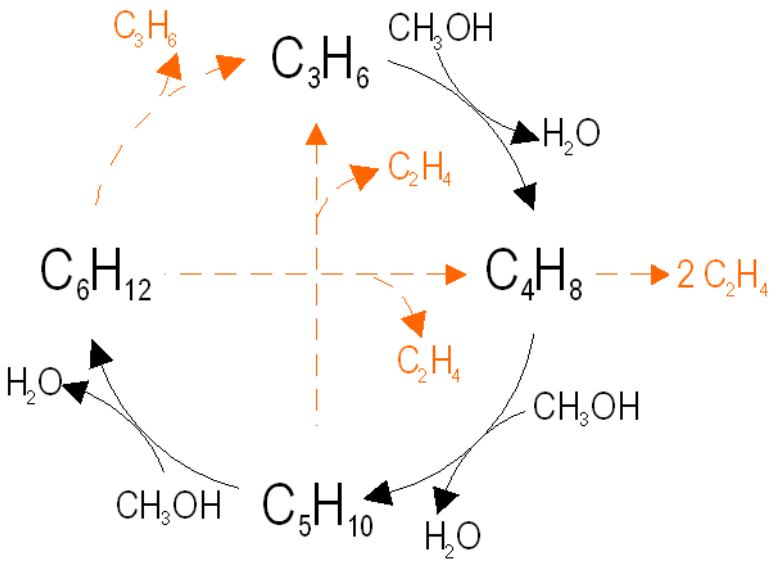

Figure 1.9: The alkene catalytic cycle in a MTO process over ZSM-5 [21,22]

mation of ethene and propene, with the reactions yielding propene among the most feasible. [21–23,25,26]

1.2.3 Olefin cracking process

A third interesting class of technologies to produce ethene and propene are the olefin cracking processes (OCP). [9,18] The aim of these OCP's is to upgrade low-value products

through the production of propene, and to some extent, ethene. Steam cracker byproducts, low-value FCC refinery streams, catalytically cracked naphtha, light gasoline or the MTO product streams can be used as feedstock. An important condition is that the feed contains sufficient amounts of C_{4+} alkenes. Several patents exist on the catalytic cracking of these olefins.[27–29]

In some countries, especially developing countries, the chemical utilization ratio of C_4 hydrocarbons is low, hence the conversion of these C_4 fractions to more valuable products becomes desirable. Production of light olefins through catalytic pyrolysis of this mixture is one of the interesting options.[30]

An olefin cracking unit can also be coupled to an existing catalytic cracking or MTO unit to increase the propene yields. Total and UOP combined their knowledge and developed an Advanced MTO process (MTO + OCP) for the production of polymer grade ethene and propene.[18] Figure 1.10 shows this Advanced MTO process schematically. In this set-up, the conventional MTO unit is coupled to an OCP unit that converts the C_4^+ fraction of the MTO outlet stream. This fraction consists for more than 95 wt% of species smaller than C_9, and between 65 and 85 wt% of butenes. Conversion takes place at temperatures around 550 °C - 600 °C and at atmospheric pressure over a MFI type zeolite catalyst with a high Si/Al ratio of 200 - 500.[27] Low pressures are necessary to suppress catalyst deactivation by coke formation. The process is carried out in a riser reactor, comparable to FCC. Part of the 'heavy' C_{4+} stream is recycled to the reactor.[27]

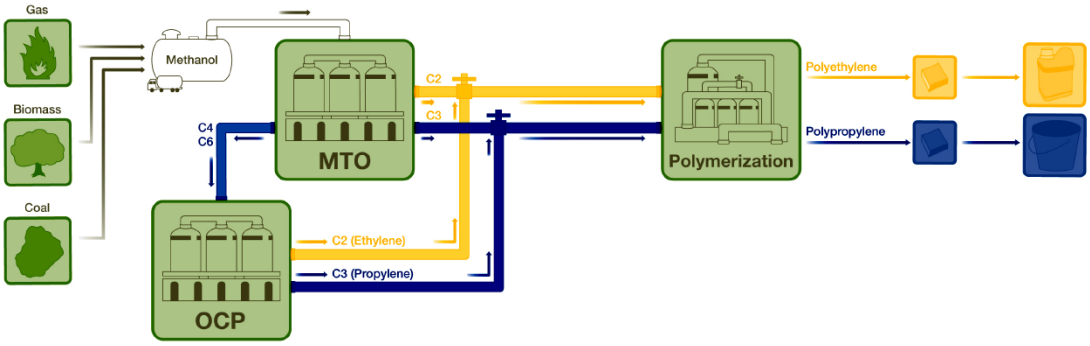

Figure 1.10: Flow diagram of the Advanced MTO process[1]

The main advantage of the Advanced MTO process is a boost of light olefin yields to 90 wt%. Furthermore, the olefin yields remain high over a wide range of propene to ethene product ratios.[18] P/E ratios of 1.5 - 2 can easily be achieved with optimal catalyst properties. The Advanced MTO Process also benefits from lower operating costs due to less methanol consumption and less energy consumption upstream from the MTO unit. Finally, it results in smaller upstream process units for methanol production and smaller

environmental impact because of reduced CO_2 emission and water consumption.[18] In Figure 1.11 the olefin yields of different processes (Naphtha cracking, MTO, MTP and Advanced MTO) are compared.

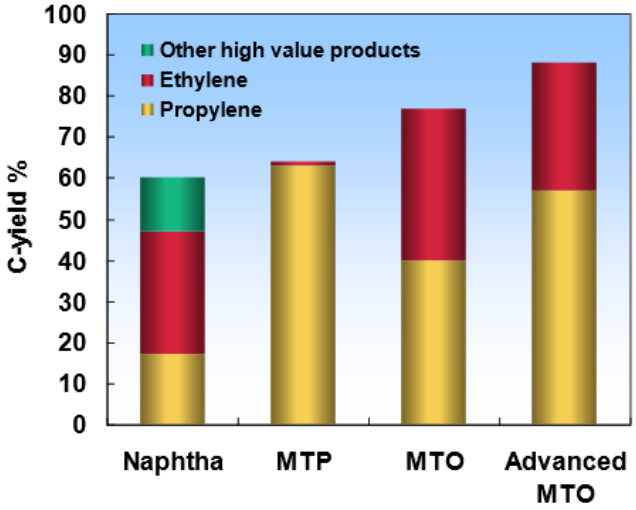

Figure 1.11: Comparison of ethene and propene yields between a conventional naphtha cracking, a MTO, a MTP and an advanced MTO process[31]

The OCP process has also been integrated with a conventional steam cracking and FCC process in a demonstration unit at the Total refinery in Antwerp. This setup allows a significant shift of the product stream composition towards propene.[32] The C_4 and higher olefin content in the C_{4+} raffinate of the steam cracker outlet or olefinic gasolines is converted selectively into propene and to a minor extent ethene. The unconverted fraction of these feedstocks has a substantially reduced olefinic content, which makes this stream more suitable to be recycled to a conventional steam pyrolysis furnace. Overall, this approach yields betters result compared to an immediate recycle of the highly olefinic feedstock.[32]

Over the last years, some on-purpose propylene technologies, based on alkene cracking, have emerged in order to meet the increasing propene demand. Kellogg Brown & Root LLC is licensor of the *Superflex* technology,[9] a catalytic cracking process that produces olefins from a C_4 - C_8 olefinic feedstock. Recycle to extinction yields of a C_4-cut pyrolysis can approximately go up to 60 wt% of propene and ethene with a P/E ratio of 2. Fuel gas and light olefins are produced as byproducts.[9]

Axens also integrated the olefin cracking process in their *Olicrack* technology,[33] a catalytic cracking process that is compatible with several refinery product streams from steam cracker up to FCC cuts. This technology is schematically shown in Figure 1.12

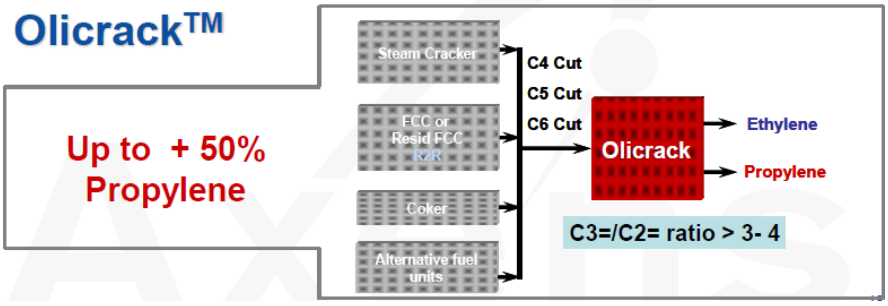

Figure 1.12: Scheme of the *Olicrack* technology[33]

They claim to obtain over 50 wt% propene yield while maintaining a high propene to ethene ratio of 3 - 4.[33]

1.3 Cracking catalysts

The most important industrial catalysts for cracking purposes are zeolites. These nanoporous materials are composed of tetrahedral units - a silicon atom or T-atom surrounded by four oxygen atoms - resulting in a three-dimensional molecular sieve structure. When some of the silicon atoms are exchanged by trivalent aluminum atoms, the framework carries a negative charge. To preserve the electroneutrality of the structure, cationic species will be present in the framework cavities. These stabilizing cations can be exchanged with protons, resulting in Brønsted acid zeolites, which are suited as cracking catalysts.

Compared to homogeneous acid catalysis, heterogeneous zeolite catalysis has the advantage that purification and product separation are easier. Additionally, the zeolite channels and pores typically have molecular dimensions, making them ideally suited as shape-selective catalysts. Three types of selectivity are considered. Spatial restriction limits the dimension of admissible reactant molecules, resulting in reactant shape selectivity. Transition state shape selectivity occurs if the formation of certain transition states is hindered by the pore dimensions. If the dimension of the formed products does not allow diffusion out of the channels or cages, product shape selectivity takes place. A third advantage is that the number of aluminum atoms can be tuned, opening up a broad range of catalysts with varying acid site density and strength. The main disadvantage of zeolite catalysts is that they are prone to coke formation and thus need frequent regeneration. If the timescale of reaction and the timescale of deactivation are of the same order, continuous regeneration is required.

One of the most used zeolite structures is H-ZSM-5 (see Figure 1.13). This material has

the MFI topology, consisting of intersecting 10-ring channels: the sinusoidal (0.55 nm by 0.51 nm) and straight channel (0.56 nm by 0.54 nm). This catalyst is ubiquitous in (petro)chemical cracking processes, justifying why it is the focus of this study. [34,35]

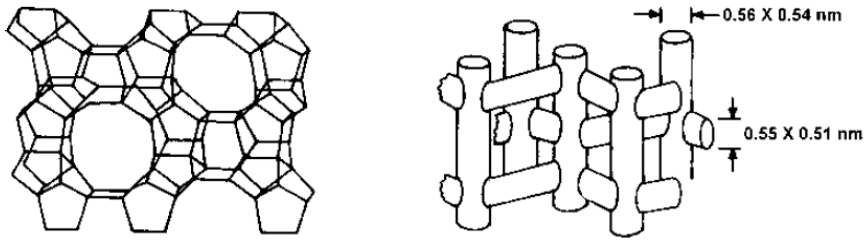

Figure 1.13: Skeletal diagram of the (100) plane (left) and channel structure (right) of ZSM-5 [34]

Other industrially important zeolite materials are the H-SAPO-34 and H-Y catalyst. The former consists of cages of 0.67 nm by 1.00 nm, interconnected by 8-ring windows with a diameter of 0.38 nm and is one of the most used catalysts in the MTO-process. The latter has large 12-ring pore windows (0.74 nm diameter) enclosing so called supercages and is one of the most used catalysts in FCC units. [34,35]

1.4 Goal of this thesis and overview of the next chapters

The goal of this dissertation is to obtain a better understanding of olefin cracking processes from a first principle approach. Mechanistic insights are required for the optimization of cracking catalysts and to obtain the desired product yields. Butene is selected as a model component and its cracking over a H-ZSM-5 catalyst is investigated.

In Chapter 2, the reaction mechanism and kinetic model of butene cracking are covered. A review of previous quantum chemical studies on alkene cracking is given. The influence of catalyst type and acid site density is also discussed. Finally, the discussion of the reactive intermediates is addressed from a quantum chemical point of view.

In Chapter 3, the different zeolite models and quantum chemical methodologies applied in this research are explained in detail.

During a butene cracking process, a broad range of different isomers can be formed as intermediates, which can all undergo cracking. In Chapter 4, static calculations on a cluster model are used to determine intrinsic kinetic parameters for some of the key reaction steps. In Chapter 5, molecular dynamics simulations are performed to clarify the exact nature of the reaction intermediates and pre-activated complexes and to evaluate

potential differences between linear and branched chains. Both techniques are combined to elucidate the reaction mechanism, to discriminate between different possible reaction steps and eventually to link these observations to the expected product distribution of butene cracking.

In Chapter 6, the main conclusions of this dissertation are summarized and an outlook for future research is given.

Chapter 2

Reaction mechanism of butene cracking

In this chapter, a literature survey is conducted regarding the different aspects concerning the reaction mechanism of butene cracking. First, an overview is given of the reaction families that take place in a catalytic cracking process. Next, a kinetic model for butene cracking is discussed, in which only the most important elementary reactions from the first part are included. In a third part, the influence of catalyst structure and acid site density is addressed. A justification for the importance of H-ZSM-5 as a cracking catalyst is given. Finally, a paragraph is devoted to the exact nature of the intermediate species.

2.1 Chemical mechanism

In all kinds of catalytic cracking processes, alkenes and alkanes are formed simultaneously. A schematic overview of the main reactions for acid catalyzed hydrocarbon conversion is shown in Figure 2.1.[36] Alkane cracking is initiated by protonation of a σ $C-C$ or $C-H$ bond, hereby forming a carbonium ion. Protolytic cracking of this carbonium ion yields a carbenium ion. If a $C=C$ bond of an alkene is protonated a carbenium ion is formed directly. These intermediates can undergo several either monomolecular reactions, e.g. isomerization, β-scission or bimolecular reactions, e.g. hydride transfer, alkylation.

2.1.1 Carbenium ion formation

Alkene cracking over acidic catalysts is generally agreed to take place at the Brønsted acid centers. Figure 2.2 shows the different interaction modes of isobutene with the

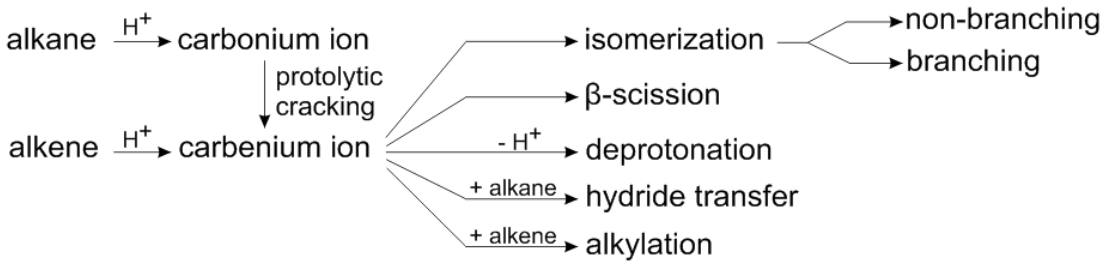

Figure 2.1: Scheme of the main reactions involved in alkene catalytic cracking [36]

zeolite acid site.

In a first stage, the physisorption, the alkene is oriented with its π - electron cloud towards the partially positive charged hydrogen atom, thus forming a π - complex. This step is relatively independent of the olefin structure. [37] In addition to the π - complex formation strength, alkene physisorption is largely determined by dispersive interactions. These interactions will become more pronounced with decreasing pore dimensions or with increasing carbon number. Nguyen et al. found that in H-ZSM-5 2-,3- and 4-alkenes have higher physisorption strengths compared to 1-alkenes owing to a different orientation in the pore structure and thus to stronger dispersion interactions. [38]

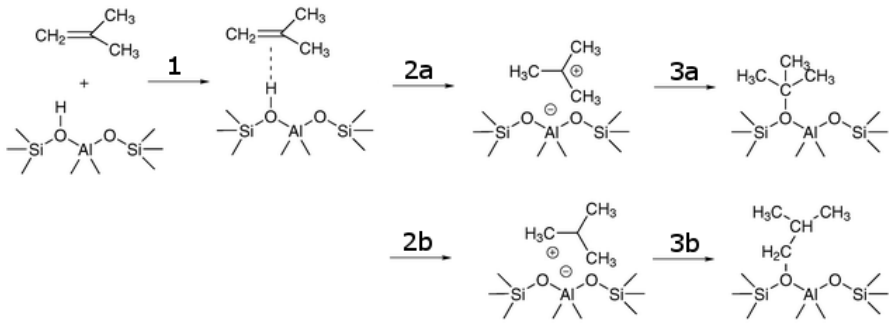

Figure 2.2: Protonation of isobutene (1: formation of physisorption complex, 2: protonation of double bond, 3: formation of chemisorption complex) at the tertiary C atom (a) and primary C atom (b) [39]

Next, this π - complex will transform into a carbenium ion by proton transfer from the zeolite to the hydrocarbon. Carbenium ions tend to decompose or isomerize into a more thermodynamically stable state, following the order primary $<$ secondary $<$ tertiary. Since metastable primary carbenium ions do not exist via adsorption, alkene protonation will always yield secondary or tertiary ions. Tertiary ions are more stable

than secondary ions due to hyperconjugation and inductive effects. These effects are also enhanced with increasing carbon numbers.[39]

Stepanov et al. have shown in experiments with deuterated zeolites that the acid proton is indeed originating from the zeolite hydroxyl groups. For linear alkenes, carbenium ion formation was also shown to take place.[40] However, carbocations are highly reactive species and therefore short living, which makes experimental observation difficult.[39]

Due to this instability, carbenium ions may transform quickly to a third stage of stable reaction intermediates. In this chemisorption stage, the carbenium ion reacts with the negatively charged framework oxygen to form an alkoxy species, bound to an AlO^- group of the framework.[41,42] The chemisorption strength is determined by the covalent $C-O$ bond strength, electrostatic and steric interactions. There is still a lot of discussion about the exact nature of the intermediate species in the cracking process. (see paragraph 2.4)

2.1.2 Non-branching isomerizations

Carbenium ions are prone to rearrangement reactions. Non-branching isomerizations, i.e., rearrangements with conservation of number of alkyl branches, occur via the Wagner-Meerwein rearrangement. In a 1,2-hydride shift (Figure 2.3), a hydrogen atom in β position is transferred, while in a 1,2-methyl shift (Figure 2.4), a β-methyl group is transferred to a positively charged carbon. A carbonium ion structure is suggested as transition state, in which respectively a hydrogen or a methyl group is shared between the vacant p orbital of the C^+ atom and the sp^3 orbital of the migrating $C-H$ bond via a coplanar structure.[36] Isotope studies have shown that 1,2-ethylshift rearrangements can also occur.[42]

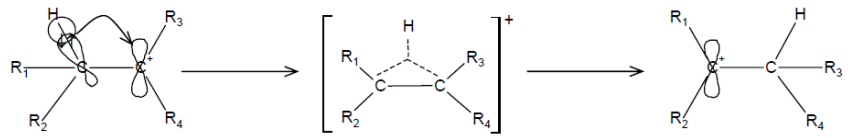

Figure 2.3: Mechanism of a 1,2-hydride shift[36]

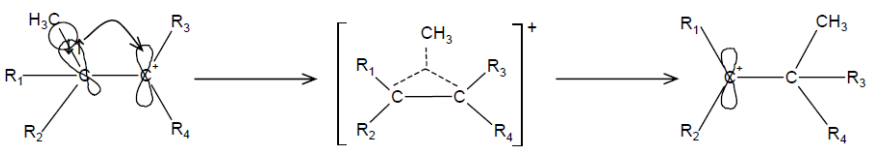

Figure 2.4: Mechanism of a 1,2-methyl shift[36]

The rate at which these rearrangements take place depends on the relative stability of the carbocations. The Hammond-Leffler postulate states that if the stability of reactant and product is comparable or if the product is more stable, the activation energy will be quite low and the isomerization rate will be high.[43] Therefore, secondary-secondary, tertiary-tertiary and secondary-tertiary transitions should be fast, while tertiary-secondary transitions are expected to be much slower.

Next to hydride or methyl shifts, double bond isomerizations can occur. Corma et al. established via post Hartree Fock methods that the reaction occurs via a concerted mechanism that involves neither ionic nor alkoxy species.[41] Although it should be mentioned that a relatively small zeolite model was employed. If the zeolite environment is properly accounted for, a stepwise mechanism could be preferred. Further research is still required in this area.

2.1.3 Branching isomerizations

A second class of rearrangement reactions are branching isomerizations. An example is shown in Figure 2.5 This type of reactions is expected to occur via a substituted protonated cyclopropane (PCP) transition state, formed via interaction of a γ located $C-H$ σ bond with an empty p orbital of the electron deficient C atom. Methyl branches for example can be formed from an edge PCP, that subsequently transforms in a face PCP. The formation of a high-energy face PCP intermediate as transition state causes the branching rearrangements to be more highly activated than non-branching rearrangements. Therefore branching isomerizations occur less frequently than non-branching isomerizations.[36]

The thermodynamic stability of the formed species is again a determining factor for the importance of branched chains. The sterical stability is a second key parameter for these isomerizations. Cracking catalysts featuring only narrow micropores, such as H-ZSM-5, show sterical limitations for the formation of highly branched chains and may therefore favor the formation of linear or lowly branched chains. However, probing with ^{13}C labeled alkenes has shown that PCP rearrangements do occur.[42] Demuth et al. established that 2-pentene isomerization pathways on H-ZSM-22 can proceed via an (edge) protonated cyclopropyl intermediate with feasible activation energies ranging between 70 and 100 kJ/mol.[44]

2.1.4 β - scission

Whitmore cracking or β - scission of carbenium ions occurs via migration of the two σ $C-C$ bond electrons in β position of the C^+ atom, yielding an alkene and a smaller carbenium ion. This is the most important reaction in the process of alkene cracking.

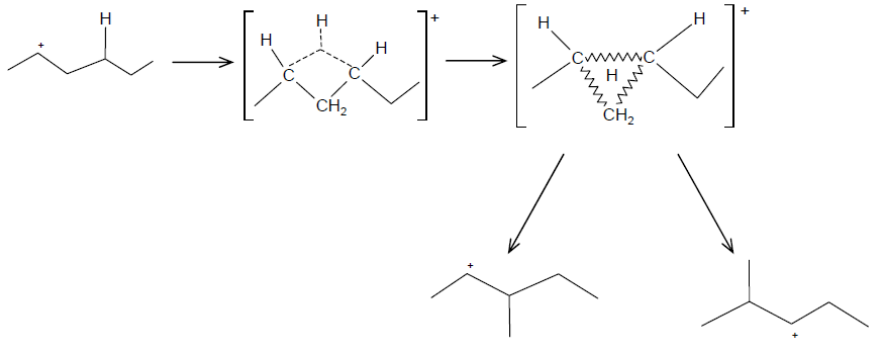

Figure 2.5: Example of the branching isomerization on a 2-hexyl carbenium ion [36]

The suggested transition state is a planar carbonium ion structure, where the σ $C-C$ electrons are shared with a third carbon atom, that will become the new electron deficient carbon. [36] The scission reaction of a 3,4-dimethyl-2-pentyl carbenium ion is shown as example in Figure 2.6.

The rate of cracking reactions will again depend on the stability of the involved carbenium ions. Primary-primary transitions are extremely unlikely to occur since unstable primary species are not confirmed as stationary point on the PES, although reactions involving either primary reactants or primary products cannot be excluded. Buchanan et al. established that tertiary-secondary and secondary-tertiary scissions are kinetically favored and will occur rather fast, while tertiary-tertiary scissions are thermodyanmically favored and will hence be slower. Tertiary-primary scissions were found to be quite slowly. [45,46] For carbenium ions with a carbon number less than six, formation of primary ions is inevitable at some time during the cracking process, while for species with higher carbon numbers, rearrangements may occur so that cracking can proceed via secondary and tertiary ions solely. This explains why alkene cracking reactivity increases rapidly with increasing carbon number. Typically, endothermic β- scissions are much slower compared to exothermic isomerization or oligomerization reactions. [42,45,46]

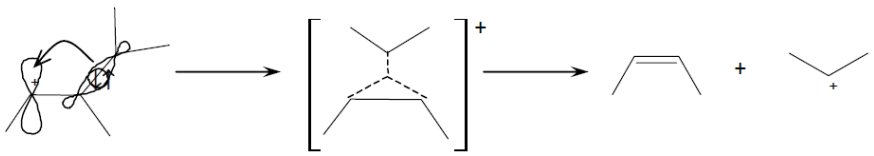

Figure 2.6: The β scission reaction of a 3,4-dimethyl-2-pentyl carbenium ion to cis-2-butene and 2-propyl carbenium ion [36]

2.1.5 Alkylation

Carbenium ions can undergo an electrophilic addition to an alkene, forming a larger carbenium ion. This reaction can be seen as the reverse reaction of a β-scission. Figure 2.7 is an example of an alkylation. A 2-propyl carbocation is added to 1-pentene, which is the reverse reaction of a scission of the 2-methyl-4-heptyl carbenium ion. [36] Dimerization and oligomerization reactions also belong to this family.

These reactions are crucial for the formation of stable carbenium ions. Isobutene, for example, will readily form oligomers in presence of acidic catalysts since this can proceed via tertiary-tertiary ion transitions. [42] For aromatic species like styrene, oligomerization is favored by resonance stabilization. For alkenes with vinylic bonds, secondary ions are involved, which show a tendency towards isomerization. Therefore, the formation of irregularly branched oligomers can be expected. [42] Quann et al. reported that propylene can be oligomerized over H-ZSM-5 up to octamers. However, the probability of exothermic n-merizations decreases compared to endothermic scissions with rising temperatures. [47,48]

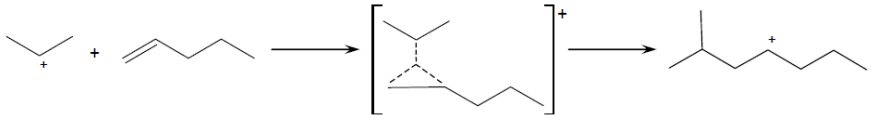

Figure 2.7: The alkylation reaction of a 2-propyl carbenium ion and 1-pentene [36]

2.1.6 Hydride transfer and protolytic cracking

A hydrogen from a $\sigma\ C-H$ bond in alkanes or alkenes can be transferred to a carbenium ion, hereby forming an alkane and a second carbenium ion over a carbonium ion transition state. Alkenes are more likely to undergo an electrophilic attack of a carbenium ion than alkanes since they may form an allylic carbenium ion, which is more stable than a tertiary alkyl ion. Also, these reactions are often part of the formation of aromatic species. [42]

If an alkane σ bond undergoes an electrophilic attack of a proton, a carbonium ion is formed with a penta-coordinated carbon atom. The decomposition of a carbonium ion into a carbenium ion occurs via protolytic or α cracking. If the proton attacks a $C-H$ bond, a carbenium ion will be created by splitting off hydrogen. If a tertiary $C-H$ bond is present, this will be the desired protonation location. However, the attack preferentially occurs at the terminal $C-C$ bond and methane will be split off. [42] At lower temperatures, cracking may also occur via the direct formation of carbenium ions. The carbonium ion mechanism yields more hydrogen, methane and ethane, while

the carbenium ion mechanism, at lower temperatures, has higher propane and butane yields.[46,49–51]

2.1.7 Deprotonation

Carbenium ions can eliminate a proton, forming alkenes. This reaction can be interpreted as a β scission of a σ $C-H$ bond and occurs therefore analogously to a cracking reaction. An electron pair in β position will be transferred from a $C-H$ bond to the C^+ atom. The H^+ will be transferred to a Brønsted basic site of the zeolite framework. Deprotonation is in fact the reverse reaction of carbenium ion formation and can yield the original alkene or a new alkene species.[36] Figure 2.8 is an example of a deprotonation reaction.

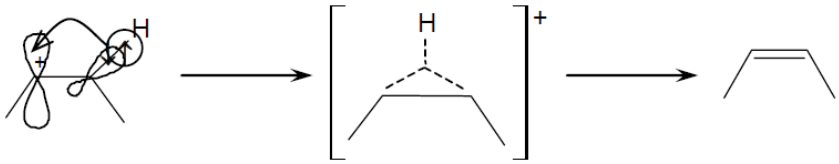

Figure 2.8: Example of a deprotonation reaction on a 3-methyl-1-butyl carbenium ion[36]

Proton elimination will usually occur such that the most stable alkene is formed. A sequence of protonation and deprotonation is the most ubiquitous reaction in alkene cracking over acidic catalysts. This sequence is known as the double bond shift.[42] For linear alkenes, the distribution of double bond shift products is determined by their thermodynamic stability. Empirical rules state that the ratio of primary alkenes to alkenes with internal double bonds in thermodynamic equilibrium is approximately 0.14 : 1.[47,52] The ratio of alkenes with internal double bonds is determined by statistics, i.e., the reciprocal of the number of positions for the double bond. The population of alkenes with an internal double bond constitutes for 68% of the thermodynamically most stable trans isomers.[42,47,52]

2.1.8 Aromatics formation

Because olefinic species are ideal precursors for coke formation, alkene cracking at high temperatures is inevitably accompanied by unwanted side reactions, leading to the formation of large aromatic compounds. In case of cracking 1-hexene, a large fraction of the products exists of alkanes, although hydrogen - necessary for hydrogenation of alkenes - was not found to be one of the main products.[52] The principal sources of hydrogen are so called hydrogen redistribution reactions. The H/C ratio in cokes is very small and the hydrogen released during coke formation is mostly consumed in alkane producing reactions. Alkane formation is partially compensated by formation of hydrogen deficient

species like cycloalkenes, cyclodialkenes or alkylaromatic compounds in the hydrogen balance.[42,52]

Condensation of olefinic species and dehydrogenation lead to ring expansion and the formation of large aromatic compounds or cokes. The formation of these large compounds also dependens on the pore size of the zeolite. The formation of extended aromatic structures on H-ZSM-5 is prohibited by shape selectivity of the cyclization and dehydrogenation reactions. A second important factor is the relatively low acid site density of H-ZSM-5.[52,53] Coke formation on H-ZSM-5 occurs mainly externally, in contrast to H-SAPO-34, for example, which suffers more from internal coking. The large cages allow formation of extended aromatic structures, but the small windows do not allow diffusion out of the cage, hereby, blocking the access to the acid sites by reactants.[17]

If the catalyst pores are blocked by stable coke components, the number of accessible active sites is reduced and a fast catalyst deactivation occurs. After a certain time-on-stream, the conversion becomes so low the catalyst needs to be regenerated. This is carried out through an oxidative treatment with air, forming CO, CO_2 and H_2O. Since high temperature steam has a detrimental effect on the catalyst activity, optimal conditions need to be selected to avoid degradation.[53,54] For FCC units, a two stage approach is widely used in which first regeneration at low temperature and in a second step regeneration at high temperature takes place. A large fraction of the hydrogen atoms of coke are indeed oxidized at low temperature.[53,54]

2.2 Kinetic model

In this paragraph, a kinetic model for butene cracking, proposed by Meng et al.[30] is discussed. A distinction can be made between different product classes. Primary products are the result from a single cracking reaction of the alkene reactant, from isomerization and dimerization reactions or from cracking of dimers. Secondary products are formed if a primary dimer, isomer or cracked species undergoes subsequent cracking, isomerization or oligomerization. Tertiary products are formed from secondary products, etc. In industry, acid-catalyzed conversion processes of hydrocarbons usually operate with a mixture of hydrocarbons as feedstock. In this thesis, cracking of n-butene as a reference component is studied.

2.2.1 Establishing a reaction network from experimental observations

The competition between alkene oligomerization and cracking makes elucidation of different cracking pathways difficult. Clearly, the complexity of reactions increases exponentially with a higher feed carbon number and higher temperatures. First principle

modeling can help in the discrimination between possible reaction pathways, which are difficult to distinguish by experimental findings. Below, several experimental insights regarding butene cracking reactivity are listed.

Alkene cracking reactivity increases with increasing carbon number.[45] The reactivity of butenes was found to be quite high in comparison to butanes, which are rather products of hydrogen transfer reactions at low reaction temperature than cracking reactants.[30] More substituted alkenes are more reactive because these can form tertiary carbenium ions, which are stabilized by a combination of the inductive effect and hyperconjugation. Product stability plays a crucial role in determining feasible reaction paths.[55] Carbenium ion stability tends to increase with higher carbon numbers, which is linked to the proton affinity of the corresponding alkene.[56]

The shape and size of the catalyst pores influences the mobility of species to a large extent and may limit access to the active centers. While linear alkenes generally have a high mobility, formation of highly branched substrates is only possible as far as allowed by the pore dimensions, i.e. transition state shape selectivity. Diffusion of reacting species into the catalyst pores can be hindered by the pore dimensions, i.e. reactant shape selectivity. Also, formed species can exhibit difficulty diffusing out of the pores, i.e. product shape selectivity.[45,57,58]

Kissin has drawn some general conclusions from a cracking study of 3,4-dimethyl-3-hexene over a H-Y zeolite based catalyst.[59] C_n alkenes tend to produce tertiary branched light products in the range C_4 - C_{n-1}. All linear and branched alkenes yield the same three olefinic products with relatively high yields: isobutene, 2-methyl-2-butene and 2-methyl-2-pentene. Methane, C_2 and C_3 yields are low at mild reaction conditions, while at higher temperatures, they become quite prominent. If the temperature increases above 200°C, the product distribution broadens. At temperatures around 400°C, reaction products from different alkenes do become indistinguishable.[30,59]

Zhu et al. also performed a series of experiments on 1-butene cracking over H-MCM-22 and proposed a kinetic model based on the results.[58] As a function of butene conversion, it was shown that initially mainly propene, C_4, C_5 and C_8 hydrocarbons were formed. At higher conversions, methane, propane, C_2, C_6 and C_7 hydrocarbon yields also increased, indicating that the latter products result from secondary transformations.[58]

Based on their experimental observations, Meng et al. proposed a reaction network for the cracking of linear butenes, shown in Figure 2.9.[30] Based on this network, a lumped 6-parameter kinetic model that was able to accurately predict experimental yields from butene cracking has been established. Note that only the main desired reactions have been included in the reaction network. Each olefin can for example be transformed into its corresponding paraffin via hydrogen transfer reactions, but these reactions are not

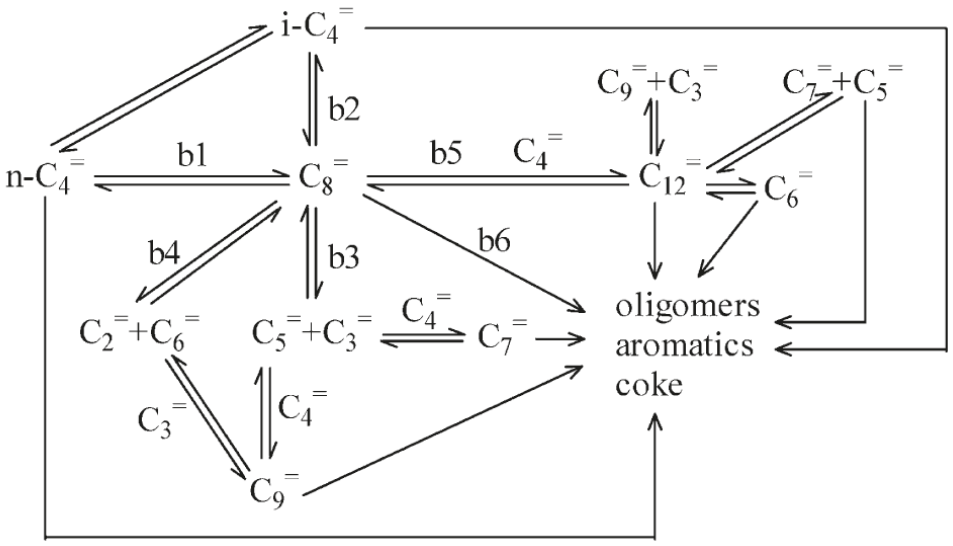

Figure 2.9: Simplified reaction network for n-butene cracking [30]

included in the network. Additionally, alkane cracking reactivity is lower compared to alkene cracking reactivity at moderate reaction temperatures, therefore thermal cracking of alkanes is not considered. [30,45,58,60–62]

N-butene can either undergo isomerization to i-butene, β - scission to ethene and an ethyl cation or dimerization to an octyl cation. I-butene can also dimerize to an octyl cation. Isomerization reactions typically have a rather low activation barrier, thus the formation of several octyl cation isomers, which can subsequently crack into secondary products, like a C_2 and C_6, C_3 and C_5 or C_4 and C_4 species are feasible. The complexity of the reaction network increases quickly once C_3 - C_8 alkenes are present in the zeolite pores which can form tertiary products: dimers, oligomers, aromatics, isomers or cracked products. If allowed by the pore dimensions, octyl cations can react with another butene molecule forming trimers (dodecyl cations), which can subsequently follow a whole series of cracking/isomerization possibilities. These oligomers are also precursors for aromatics formation and cokes condensate can also occur as side reaction.

Two main pathways exist for the cracking of butene that yield ethene and/or propene as the main products. First, in monomolecular cracking, a single butene molecule undergoes a β - scission. Secondly, in bimolecular cracking, two butene molecules dimerize before cracking towards small olefins occurs. However, detailed information about the individual reaction steps is still lacking.

Regarding the **monomolecular cracking mechanism**, i.e. the direct scission of a protonated 1-butene species, three possibilities for butene cracking can be written down

as shown in Figure 2.10: a primary carbenium ion can crack into ethylene and ethyl carbenium ion (Reaction a4), a secondary carbenium ion can undergo β scission into propylene and a methyl carbenium ion (Reaction a5) and a tertiary carbenium ion can undergo hydrogen abstraction with formation of isobutene and a proton (Reaction a6). If this pathway would be the prevailing way to produce light olefines, a lot of hydrogen, methane and ethane would be produced as side products. This is not experimentally confirmed, which was attributed to thermodynamically unfavorable mechanism as a consequence of the formation of poorly stabilized primary carbenium ions or protons. Due to the formation of unstable methyl cations upon cracking, reaction step a5. Reaction step a6 is in fact not a cracking reaction, but a deprotonation to the framework and can hence also be excluded.[60] Therefore, it has been suggested to take only path a4 into account in the kinetic model. It should be noted that in this reaction also a primary ethyl carbenium ion is formed, such that the entire monomolecular cracking pathways can been called into question.

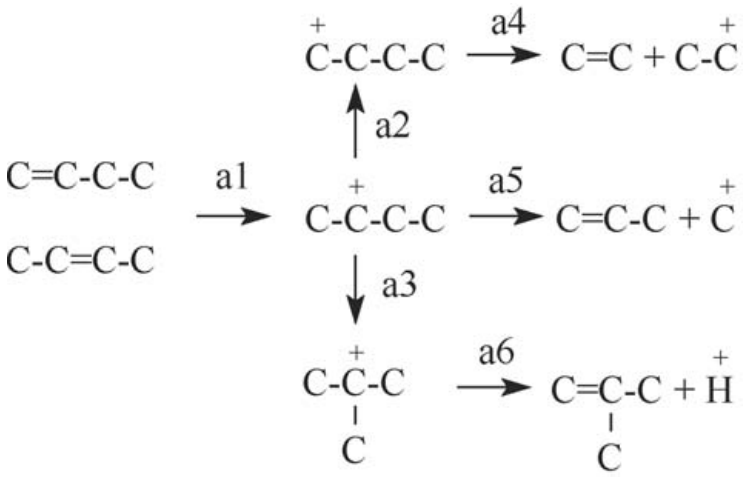

Figure 2.10: Overview of reactions involved in the monomolecular cracking mechanism[60]

Since n-butene can quite easily dimerize to an octyl carbenium ion, catalytic pyrolysis of butene is believed to proceed via a so called **bimolecular cracking mechanism**. N-butene first forms C_8 dimers, which can subsequently crack. In most cases, isomerization will be required to produce new species. It can also be expected that the most stable isomers will be formed preferentially. Therefore, primary carbenium ions are highly unlikely to occur as cracking reactants. Reaction path b4 (Figure 2.9) is less prominent because most reactions involve formation of a less stable ethyl carbenium ion.[45,60]

As stated previously, the pore structure of the molecular sieves is also extremely important with respect to the reaction rate. First, the dimerization reaction in this mechanism can suffer from diffusion limitations. Secondly, the formation of highly branched C_8 iso-

mers was found to be difficult in the H-ZSM-5 channels. This could explain why a lower yield for isobutene than for propene is experimentally observed.[60,62] Isobutene is mainly produced from the cracking of carbenium ions with a high branching degree, which theoretically should have been fast due to the involvement of tertiary cations. It was asserted that cracking path b2 is a possible, but not the most important route. Reaction path b5 is also predicted to be difficult in the relatively narrow pores of ZSM-5.[21,60,62,63]

According to this mechanism, a lot of propene, i-butene, pentenes and aromatics will be formed, which is in agreement with experimental predictions. The main reactions in the network are claimed to be step b1 and step b3. A second experimental proof is the observed initial temperature rise in a reactor at low reaction temperatures due to the exothermic polymerization reactions before a temperature drop indicates the start of endothermic cracking reactions.[60,62,63] Several experimental studies support this bimolecular kinetic mechanism.[45,59,62,64,65]

2.2.2 Overview of ab initio studies

Over the last years, many first principle studies have been performed on the subject of alkene cracking. The most relevant findings of these studies are reviewed in this paragraph. First, the dimerization is briefly addressed, followed by the cracking itself. Computational resources have increased drastically the last decade, therefore the studies are ordered from older to more recent, from a lower to a higher level of theory.

The first step in the bimolecular cracking mechanism is the dimerization. Svelle et al. studied this step for a few olefinic compounds (ethene, propene, 1-butene and trans-2-butene) in a DFT study on a 4T cluster. Two mechanisms were proposed. First, a stepwise mechanism that involves protonation and alkoxide formation as a first step and C-C bond formation with another adsorbed olefin as a second step. Secondly, a concerted mechanism that involves simultaneous protonation and electrophilic attack of a second olefin. The activation barrier of the concerted reaction lies in between the first and second barrier of the stepwise mechanism. Although trans-2-butene is expected to be more reactive than 1-butene based on the inductive effect, the contrary was proven to be true, which can possibly be attributed to steric limitations in the transition state. It should also be noted that the stepwise mechanism may be kinetically favored since this does not require two physisorbed butene molecules to meet at the acidic center. However, the lack of an accurate description of the stability of the intermediates is a serious limitation of the small cluster model, such that a clear distinction between both mechanisms could not be made.[66]

Vandichel et al. studied dimerization reactions in the context of the MTO process with the ONIOM (B3LYP:MNDO) method on a 46T-cluster model of H-ZSM-5.[67] Their

results indicated that the stepwise mechanism is generally preferred over the concerted mechanism if the zeolite environment is taken into account. Three oligomerization routes were discussed. The pathway with the highest reaction rate was found to be the dimerization of propene and a 1-propoxide molecule, yielding the 2-hexyl carbenium ion, closely followed by the oligomerization of an ethene molecule and an ethoxide to 1-butene. 4-methyl-1-pentene as a dimer from iso-propoxide and propene was estimated to be a less viable route. Although, the latter appeared to be the most interesting pathway for cracking (reverse reaction), confirming that branched alkenes are more prone towards cracking than linear alkenes.[21,67]

Guo et al. proposed a mechanism for cracking of a homologous series C_4 - C_{10} α - olefins, in which a secondary carbenium ion cracks into propylene and a primary alkoxide. 3T-cluster calculations have indicated that the intrinsic barrier is independent of olefin chain length and that the difference in apparent barriers can be mainly attributed to Van der Waals interactions. Furthermore, the intermediate species were found to be mainly short-living carbocations.[68]

Hay et al. performed a theoretical investigation for cracking of 1-pentene and 4-methyl-1-pentene on a 3T cluster model. The former scission produces propene (see Figure 2.11) and an ethyl cation, while the latter produces propene and a 2-propyl cation. Based on gas phase calculations one would expect that the cracking of 4-Me-1-pentene is less endothermic due to the formation of a secondary ion. In a 3T cluster however, assuming immediate transformation of the ion into an alkoxide, the endothermicity of both reactions is comparable due to the little structural difference between an ethoxide and a 2-propoxide. The activation energy for cracking of the branched alkene is somewhat lower, indicating that kinetic rather than thermodynamic factors play a significant role in the cracking chemistry.[69]

More recent studies however have proven the necessity to account for the entire zeolite environment to include pore confinement effects. Mazar et al. investigated β scission for a series of C_6^+ and C_8^+ isomers by performing periodic PBE-D calculations on a H-ZSM-5 periodic unit cell. Reactant and product states were optimized starting from a well oriented alkoxide conformer structure as initial guess. T-butoxide species were found to rearrange to a t-butyl structure in their optimized state, indicating that this alkoxide is energetically not the most favorable product despite the t-butoxide formation can occur via an endothermic, relatively high activated, reaction. Alkoxide adsorption and desorption were also established to be fast compared to cracking. Cracking reactions are classified in different categories according to the involvement of primary, secondary or tertiary ions as reactant or product state. From each class a representative reaction is studied. The activation energies of these reaction classes are represented in a bar plot, shown in Figure 2.12. Note that some transitions occur more than once since

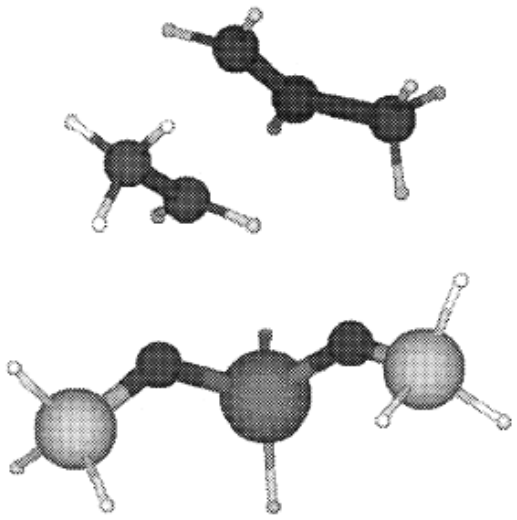

Figure 2.11: 3T cluster model transition state for 1-pentene cracking [69]

free carbenium ions can rearrange to rotational conformers with access to a β scission pathway with lower activation energy. [70]

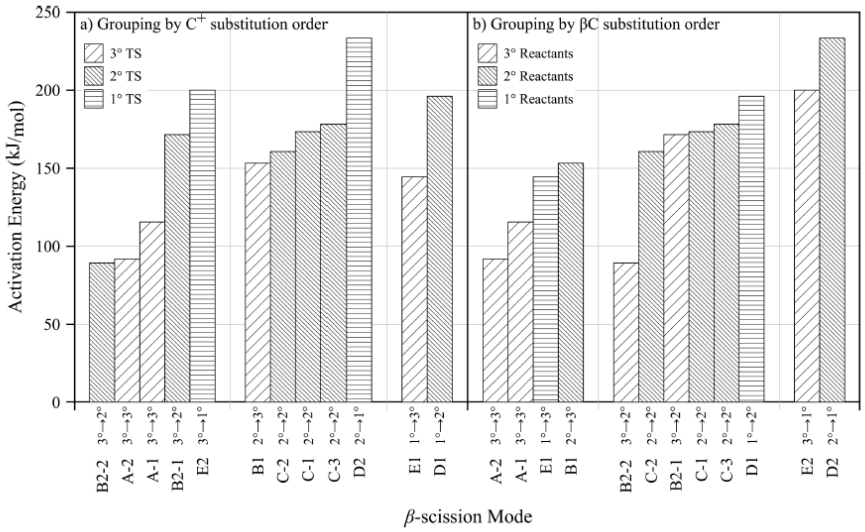

Figure 2.12: Activation energies for the β - scission of C_6 and C_8 isomers, grouped by nature of the reactant (a) and by nature of the transition state / product state (b), obtained with theoretical PBE-D periodic calculations on a H-ZSM-5 unit cell. [70]

Some general trends can be observed by considering the stability of reactant and transition state species (see Figure 2.12). The activation energies are primarily determined by the degree of substitution of the β - C atom of the carbocation like transition state, which will receive the positive charge in the product state. The trend for the same class of reactants is an increasing barrier height following the order tertiary $<$ secondary $<$ primary transition state carbocations. To a minor extent, the activation barrier is also determined by the degree of substitution of the reactant positively charged carbon. The trend for the same class of products is an increasing barrier height according to tertiary $<$ secondary $<$ primary reactant carbocations. This is equivalent to saying that a linear correlation exists between the change in charge, required for the reactant β - C transforming to its transition state, and the activation energy.
Finally, note that species with a different number of carbon atoms have been compared, which may result in a somewhat distorted view. For example, the secondary - tertiary transition is higher activated than the primary - tertiary transition. The former is bulkier, will have higher dispersion interactions and will therefore be stronger chemisorbed resulting in a higher barrier.[70]

Sun et al. carried out ONIOM (MP2//B3LYP:UFF) calculations on 1-butene cracking over a 38T:140T H-ZSM-5 cluster model. Only a central 5T cluster around the reaction center was allowed to relax, while the remaining cluster atoms were held fixed at their atomic positions. Four possible catalytic reactions were investigated of which two involve a primary butoxide and two a secondary butoxide as intermediate species, as shown in Figure 2.13. The butene complex physisorption energies consist of a constant QM contribution and a zeolite dependent MM contribution. The pore size thus mainly influences long range interactions.[55]

Pathway I and III are examples of monomolecular cracking. Quite high barriers were found for these cracking cracking reactions (158 kJ/mol and 156 kJ/mol respectively). The scission in pathway III is also more endothermic and the products are less stable, which can be attributed to the unstable methyl ion (methoxide) formed. The exothermic dimerization is a factor in favor of the bimolecular cracking paths as shown from cycle II and IV. The activation energies are comparable (111 kJ/mol and 117 kJ/mol respectively) and are mainly determined by QM contributions, only including the short range interactions. This is not surprising since the nature of the involved reactant and product state are comparable. Interesting to note is that the cracking reactions - with alkoxides as reacant and product state - are exothermic for bimolecular cracking and endothermic for monomolecular cracking.[55]

Lesthaeghe et al. studied cracking of n-butene, n-pentene and n-hexene within the context of the alkene route in the MTO process.[21] They modeled β - scission on a secondary carbenium ion with the ONIOM (B3LYP:MNDO) method on a 8T:46T H-

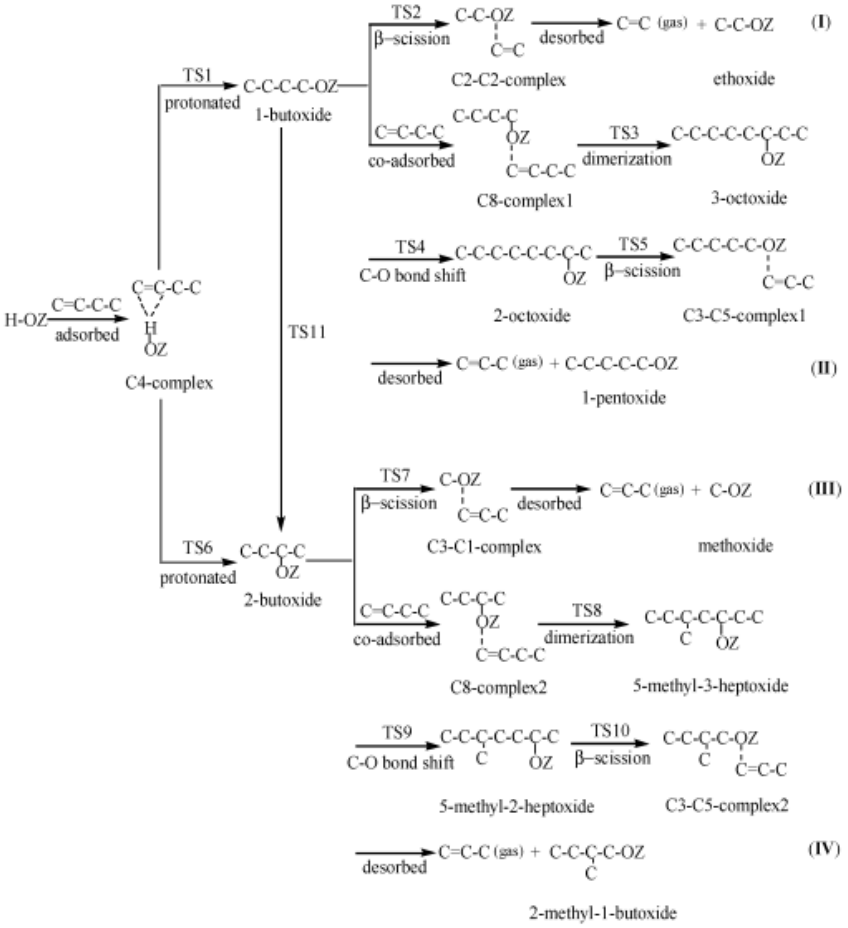

Figure 2.13: Different pathways of cracking 1-butene to propene and ethene [55]

ZSM-5 cluster. Cracking of alkenes to form propene was found to have higher rates than cracking to form ethene, in agreement with experimental observations. [42] Nonetheless, formation of ethene cannot be excluded. The barriers for cracking of a butyl cation were higher than those of a pentyl cation, whereas the lowest barriers were found for cracking hexyl cations. [21]

Guo et al. studied cracking of 1-hexene on a 10T:88T cluster model with the ONIOM (B3LYP:UFF) method, in which only the 10T cluster was allowed to relax. The hexene molecule is larger than the ZSM-5 pore size, implying that interaction with the framework and possible steric hindrance are important factors determining the adsorption properties of hexene. A stable 2-hexyl cation was found as reactive intermediate which will rapidly undergo scission to propylene and 1-propoxide with a barrier of 66 kJ/mol. [71]

2.3 Influence of zeolite catalyst properties

2.3.1 Influence of micropore structure

As for all hydrocarbon reactions, the product distribution is a function of the catalytic performance and this is strongly influenced by the zeolite pore structure and acidity. Zhu et al. investigated experimentally the influence of structural effects on the cracking of C_4 alkenes.[72] Figure 2.14 shows the resulting conversions and product distributions.

From high to low acid site density, the studied catalysts follow the order: H-Y > H-ZSM-35 ≈ H-SAPO-34 > H-β ≈ H-MCM-22 ≈ H-ZSM-5 > H-ZSM-23 > H-ZSM-22. Except for H-ZSM-22, all zeolites possess a large number of strong acid sites. The zeolite pore diameters decrease in the following order: H-Y > H-β > H-MCM-22 > H-ZSM-5 > H-ZSM-22 > H-ZSM-23 ≈ H-ZSM-35 > H-SAPO-34.

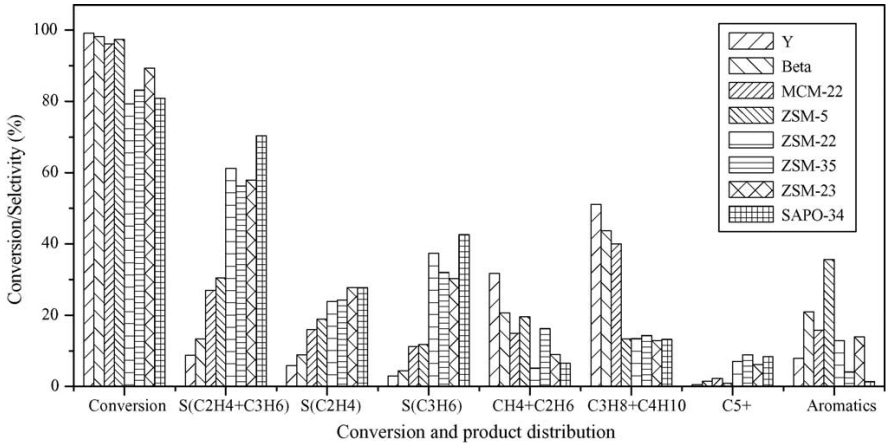

Figure 2.14: Comparison of conversion and product selectivities between different zeolites from experimental results of cracking a 1-butene feed in a continuous plug flow reactor at 620°C, 1 bar, 2 minutes TOS and a WHSV of 3.5 h^{-1} [72]

Two effects play an important role in the conversion of butene. First, the mass transfer of reactants and products is highly enhanced by the empty channel space and thus by the pore diameter. Secondly, the butene transformation itself is influenced by the acid site density. This explains the high conversion for H-Y and H-β.[58] Although the acid site density is quite high in H-SAPO-34 and H-ZSM-35, their small pore channels suppress the diffusion of reacting species, resulting in a lower conversion.[58,64,72]

Both ethene and propene selectivity shows an inversely proportional relationship with the pore diameter. Ethene formation was suggested to occur via the energetically less favorable monomolecular cracking pathway. Although this is probably not the most prominent reaction, interaction of the adsorbed carbenium ions with the zeolite wall can

provide stabilization of these species.[58,64] Propene formation, which was suggested to occur via bimolecular cracking, was found to depend on the extent of hydrogen transfer reaction to alkenes suppression, resulting in the formation of bulky intermediates. Small pore zeolites are hence more shape selective towards light olefins.[58,64,72]

Methane and ethane are primarily produced via protolytic cracking of alkanes and dealkylation of aromatics. These reactions are positively influenced by an increasing acid site density with the exception of the H-SAPO-34 catalyst, where the formation of the aromatic precursors is suppressed by the small pore channels. Aromatics can therefore only be formed at the external surface of the zeolite. In contrast, the particular structure of H-ZSM-5 zeolite has a high tendency for aromatics formation.[73]

Compared to alkane cracking, the alkene/alkane product ratio for alkene cracking is higher. This is reasonable since alkene cracking theoretically yields two alkene products, while alkane cracking yields both an alkane and an alkene product.[64]

The large pore zeolites with supercages (H-Y and H-MCM-22) enhance condensed aromatics and coke formation which adsorb strongly at the acid sites and hereby deactivate the catalyst in a short time scale. H-SAPO-34 shows rather poor stability and the fast deactivation may be a result of cokes blocking the small one dimensional 8 ring pores. From all the tested zeolites, H-ZSM-5 shows the best stability. Due to its particular three dimensional structure condensed ring aromatics formation is to a large extent prevented. In addition, pore blocking is more difficult due to the interconnected channel structure.[53,54]

H-ZSM-5 is one of the best catalysts for alkene cracking processes due to its optimal balance between stability against coke formation, its activity for butene conversion and its relatively low selectivity for light alkanes (ethane, propane,...).

2.3.2 Influence of acid site density

Zhu et al. investigated experimentally the influence of SiO_2/Al_2O_3 ratios - a higher SiO_2/Al_2O_3 ratio is equivalent to a lower acid site density - on a H-ZSM-5 catalyst. The resulting conversion and product selectivities are shown in Figure 2.15. For lower acidity catalysts, the cracking severity will be lower. Butene conversion will thus show a decreasing trend with increasing SiO_2/Al_2O_3 ratios.[74]

Ethene and propene selectivity and yield show a proportional relationship with increasing SiO_2/Al_2O_3 ratios for high acid density catalysts.[72] In contrast, for low acid density zeolites, ethene selectivity will remain approximately constant, while propene selectivity keeps increasing. Lower acidity implies a less important contribution of hydrogen transfer reactions to propene, resulting in a higher selectivity of propene. This effect is less

present for ethene, explaining the constant ethene selectivity versus the growing propene selectivity at low acidity catalysts.[72,74,75]

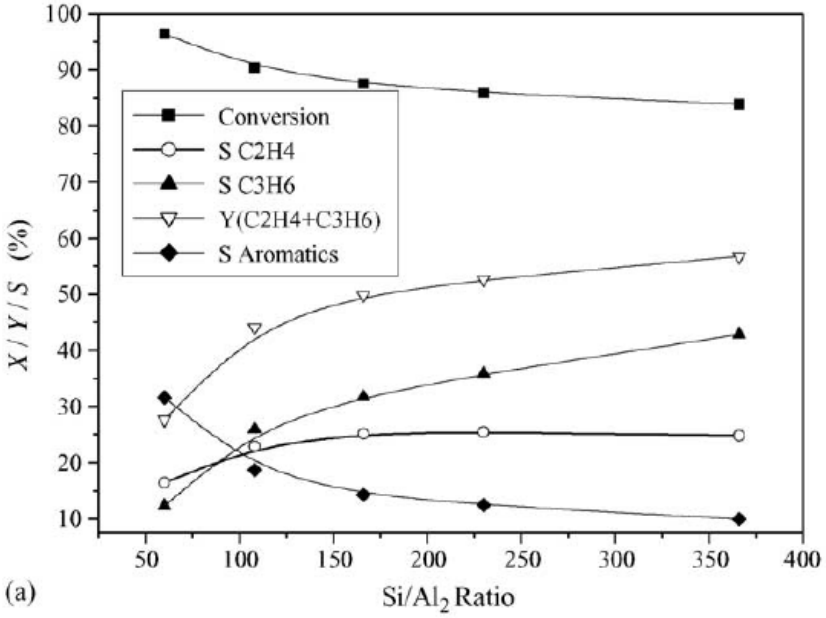

Figure 2.15: Comparison of conversion and product selectivities between zeolites with different Si/Al_2 ratios from experimental results of cracking a 1-butene feed in a continuous plug flow reactor at 620°C, 1 bar, 2 minutes TOS and a WHSV of 3.5 h^{-1} [72]

As explained above, the formation of condensed aromatics is the key factor in the catalyst stability against coke formation. The selectivity for aromatics strongly depends on the acid site strength and shows a decreasing course with SiO_2/Al_2O_3 ratios as expected. At lower acidities, alkene aromatization will be suppressed.[72,75] Catalyst stability is thus effectively prolonged with higher SiO_2/Al_2O_3 ratios due to the lower aromatics selectivity. For a SiO_2/Al_2O_3 ratio below 100 the conversion diminishes drastically as a function of time on stream. Especially the strong acid sites deactivate rapidly. For a SiO_2/Al_2O_3 ratio above 350 on the other hand, a very small decrease in conversion as a function of time on stream is observed.[72,74,76]

The above considerations explain why industrially, high SiO_2/Al_2O_3 ratio zeolites are often selected for olefin cracking.[27,28] These observations are in contrast with alkane cracking, where relative stronger acidity is required to activate the alkane species. In alkene cracking, on the other hand, this would enhance secondary reactions of alkenes, resulting in an overall lower olefin yield.[72,75]

2.4 On the nature of the intermediate species: carbenium ion vs. alkoxide

To date, experimental spectroscopic observations (NMR, IR,...)[77–79] have failed to prove the existence of "free", non-cyclic, non-aromatic carbenium ions in the zeolite pores. Therefore, theoretical calculations can assist in the elucidation of the intermediate nature. At first sight, alkoxides bound to the aluminosilicate framework, appear to be stable intermediate species, i.e., a local minimum on the potential energy surface. However, if a mechanism is assumed that will first form surface alkoxide species which then decompose, it will probably have a too high activation energy.[46]

In the case of branching isomerizations of linear butenes, Corma et al. proposed a mechanism that involves formation of secondary alkoxy intermediates, which rearrange to branched primary alkoxy species that subsequently can desorb to form isobutene.[41] Gas-phase calculations indicated that the 2-butyl, t-butyl and primary isobutyl species do not exist as free carbenium ions on the zeolite surface. Other studies confirmed that no "free" carbenium ions, but alkoxides occur as intermediates, formed over a carbocation like transition state.[37,80,81] However, some recent studies support the existence of the t-butyl carbenium ion as intermediate[79,82–84] and even the existence of protonated olefins longer than propene in general.[71,85]

Carbenium ion stability

Two main effects play a crucial role in carbenium ion stability: stabilizing electronic effects and destabilizing steric constraints. On the one hand, the electronic effects consist of both the long range electrostatic attraction between the positively charged carbon and the negatively charged framework oxygen as well as the van der Waals interactions of the hydrocarbon with the zeolite framework. For H-ZSM-5, Fang et al. concluded that no stable isopropyl ion can be found on the PES due to a high accessibility of the C^+ atom by the zeolite oxygen, resulting in immediate alkoxide formation.[86]

On the other hand, Fang et al. also pointed out that tertiary carbenium ions like the t-butyl cation did appear to occur inside the H-ZSM-5 pores.[86] Compared to the large pore catalysts H-Y and H-β, the t-butyl ion was more stable in H-ZSM-5 due to enhanced interaction with the zeolite wall in the smaller channels, while alkoxide formation is prohibited by the steric repulsion. Larger ionic fragments were found to show enhanced stability in H-Y compared to H-ZSM-5 due to reduced steric constraints. Rozanska et al. established that in small pore zeolites, like H-ZSM-22, the stabilities of the t-butoxide and the t-butyl cation were nearly the same.[84] The degree of stabilization will therefore depend also for a large extent on the accommodation and the fitting of the hydrocarbons in the zeolite cages.[84,86]

Adsorption enthalpy of alkoxides

Experimental heat of adsorptions are difficult to measure due to the relatively fast oligomerization reactions. Nieminen et al. performed a theoretical study on the stability of intermediate alkoxide species (C_2 - C_5 species) on a H-FER zeolite.[87] The resulting alkoxide chemisorption energies are depicted in Figure 2.16. Several effects can be observed. First, an increasing carbon number was clearly shown to lower chemisorption energies for homologous alkoxides (e.g. the series 2-propyl, 2-butyl, 2-pentyl). The bulkiness also plays a crucial role, for example isobutyl and 2-methylbutyl alkoxides are less stable than their linear analogues. Thirdly, the general stability order of the alkoxides is primary > secondary > tertiary. This can be explained by steric effects, tertiary alkoxide species are more compact and show more repulsion between the methyl groups and the zeolite wall. Therefore, tertiary alkoxides, like t-butyl, are not very stable compared to secondary (2-butyl) or primary ones (1-butyl) and will try to rearrange.[39,87,88]

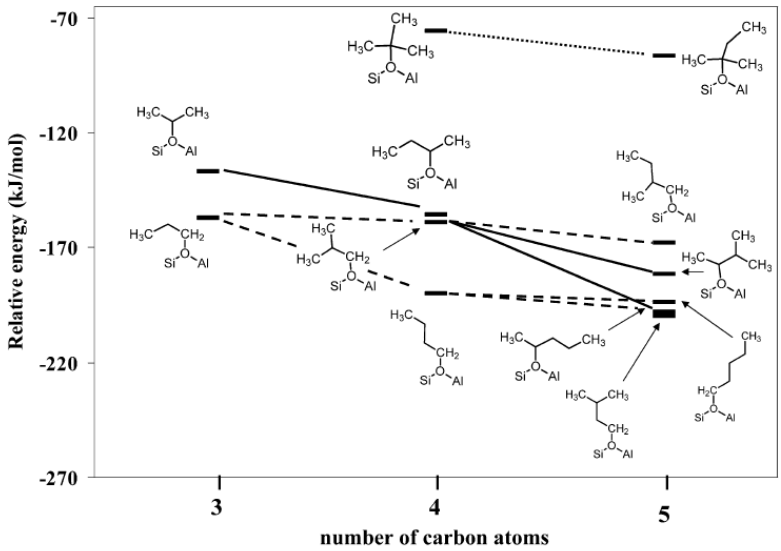

Figure 2.16: Energies of different alkoxide species as a function of carbon number, relative to the energy of the corresponding alkene and zeolite at infinite distance of each other.[87]

The alkoxide stability order is however in sharp contrast with what is expected from the relative carbenium ion stability order. A mechanistic view can explain this apparent contradiction. Assuming the chemisorption as a sequence of two reactions: alkene protonation forming a carbenium ion (Reaction 2.1) followed by alkoxide formation by forming the C-O bond with the negatively charge zeolite.(Reaction 2.2). The heat of

adsorption is then given by summing over both reactions.

$$H{-}Z + C_nH_{2n} \longrightarrow Z^- + C_nH^+_{2n+1} \tag{2.1}$$

$$Z{-}O^- + C_nH^+_{2n+1} \longrightarrow H_{2n+1}C_nO{-}Z \tag{2.2}$$

The contribution of Reaction 2.1 depends on the carbenium ion stability. The contribution of Reaction 2.2 includes the energy of bond formation and van der Waals interaction with the zeolite wall. The formation of secondary alkoxides is exothermic and higher carbon numbers will yield higher Van der Waals contributions.[80,87] Tertiary alkoxides are more compact and their formation is endothermic because the steric hindrance (repulsion between methyl groups, both mutual and with zeolite wall) does not allow the formation of an optimal C-O bond distance (Reaction 2.2). These effects overcompensate the larger stability for tertiary carbenium ion (Reaction 2.1). The formation of secondary (and primary) alkoxides is less hindered, resulting in an exothermic reaction, thus explaining the reverse order.[80,87] Analogous results can be expected for a ZSM-5 zeolite.

In a similar study, Nguyen et al. established that t-butyl minima do exist on H-ZSM-5 in contrast with H-FAU in which the large pores allow t-butoxide formation without steric hindrance.[89] Despite the sterical repulsion in the rather narrow pore structure of H-ZSM-5, the t-butoxide chemisorption strength was found to be unexpectedly high, which was attributed to the high flexibility of the framework in the vicinity of the acid site. In agreement with Nieminen et al.[87], the primary isobutoxide was found to show a higher chemisorption strength compared to t-butoxide.[89]

Free energy of alkoxides

Adsorption entropies are negative values and entropy losses corresponding to chemisorption are much higher than for physisorption due to the relatively little degrees of freedom of an 'immobile' alkoxy species. Combined with their relative high instability, formation of tertiary alkoxides is therefore particularly difficult for some active sites or even impossible, especially at higher temperatures.[90] Entropy should be taken into account when considering the nature of the intermediates.

Tuma et al. studied the protonation of isobutene in H-FER.[91] The considered intermediates and free energy curves are shown in Figure 2.17. They have shown that due to the negative entropy contribution, from temperatures of 120K or higher, the t-butyl carbenium ion becomes more stable than the isobutoxide or t-butoxide and that the t-butyl carbenium should exist as a local minimum on the PES for isobutene cracking, although it has not yet been experimentally confirmed.[90,91]

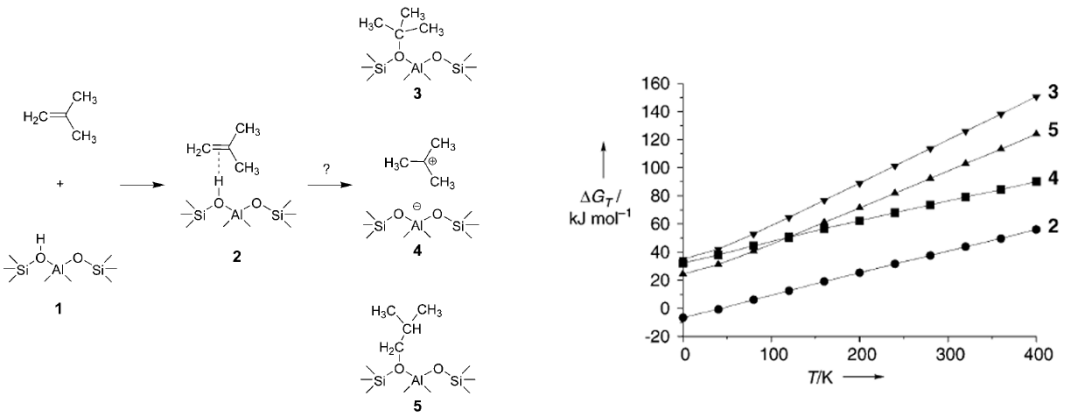

Figure 2.17: Left: Possible reactions of isobutene protonation; Right: Gibbs free energy plot of different isobutene species as a function of temperature [91]

Nguyen et al. also studied the entropic contributions in isobutene protonation on H-ZSM-5. Entropy losses were found to be inversely correlated with pore size and are larger for the t-butoxide than the isobutoxide. [89] Free energy evaluations have shown that due to their high entropy loss, chemisorption complexes are significantly less stable than physisorption complexes. The stability of the t-butyl carbocation appears to be less stable than a physisorbed complex, while still more stable than the corresponding alkoxide species from temperatures of 500 K or higher, an effect that can be entirely attributed to the loss of entropy. At industrial relevant temperatures, tertiary carbenium ions are therefore much more likely to play a role as stable intermediate than tertiary alkoxides. Assuming a tertiary or primary carbocation like transition structure, protonation of isobutene forming a t-butyl cation can be expected to have a lower barrier than forming an isobutyl cation. [38,89]

Corma et al. studied the protonation of isobutene on a different catalyst, H-MOR. [92] The transformation of t-butyl carbenium ion in t-butoxide in H-MOR is an endothermic reaction with a quite high activation energy. Hence, at first instance a "free" carbenium ion will be created. [92] However, depending on the type of active site (T-atom and environment), formation of the alkoxide may or may not be stabilizing. The alkoxide stability depends on the AlOSi angle in the complex, implying that this can be influenced by the synthesis conditions. [92]

An important consideration on the above studies is whether the harmonic oscillator approximation remains valid when the entropy contribution to the Gibbs free energy becomes dominant (cfr. Section 3.2.2).

Conclusion

Knowledge of the nature of the process intermediates is very important to attain complete insight into the reaction mechanism and eventually to predict product formation rates and product selectivities. If alkoxide species play a role in the cracking process, this may influence the relative activation energies. The more stable the alkoxides (primary or secondary) occurring along the reaction path, the more the activation barrier will increase compared to the gas phase reactants. [87]

The issue of the nature of the reacting species remains until now unresolved and is seriously complicating the comparison of QM calculated activation barriers with experimental recorded data. Especially information on secondary carbenium ions is still lacking. To solve the mystery of the existence of short living intermediates, molecular dynamics simulations (see Chapter 5) or quantumchemical spectroscopy techniques can be particularly useful.

Chapter 3

Zeolite models and quantum chemical methods

Different methods can be employed to describe a system quantum chemically. All these techniques are based on solving the Schrödinger equation, describing the electronic many-body problem. In this chapter, an overview of the applied methods in this thesis is given. First, an overview of the methods for modeling the zeolite environment is covered. Secondly, static modeling of zeolite catalyzed reactions and the derivation of kinetics from transition state theory is discussed. Finally, the principles of the molecular dynamics simulation are elucidated.

3.1 Modeling the zeolite environment

The H-ZSM-5 zeolite framework is composed of pentasil units linked together by oxygen bridges, resulting in a complex 3D structure of interconnected sinusoidal and straight channels. It is computationally expensive to describe the entire H-ZSM-5 unit cell (289 atoms) with ab initio methods. However, when studying reactions at the Brønsted acid site, it is necessary to account for the interactions with the zeolite framework since this influences the chemical kinetics to a large extent as discussed in Paragraph 2.2.2. Therefore, several models were developed to account for the nanoporous environment.

3.1.1 Small Cluster model

The small cluster method is the most simple method to simulate a zeolite. The chemically interesting part, the active center of the framework, typically consisting of 5 or more T-atoms is simply cut out from the zeolitic environment. This structure is chemically unstable due to broken Si-O bonds, therefore the dangling bonds are saturated with

hydrogen atoms. The zeolite is in fact replaced by a small gas phase molecule.

The main advantage of such small models is the significant reduction of the computational effort, hence a high level of theory can be used to study the reaction (DFT or post-HF calculations).[93,94] However, small cluster models have important limitations. First, the small cluster is independent of the zeolite type, which is an important disadvantage since activity is typically catalyst dependent. Secondly, adsorbed hydrocarbons are essentially stabilized by Van der Waals interactions. Naturally, these dispersion interactions cannot be correctly included in small cluster models.[93,94] Today, this approach is merely interesting to find initial geometries for transition state configurations, which can be transposed to more complex models.

3.1.2 Hybrid techniques

Next to quantum chemical techniques, classical force field techniques can be used to describe the structure and relaxation of the zeolite framework or diffusion of species in the cage structure. Unfortunately, these computationally inexpensive methods are useless for the description of bond breaking and formation. A thorough investigation of chemical reactions requires ab initio solving of the electronic many body problem. For extended systems DFT methods ar nowadays frequently used. However, these methods typically give a poor description of long range interactions between the guest molecules and the zeolite, which are determining the adsorption strength in the zeolite. Also, a model with a large number of atoms is computationally demanding.

An optimum between these two techniques was found in the hybrid methods or so-called QM/MM methods (Quantum mechanical / Molecular mechanical method). The system is divided in subsystems to obtain an efficient use of computational time.[94] The guest molecules and the active site with a few neighboring T-atoms are described quantum chemically (DFT methods). This part of the cluster is called the high level (HL) region. The surrounding part of the cluster is described by molecular mechanics (Force field methods) or semi-emprical methods. This part is called the low level (LL) region.[93,95]

An example of these hybrid methods is ONIOM (**O**ur-own-**N**-layered **I**ntegrated molecular **O**rbital + molecular **M**echanics). This method is implemented in the Gaussian09 software package.[96] The real system is divided in an Inner Region (I) and Outer Region (O). For H-ZSM-5, the inner shell consists of an 8T-atom cluster and the guest molecules, embedded in a larger 46T-atom cluster. The dangling bonds are saturated with infinite mass hydrogen atoms, allowing the cluster to relax within a fixed frame. Both regions are connected via a number of oxygen atoms, forming together the Link Region (L). These link atoms are replaced by hydrogen atoms in the Inner Region where they serve as saturating atoms.[93,97]

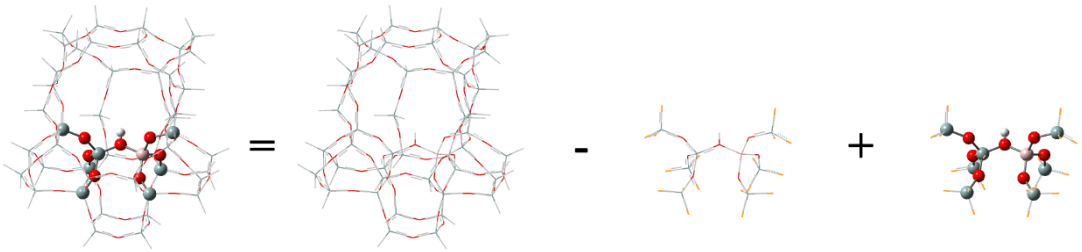

Figure 3.1: 2-layer ZSM-5 ONIOM model (8T:46T) [94]

The two-layer ONIOM energy is calculated as

$$E_{ONIOM} = E^{LL}_{(I+O)} - E^{LL}_{(I+L)} + E^{HL}_{(I+L)}$$

This is illustrated for the 46T-cluster in Figure 3.1. Depending on the choice for the low and high level of theory, several combinations are possible. Comparison with experimental data is essential to find the ideal combination. [94] Note that also QM/QM methods are an option in which the outer shell is described by a low level of theory quantum mechanical method or semi-empirical method.

3.1.3 Periodic calculations

A third possibility to accurately incorporate the zeolite framework is through periodic calculations. The complete unit cell of the framework is periodically extended in 3 dimensions. The interaction of the guest molecule with this periodic unit cell is entirely described by quantum chemical techniques. This method is typically computationally demanding, but achievable with the current computational power. Some important industrial zeolites are composed of large unit cells, in particular H-ZSM-5 with 289 atoms per unit cell (see Figure 3.2). Today, periodic calculations on theses systems are feasible although they used to be only possible for small unit cell zeolites, e.g. CHA. While small unit cells seem interesting from a computational point of view, the results may suffer from artificial self interactions if the guest molecules in each repeated unit cell are located too close to each other. [94] In that case, more computationally demanding super-cells, consisting of multiple unit cells, can be used as repetitive unit. Periodic models are especially suited for molecular dynamics simulations (see Chapter 5). [93]

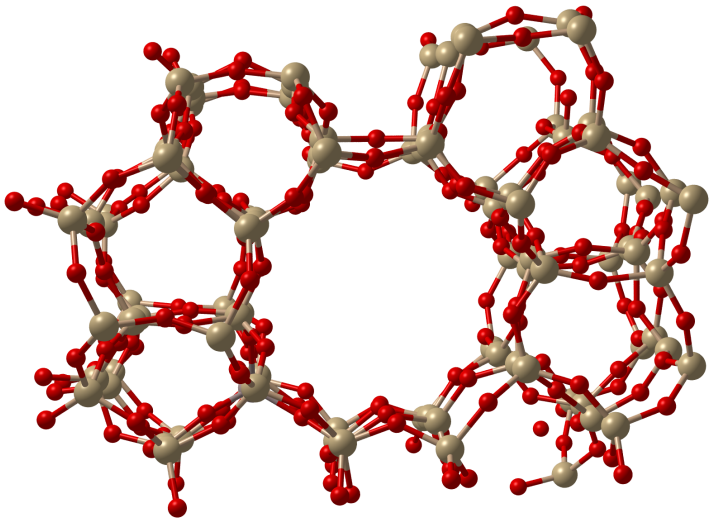

Figure 3.2: Straight channel view of a ZSM-5 periodic unit cell

3.2 Static calculations

3.2.1 Level of theory

In static calculations, the electronic many-body problem is solved, i.e., finding appropriate solutions for the Schrödinger equation. Within the Born Oppenheimer approximation, the wave functions ψ_{el} as a function of the electron and nuclei coordinates are found by solving the time-independent electronic Schrödinger equation with $\hat{\mathrm{H}}_{el}$, the electronic Hamiltonian, ψ_{el} the electronic wave function, x_i (i = 1,...,N) the coordinates of the N electrons, X_j (j = 1,...,P) the coordinates of the P nuclei and U, the potential energy.[93]

$$\hat{\mathrm{H}}_{el}\ \psi_{el}\ (\{x_i\}^N, \{X_j\}^P)\ =\ U\ (\{x_i\}^N, \{X_j\}^P)\ \psi_{el}\ (\{x_i\}^N, \{X_j\}^P)$$

The static calculations in this thesis are performed with the Gaussian09 software package.[96] For geometry optimizations, 2-layer ONIOM calculations are performed on a 46T-cluster model to account for the zeolitic environment of H-ZSM-5. The high level, a central 8T-cluster and guest molecules, around the active site is described by the well-known B3LYP hybrid DFT-functional.[98,99] The low level is described by the semi-empirical pm3 method.[100]

This approach yields accurate results regarding the geometries, however the calculated ONIOM energy values are less reliable. Therefore, a single point energy calculation at

high level is performed on the entire 46T-cluster for each geometry with the $\omega B97X-D$ functional.[101]

A classical problem of most DFT functionals is their lack of a correct description of long range electron correlations that are responsible for van der Waals forces. These interactions play a crucial role in the confined space of the zeolite cages. To account for this shortcoming, a dispersion-corrected functional is applied. Grimme first introduced this dispersion correction by means of a semi-empirical add-on energy term, which does not has a significant impact on the computational expense.[102] The $\omega B97X-D$ functional used in this study is a long-range corrected hybrid functional that includes a Grimme-type dispersion term. All parameters in the functional are self-consistently optimized, is used.[101]

The basis set used for the DFT calculations is *6-31+g(d,p)*, including polarization functions to account for deformation of atomic orbitals and diffuse functions to improve the description of long-range interactions. Since proton transfer plays a crucial role in heterogeneous catalyzed reactions, polarization functions are also included for hydrogen atoms.[93,94]

3.2.2 Chemical kinetics

One of the main objectives of this work is studying chemical kinetics of zeolite-catalyzed reactions. For the determination of kinetics, it is presumed that all reactants and products are already adsorbed on the active site of the catalyst. These species will therefore undergo unimolecular reactions. The reaction rate $r[mol\ m^{-3}\ s^{-1}]$ is then given by

$$r(T) = k(T)c_R$$

with $c_R[mol\ m^{-3}]$, the reactant concentration and $k(T)[s^{-1}]$, the temperature dependent rate coefficient. This dependency is given by the Arrhenius relation

$$k(T) = Ae^{-\frac{E_a}{RT}}$$

in which $A\ [s^{-1}]$ is the pre-exponential factor, $E_a\ [kJ\ mol^{-1}]$ is the activation energy and R is the universal gas constant. The exponential part of the expression describes which fraction of the reactants possess sufficient energy to cross the barrier and can therefore also be associated with reaction enthalpy. The influence of different possible orientations on the chance of a successful barrier crossing is expressed in the pre-exponential factor and can therefore be associated with the reaction entropy. For many reactions, the pre-exponential factor and activation energy can assumed to be constant in a small temperature interval.

To determine the parameters in the Arrhenius equation on a microscopic basis, transition state theory (TST) is used.[103,104] In an ideal situation, a calculation of all possible reaction paths along the potential energy surface (PES) is required and the reaction rate can then be found by averaging. This approach is however computationally too demanding. In TST, macroscopic quantities are linked to microscopic rate parameters.

The main hypothesis of TST is the existence of a critical point (the transition state or activated complex), which is part of every successful reaction path. Furthermore this point is a saddle point on the potential energy surface: a minimum in all degrees of freedom except for the reaction coordinate, where it is a maximum. A molecule that possesses sufficient energy to proceed via the transition state from one local minimum to another, follows the reaction path on the PES with the lowest energy between those minima. This path is the so-called *intrinsic reaction coordinate* (IRC). The minima are also called the reactant and the product valley. Furthermore, some other assumptions are made:[103,104]

- Once the critical point is reached in the direction of the products P, the system will immediately proceed to the product valley and will not return to the reactant state. Reaction paths that have multiple crossings of the saddle point are not considered.
- The reactants R are supposed to be in quasi-equilibrium both mutually and with the activated complex ‡, even when the system is in non-equilibrium.

$$R \rightleftarrows \ddagger \longrightarrow P$$

- The motion that corresponds to the reaction coordinate, i.e. bringing the system over the activation barrier, can be separated from all other motions.
- The motion corresponding to the reaction coordinate can be described in a classical way. Quantum effects like tunneling through the potential barrier are not allowed.

In the TST approximation it is sufficient to localize three points on the potential energy surface: two minima corresponding to the reactant and product state and the transition state saddle point connecting those two.

The forward rate coefficient for a unimolecular reaction is given by

$$k(T) = \frac{k_B T}{h} \frac{q_\ddagger(T)}{q_R(T)} e^{-\frac{\Delta E_0^\ddagger}{k_B T}}$$

with k_B representing the Boltzmann constant, h the Planck constant, $q_\ddagger$ and q_R the temperature-dependent molecular partition functions of the transition state with respect to V=0, i.e. without the motion along the reaction coordinate, and the reactant

respectively, and $\Delta E_0^{\ddagger}$ the energy barrier at 0 K, including zero-point energy (ZPE) corrections.[93]

$$\Delta E_0^{\ddagger} = E_0^{\ddagger} - E_0^R$$

The energies and partition functions follow from the ab initio calculations. For the evaluation of the molecular partition functions, the electronic, translational, vibrational and rotational motions are decoupled.[93]

$$q(T) = q_{el} \cdot q_{trans} \cdot q_{rot} \cdot q_{vib}$$

The Born-Oppenheimer approximation assumes that the molecules are in the ground state of the PES. Therefore, the electronic part of the partition function is given by

$$q_{el} = e^{-\frac{E_0}{k_B T}}$$

For gas phase molecules, the translational partition function is given by the one of the ideal gas.

$$q_{trans} = \left(\frac{2\pi m k_B T}{h^2}\right)^{3/2} \text{(per unit volume)}$$

The second contribution, the rotational partition function, represents the external rotation of the global, rigid molecule. As a global approximation, the partition function of a non-linear polyatomic molecule is typically applied.

$$q_{rot} = \frac{\pi^{\frac{1}{2}}}{\sigma}\left(\frac{8\pi^2 k_B T}{h^2}\right)^{\frac{3}{2}} (I_X I_Y I_Z)^{\frac{1}{2}}$$

Herein represents σ the symmetry number of the molecule, describing the number of non-distinguishable rotational configurations of the molecule and I_X, I_Y and I_Z are the three moments of inertia of the rigid molecule.

The vibrational partition functions are determined within the harmonic oscillator approximation. Herein the total vibrational motion of a non-linear molecule with N atoms is expressed as a sum of $3N-6$ independent harmonic oscillators corresponding with each of the normal modes of the molecule. Therefore, the vibrational partition function can be factorized.

$$q_{vib} = \prod_{i=1}^{3N-6} q_{vib,i} = \prod_{i=1}^{3N-6} \frac{1}{1 - e^{-\frac{h\nu_i}{k_B T}}}$$

with $q_{vib,i}$ the vibrational partition function corresponding to the normal mode with frequency ν_i. Note that the ZPE contribution is excluded from the vibrational partition function since this part is included in the molecular energy difference $\Delta E_0^{\ddagger}$. One

disadvantage is that the harmonic oscillator approximation prohibits considering different rotational motions of the molecule. Partial Hessian vibrational analysis (PHVA) is applied on the zeolite model with fixed hydrogens, hence no global translations and rotations are considered. Certain low vibration modes may correspond to translations or rotations of the guest molecule. In a more accurate approach, these modes can be replaced, e.g., by the 1D-hindered rotor.

A vibrational analysis is performed on each geometry - at the same level of theory as for geometry optimizations - to check if the reactant product state exhibit only real frequencies (local minima) and if the transition state structure exhibits exactly one imaginary frequency (saddle point). Furthermore, this imaginary frequency should correspond to the translative motion of bond breaking / bond formation of the reaction.[93,94]

If the logarithm of the microscopic calculated rate coefficient is plotted versus the reciprocal of the temperature, linear regression allows determining the Arrhenius parameters A and E_a within the considered temperature range. Finally, note that these parameters are usually highly correlated, rendering independent determination of their numerical values difficult. Therefore, it is often a more reliable approach to compare directly rate coefficient values.[93]

Kinetic parameters are determined with the TAMkin software module[105] at 833 K or 560 °C, which is an industrial relevant temperature for catalytic alkene cracking.

3.2.3 IRC method

Modeling a reaction starts with the search for the geometry of the activated complex. An appropriate initial guess is required to start a geometry optimization. Identifying the transition state geometry is the most complex task of static cluster calculations. It is therefore desirable to perform a first geometry optimization with fixed breaking/forming bond length, allowing the remainder of the cluster and guest molecules to relax. Once this preliminary saddle point has been found, a second optimization of this point, in which the entire cluster is allowed to relax, will lead more easily to the real transition state.

Due to the complexity of the potential energy surface, it may be unclear from only the motion along the imaginary frequency what the minimum of the reactant and product will be. Therefore, in this thesis, the IRC method[107,108] is applied to localize the reactant and product complexes corresponding to each transition state. This algorithm follows the intrinsic reaction coordinate in both directions, starting from the transition state structure. A sufficient number of steps is required to ensure the correct geometries will be found. The IRC method can also be used to get a clear view if the transition state corresponds indeed to the desired reaction. The resulting states down the hill can

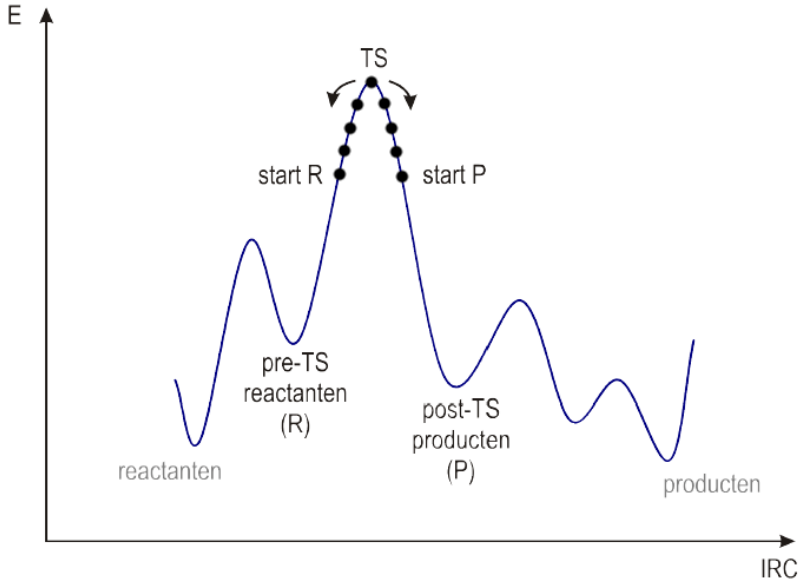

Figure 3.3: Scheme of the IRC approach on an energy diagram [106]

be used as initial guesses to start the reactant or product optimization, as shown in Figure 3.3. [107,108]

3.3 Molecular dynamics simulations

Ab initio molecular dynamics (MD) simulations are a powerful technique to study the dynamic or statistical properties of a molecular system. MD can be used to study for example the interactions of species with the zeolitic environment or to evaluate the temperature effect on adsorption. This technique samples a trajectory of a system on the potential energy surface (see Figure 3.4), which has the advantage that there are no conformational limitations as encountered in the harmonic oscillator approximation in the case of static calculations. Entropy contributions due to different conformers are inherently accounted for (i.e. conformational entropy). [93]

3.3.1 The algorithm

Newton's law of motion

The simulations in this work make use of the time-dependent Born Oppenheimer approximation. In the Born Oppenheimer approximation the system remains in the electronic ground state. The motion of the atomic nuclei is described by the classical Newton's

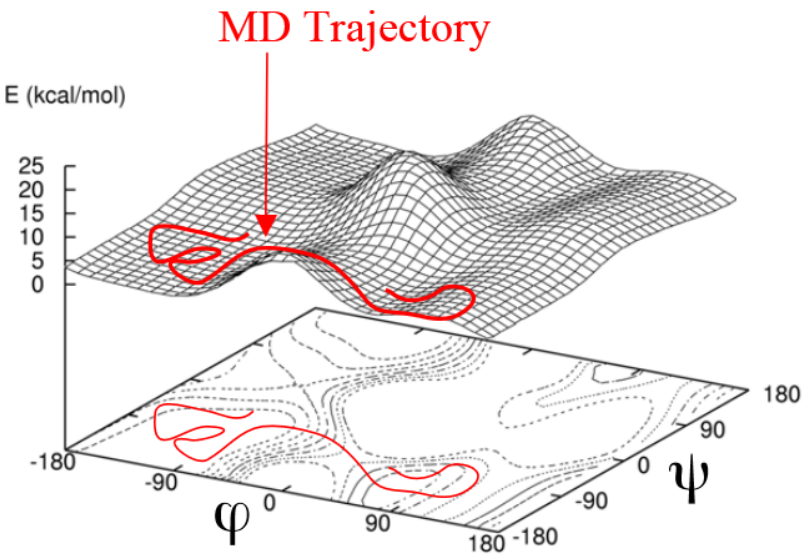

Figure 3.4: Example of an MD sampling trajectory (NVE) on a 2-dimensional potential energy surface of dialanine [109]

law of motion. [110]

$$m_i \ddot{\bar{R}}_i = \bar{F}_i = -\bar{\nabla}_i V$$

If the forces on all atoms at their current position are known, the atoms can be propagated. The new velocity vector $\bar{v}$ and position vector $\bar{R}$ are calculated for each atom. During the sampling period, Δt, the forces are assumed to be constant. In the first step, the initialization, the atomic coordinates are read from an input geometry and random initial velocities (a fictitious kinetic energy) are assigned to each atom. The equations of motion are then numerically integrated, for example by the simple Verlet algorithm. [110]

$$\bar{\boldsymbol{R}}\ (t+\Delta t) = \bar{\boldsymbol{R}}(t) + \bar{\boldsymbol{v}}(t)\Delta t\ + \frac{1}{2}\frac{\bar{\boldsymbol{F}}(t)}{M}\Delta t^2$$

$$\bar{\boldsymbol{v}}\ (t+\Delta t) = \bar{\boldsymbol{v}}(t) + \frac{1}{2}\frac{\bar{\boldsymbol{F}}(t) + \bar{\boldsymbol{F}}(t+\Delta t)}{M}\Delta t$$

This is an efficient algorithm because no derivatives of the force vector are required. Note that the last term of the right hand side corresponds to the acceleration vector. This is a deterministic approach since the state of the system at any future time can be predicted from its current state. By considering second order derivatives in the laws of motion, the system is allowed to move upwards on the potential energy surface, i.e., the system may leave a local minimum. However, the added fictitious energy is small and the probability for a certain state transition is determined by the Boltzmann factor

$e^{-\frac{\Delta E}{k_B T}}$. It is therefore almost impossible to sample states with an activation barrier higher than the thermal energy, $k_B T$ (2.5 kJ/mol at room temperature).[93,109] This is also shown in Figure 3.4, representing a NVE molecular dynamics trajectory on a 2-dimensional fictitious potential energy surface as a function of two dihedral angles within a dialanine molecule. As indicated, two minima separated by a barrier of about 5 kJ/mol are sampled, while a transition over the 20 kJ/mol barrier is difficult to observe in a short simulation time.

The choice for the integration time step Δt depends on the time scale of the particular motion that needs to be investigated. When studying reactions or the behavior of guest molecules inside a zeolite, the chemical vibration is of interest, which has a time scale in the order of 1 fs or smaller at higher temperatures. For the simulations performed in this thesis, at a temperature of 560 °C, a sampling period of 0.5 fs is therefore a justifiable choice. If a time step is chosen too large, the energy will no longer be conserved by the numerical scheme. As a consequence of this small sampling period, only simulation times of 50 - 100 ps are computationally achievable within ab initio MD.[110]

The electronic many-body problem

The atomic forces at each time step are computed by taking the space derivative of the potential energy. Newton's law of motion is coupled with the electronic many-body problem equations since the potential energy is also dependent on the electronic wave function. The latter varies each time step since the atomic positions will change. Therefore at each time step the Schrödinger equation needs to be solved with ab initio DFT methods. The Hellmann - Feynman theorem states that once the electronic wave functions are known the forces working on the atomic nuclei can be determined, which is the most intensive step. Solving the many-body problem each time step from 'scratch' would require too much computational effort. To overcome this problem, it is assumed that the wave functions will not vary significantly between two consecutive time steps. The wave function of the previous time step is thus chosen as initial estimate for the next step, effectively reducing computational time. Only in the first step, the electronic wave function is calculated starting from the individual atomic orbitals.[93,110]

Typically, periodic boundary conditions are used in MD simulations. Sufficiently large unit cells are required to avoid an influence of the periodic boundary conditions on the dynamic behavior. Because of the periodicity, a plane wave basis set can be used. However, if all electrons are explicitly taken into account, a large number of basis functions would be required for the plane wave expansion to describe the complicated, rapid variations of the core states. As the core electrons vary almost independently from their atomic environment, and only the valence electrons contribute significantly to the interatomic interactions, pseudo-potentials are used to reduce the number of required plane

wave functions. With pseudo-potentials, the valence states are replaced by pseudo-wave functions with a smooth course at the core, but outside cocurrent with the atomic wave function.[93]

Ab initio MD simulations in this thesis are performed with the CP2K software package[111] on a periodic ZSM-5 unit cell. As DFT functional the revPBE functional[112] with additional Grimme D3 dispersion corrections is selected.[113][114] A DZVP basis set with GTH pseudopotentials[114], a combination of Gaussian and plane wave (GPW)[115] basis sets (with a cutoff energy of 320 Ry for the plane wave basis set), is used.

3.3.2 Statistical mechanics

A molecular system is characterized by the atomic coordinates $\bar{R}_i$ and momenta $\bar{p}_i$, varying with time. A collection of points in the phase space, which all satisfy the conditions of a specified thermodynamic state is called an ensemble. MD simulations sample a sequence of states, corresponding with varying atomic positions (different conformers) and varying momenta, which are all belonging to the same ensemble. Different ensembles can be considered.

The microcanonical ensemble

The microcanonical ensemble or NVE ensemble comprises states with a conserved number of atoms (N), volume (V) and energy (E). This corresponds to an adiabatic process without heat exchange. Sampling in a microcanonical ensemble is obtained by integration of the Newtonian dynamics. In this theory, the total energy is conserved, therefore a MD trajectory simply simulates potential and kinetic energy exchanges. However, NVE ensembles will rarely represent realistic experimental conditions, for example an isothermal system.[116,117] Secondly, energy dissipation will in reality occur very fast among the other atoms. Due to the relatively small number of atoms, this can result in an unexpected temperature increase.[109]

The canonical ensemble

In a canonical ensemble or NVT ensemble, the number of atoms (N), the volume (V) and the temperature (T) are conserved. Boltzmann showed that the canonical probability of a microstate i is given by

$$P_i = \frac{1}{Q} e^{-\frac{E_i}{k_B T}}$$

with Q, the partition function

$$Q = \sum_i e^{-\frac{E_i}{k_B T}}$$

Due to velocity fluctuations of the atoms, the instantaneous temperature will vary and the law of conservation of energy will be violated. One possibility to correct for these thermal calculations is a velocity rescaling based on the physical principle $T \sim v^2$. Although it is easy to implement, this algorithm is not time reversible and does not correspond to a real ensemble. The Nosé Hoover algorithm [118] introduces a new dynamic variable, representing a heat bath or thermostat, which is an infinite energy reservoir at constant temperature. The system can exchange energy with the heat bath, so different energy states are possible. The introduced variable will alter the kinetic energy and thus the Hamiltonian of the system. The total energy of system and heat bath (thermostat) is conserved. [116,117]

Next to the deterministic Nosé Hoover thermostat, stochastic thermostats exist, which introduce an additional stochastic factor, for example the 'Canonical Sampling through Velocity Rescaling' (CSVR) thermostat, [119] which is used in this thesis to perform the simulations.

Despite the instantaneous temperature fluctuations, the ensemble-averaged temperature will be constant. The ergodic hypothesis states that the ensemble averages are equal to the time average over the sufficiently long simulation. The validity of this hypothesis depends on the quality of the sampling. [109]

$$\frac{1}{Q}\sum_i T(R_i,p_i)e^{-\frac{E_i}{k_BT}} = \frac{1}{t_{sim}}\sum_{t=0}^{t=t_{sim}} T(t)$$

The isothermal - isobaric ensemble

In the isothermal - isobaric ensemble or NPT ensemble, the number of atoms (N), the pressure (P) and the temperature (T) are conserved. In this case, the volume of the system is no longer constant. Next to a thermostat to exchange heat with, an analogous barostat or volume bath is required. The system can exchange volume (and thus work) with the infinite volume bath, so that the time averaged pressure will be constant. The instantaneous pressures will of course show fluctuations. Again, the total energy (system + baths) is conserved. [116,117]

In this study, MD simulations are performed within the NPT ensemble at a pressure of 1 bar and a temperature of 560 °C. The quite large species in the zeolite can result in a volume change of the flexible cage, so a constant volume is not guaranteed.

Chapter 4

Static cluster calculations on mono- and bimolecular butene cracking

In this chapter, different reaction pathways from the suggested kinetic model for butene cracking (see paragraph 2.2.1) are investigated using static calculations. Both monomolecular and bimolecular cracking routes are investigated.

Static calculations using the ONIOM scheme have been performed on a 46T-cluster of a H-ZSM-5 zeolite. The active site is placed at the intersection of the straight and sinusoidal channel. This allows to explicitly take shape selectivity and interactions with the framework into account. Free energy barriers, reaction enthalpies and entropies are evaluated at 560 °C. Kinetic coefficients are fitted to an Arrhenius relationship in the temperature interval 460 °C - 660 °C. The different β - scissions will be compared and the limitations of a finite cluster model will be discussed.

4.1 Monomolecular butene cracking

As stated in section 2.2.1, a single butene molecule can undergo so-called monomolecular cracking. Once a butene molecule has diffused to an acid site, it may get protonated. The most stable carbocation that can be formed is a 2-butyl cation. However, the only viable cracking reaction is a β - scission of the unstable primary 1-butyl cation ${}^{+}C_1 - C_2 - C_3 - C_4$ (Figure 4.1).

The products of this β - scission are ethylene and an ethyl carbenium ion. The latter is a very unstable species and will therefore stabilize by covalently binding to an AlO^-

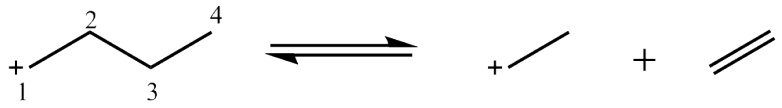

Figure 4.1: β - scission of 1-butyl carbenium ion

group of the framework, i.e., by forming an ethoxide. All reaction states (reactants, intermediates, transition states, products) are shown in Figure 4.2.

The modeled transition state of this reaction resembles the product state: the carbon atoms in the ethylene fragment, $C_1 - C_2$, are sp^2 hybridized and the $C_1 - C_2$ bond distance is 1.35 Å, while a usual $C = C$ double bond distance amounts to 1.33 Å.[120,121] The breaking bond $C_2 - C_3$ distance is 2.50 Å. However, the ethoxide has not yet been formed with an $O - C_3$ distance of 2.29 Å, which reduces to 1.49 Å in the product state. A formal primary ethyl cation is hence formed in the transition state. The small ethene fragment shows little interaction with the zeolite wall and tends to diffuse away from the active site during product optimization.

As indicated in Figure 4.1, a primary butyl carbenium ion is expected to be found as reactant for this β - scission, resulting from the IRC calculation. However, this is not the case: during the geometry optimization, spontaneous isomerization of the 1-butyl cation to a more stable 2-butyl cation takes place. A seemingly barrierless proton shift occurs over a corner protonated cyclopropyl intermediate (see Figure 4.2(d)). In contrast with the 2-butyl cation, the 1-butyl cation is not a minimum on the potential energy surface and will spontaneously rearrange. Vandichel et al. found for the same reaction on a 5T-cluster model,[67] that a protonated methylcyclopropane species was formed as reactant state. With inclusion of electrostatic and van der Waals interactions with the extended surrounding framework, this is no longer the most stable configuration.

Although the 2-butyl cation does exist as a local minimum on the PES, the question remains if this species is sufficiently stable to remain long living in its protonated state in the zeolite cage. The inductive and hyperconjugative stabilization increases with increasing carbon numbers, such that from a certain carbon number the protonated alkenes can be expected to survive 'freely' in the zeolitic environment. Nicholas et al. proposed as empirical rule that carbenium ions can be long-lived stable species if the proton affinity is larger than 870 kJ/mol.[56,122] However, the proton affinity of 2-butene (747 kJ/mol) falls below this threshold.[123] Based on our calculations, it seems therefore plausible that a 2-butyl carbenium will bind to an active site (a framework oxygen), forming a 2-butoxide species. 1-butoxide formation can be ruled out due to the fast isomerization of 1-butyl carbenium ions to 2-butyl carbenium ions. Alkoxide species

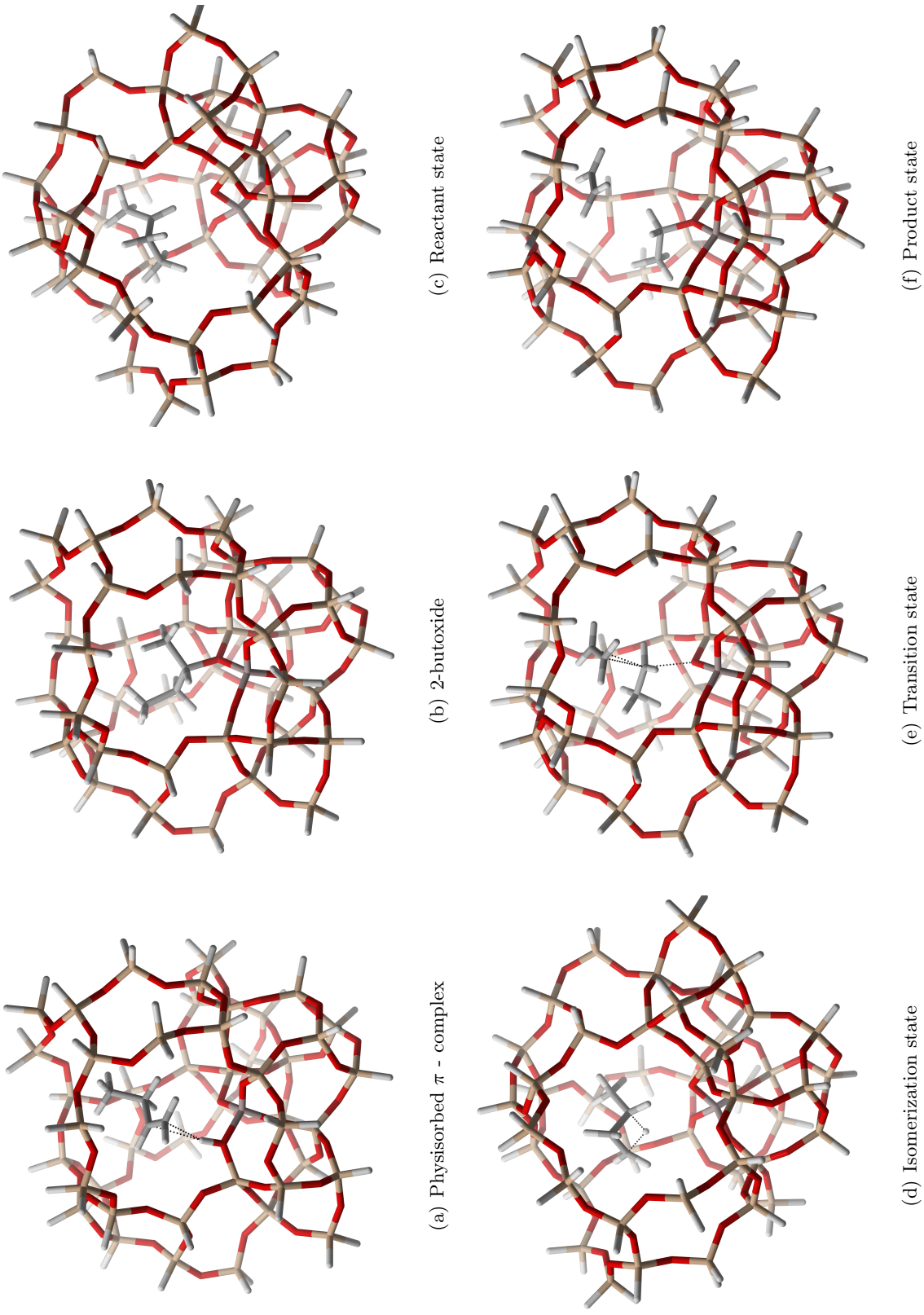

Figure 4.2: Optimized geometries for the monomolecular cracking of 1-butene

are stable products, which implies that cracking would involve an activated desorption step before scission. The activation barrier would thus be rather high, reducing the probability of cracking via this route.[46]

Another important issue is which reactant level should be used to compare computed with experimental activation barriers: either the chemisorbed 2-butoxide or the physisorbed π-complex. Figure 4.3 is an electronic and free energy diagram of the modeled cracking reaction, including the energy levels of the physisorbed π - complex and the chemisorbed 2-butoxide with the gas phase 46T-cluster and 1-butene molecule at an infinite distance as reference state. The chemical structures of the shown states are depicted in Figure 4.4.
In the remainder of the chapter, reactions with a cation as reactant state will be referred to as intrinsic reactions. The corresponding electronic and free energy barriers are abbreviated by $G^{\ddagger}_{int}$ and $\Delta E^{\ddagger}_{int}$ respectively. For the reaction with the chemisorbed alkoxide as reactant state, the electronic and free energy barriers are denoted as $\Delta G^{\ddagger}_{chem}$ and $\Delta E^{\ddagger}_{chem}$ respectively. For the reaction with the physisorbed π - complex as reactant state, the electronic and free energy barriers are denoted as $\Delta G^{\ddagger}_{phys}$ and $\Delta E^{\ddagger}_{phys}$ respectively. Table 4.1 and Table 4.2 summarize the kinetic and thermodynamic parameters at 560 °C, including reaction barriers from the three different reactant states.

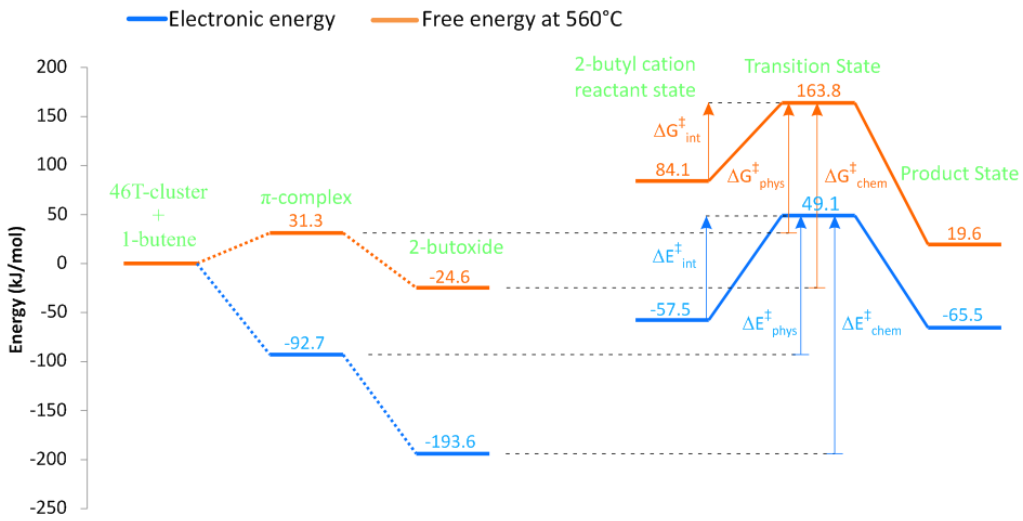

Figure 4.3: Monomolecular cracking (free) energy diagram with indication of the different states along the reaction path: π - complex, 2-butoxide, 2-butyl cation and the gas phase 46T-cluster and 1-butene at infinite distance as reference level

First, in Figure 4.3, it can be seen from the electronic energies that the physisorbed π - complex is more stable than the gas phase reference level, i.e., without any interaction

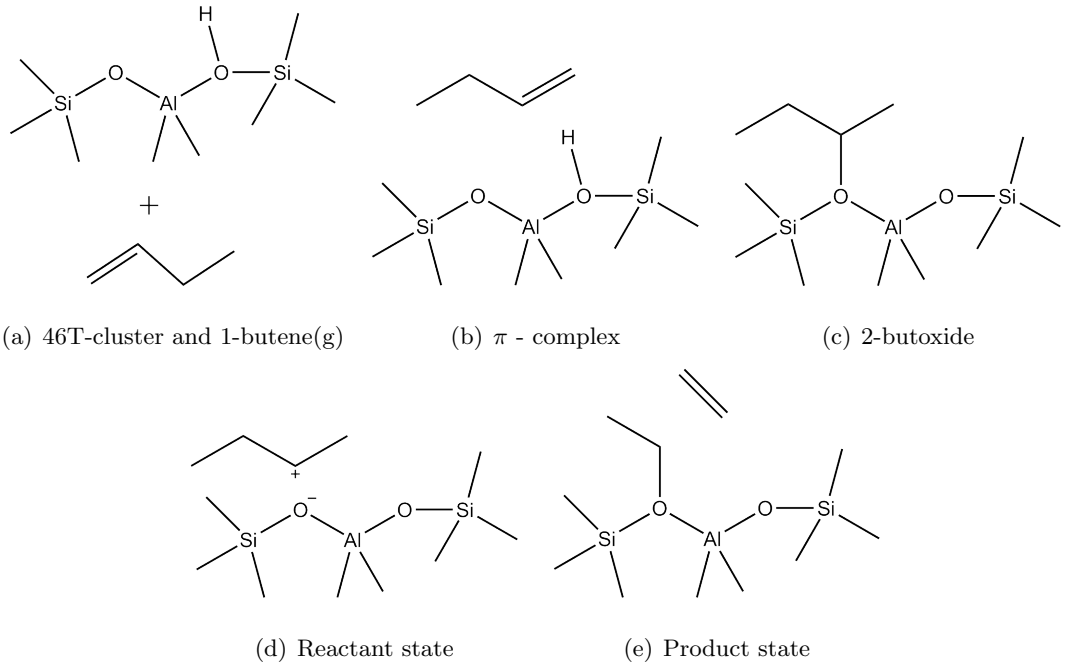

(a) 46T-cluster and 1-butene(g) (b) π - complex (c) 2-butoxide

(d) Reactant state (e) Product state

Figure 4.4: Chemical structures of the different states along the reaction pathway

($\Delta E_{phys} = -92.7 kJ/mol$). The chemisorbed 2-butoxide is in turn about 100.9 kJ/mol more stable than the π - complex and 193.6 kJ/mol more stable than the gas phase reference level. The covalent bond interaction is clearly much stronger than the π - complex interaction. The cationic reactant state is 35.2 kJ/mol less stable compared to the physisorbed 1-butene state. The stabilization of the 'free' 2-butyl cation state is determined by a major contribution of electrostatic interactions with the framework (next to dispersion interactions), while for the π - complex Van der Waals contributions next to the interaction of the H 1s orbital and the π - electrons are dominant. Apparently, the adsorptive stabilization will have a serious influence on reaction energies.

Secondly, it is necessary to evaluate free energy differences next to the enthalpic contributions. At 560 °C, entropy effects are indispensable for the evaluation of reaction barriers. Due to the loss of entropy with the formation of a covalent $C-O$ bond in the chemisorption state, 2-butoxide becomes at 560 °C about 169.0 kJ/mol less stable, compared to the electronic energy. The 2-butyl cation state is also 141.6 kJ/mol less stable, compared to the electronic energy. The difference between free energy and electronic energy is less pronounced (114.7 kJ/mol) since the transition state has a larger number of degrees of freedom than the reactant.

The intrinsic activation energy, $\Delta E^{\ddagger}_{int}$ is 106.6 kJ/mol, a high barrier, which is in agreement with the unstable transition state involving a primary ethyl cation. However, the $\Delta E^{\ddagger}_{phys}$ barrier has a much higher value of 141.8 kJ/mol. Due to the high stability of

Table 4.1: Kinetic parameters at 833 K for the monomolecular cracking of 1-butene with three different reactant levels: the 2-butyl cation (int), the 2-butoxide (chem) and the π - complex (phys) (LOT : ωB97X-D/6-31+g(d,p)//ONIOM(B3LYP/6-31+g(d,p):pm3))

Reference	A s^{-1}	E_a $kJ\ mol^{-1}$	k_{fwd} (833 K) s^{-1}
int	8.7 10^{14}	106.8	1.7 10^{8}
chem	2.4 10^{16}	238.4	2.6 10^{1}
phys	5.6 10^{13}	112.2	1.6 10^{4}

a butoxide species, $\Delta E^{\ddagger}_{chem}$ is 242.7 kJ/mol, which is very high. Sun et al. found a $\Delta E^{\ddagger}_{chem}$ barrier of 158.2 kJ/mol for monomolecular butene cracking on a 140T cluster at 0 K.[55] However, they considered a 1-butoxide species as reactant. Our calculations have shown that a 2-butoxide species is approximately 90 kJ/mol more stable than a 1-butoxide species ($\Delta E_{phys} = -103.8 kJ/mol$). The results of Sun et al. are thus in good agreement with the calculations in this thesis.

The intrinsic free energy barrier amounts to 79.7 kJ/mol. The barrier $\Delta G^{\ddagger}_{chem}$ however remains rather high (188.5 kJ/mol), while the barrier $\Delta G^{\ddagger}_{phys}$ (132.5 kJ/mol) has a less pronounced temperature dependency due to the low entropy difference between the physisorbed reactant and the transition state: The π - complex has still a relatively high degree of freedom, resulting in a low entropy barrier increase towards the transition state.

The positive $\Delta H_{r,chem}$ and $\Delta H_{r,phys}$ values indicate that the reaction is indeed endothermic, which meets the expectations for a cracking reaction. Due to the high reaction entropies, the effect is more nuanced in the free energy. The free energy of the reaction with 2-butoxide as reactant is strongly positive (44.2 kJ/mol), while for the reaction with the π - complex as reactant is slightly negative (-11.8 kJ/mol). The intrinsic reaction, however, is slightly (-5.4 kJ/mol) exothermic, which should not be surprising since the product state involves only covalently bonded stable molecules, while the reactant state consists of charged species. The free energy of the intrinsic reaction is aigan more pronounced (-64.6 kJ/mol) due to the high reaction entropy.

Based on previous positive validation of the 46T-cluster model for description of methylation reactions with small adsorbates,[124] it is expected that for similar reactions like

Table 4.2: Thermodynamic parameters (enthalpic, entropic and free energy barriers, enthalpy, entropy and free energy of reaction) at 833 K for the monomolecular cracking of 1-butene with three different reactant levels: the 2-butyl cation (int), the 2-butoxide (chem) and the π - complex (phys) (LOT : ωB97X-D/6-31+g(d,p)//ONIOM(B3LYP/6-31+g(d,p):pm3))

Reference	$\Delta H^{\ddagger}$ $kJ\ mol^{-1}$	$\Delta S^{\ddagger}$ $J\ mol^{-1}K^{-1}$	$\Delta G^{\ddagger}$ $kJ\ mol^{-1}$	ΔH_r $kJ\ mol^{-1}$	ΔS_r $J\ mol^{-1}K^{-1}$	ΔG_r $kJ\ mol^{-1}$
int	99.9	24.3	79.7	-5.4	71.1	-64.6
chem	231.6	51.8	188.5	126.3	98.6	44.2
phys	133.6	1.4	132.5	28.3	48.2	- 11.8

monomolecular butene cracking, this model can also yield quite reliable estimations of the kinetic parameters. Assuming 'free' butyl carbenium ions exist within the zeolite pores at 560 °C, the monomolecular cracking reaction is a feasible, but highly activated pathway.

4.2 Bimolecular butene cracking

A more interesting route for butene cracking is the bimolecular or dimerization cracking mechanism. Generally speaking, the rate of β-scissions is proportional to the number of possible isomers, which is a reflection of the increasing stability trend with increasing carbon number.[45,86] Only a limited number of octyl carbenium ions can be formed from reaction of 1-butene with a 1-butyl or 2-butyl cation with a small number of cracking possibilities. However, it can be safely assumed that the time scale for isomerization is much smaller than the time scale for cracking, hence a variety of octyl cation isomers will be present in the zeolite pores.[12,52,60,62,63] Some of these isomers can undergo β - scission to two C_4 species, varying from 1-butene over cis- or trans-2-butene, to isobutene. This type of cracking reactions is in fact the reverse of butene dimerization. Other octyl cation isomers can undergo β - scission to either a C_3 and C_5 or C_2 and C_6 species. The latter are less prominent reactions in the kinetic mechanism[60,125–127] and will therefore not be investigated in this work. These types of cracking reactions yield the desired ethene and propene products, next to pentenes and hexenes, which are prone to secondary reactions.

Writing down all possible octyl carbenium ion isomers and the accompanying cracking reactions is an elaborate task and it would be too time intensive to study all possibilities.

To reduce the number of reactions to be investigated, the various steps are divided into different classes according to the type of cationic transition between reactant and product: primary - primary, primary - secondary, primary - tertiary, secondary - primary, secondary - secondary, secondary - tertiary, tertiary - primary, tertiary - secondary and tertiary - tertiary. From each class one or more representative reactions are selected. Due to their unstable nature, primary cations will rarely occur in the catalyst pores - and if they do, rearrangement to a more stable configuration is almost instantaneous (e.g. the 1-butyl cation in Section 4.1), hence eliminating the importance of primary transition reactions.[45] Therefore, only secondary and tertiary reactant transitions are considered in this section.

There are 20 possible reactions yielding C_4 alkenes (12 with exclusion of primary carbenium ion reactants). There are 34 plausible reactions yielding C_3 and C_5 alkenes of which 13 reactions can be eliminated due to the presence of primary carbenium ions. For cracking reactions yielding C_2 and C_6 40 possibilities can be written down of which 23 reactions can be omitted due to the presence of primary cations.

For all reactions only the intrinsic kinetics have been determined and compared. This implies that the reactant state is a conformer ready to undergo scission, which is not necessarily the most stable configuration for the carbenium ion itself. The scission products, besides alkenes, are relatively small carbenium ions, which are typically short-lived species, that will tend to rearrange to stable alkoxide species.

Tertiary - primary transitions

Two reactions from the tertiary - primary transition type have been investigated: Cracking of a 2-methyl-2-heptyl carbenium ion yielding isobutene and a 1-butyl cation (Reaction (4.1)) and cracking of a 3-methyl-3-heptyl carbenium ion yielding 2-methyl-1-butene and a 1-propyl cation (Reaction (4.2)). The optimized geometries of both reactions are very similar, therefore only geometric aspects for Reaction (4.1) will be discussed below.

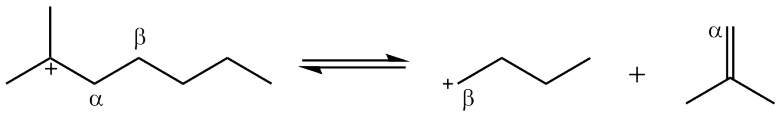

(4.1)

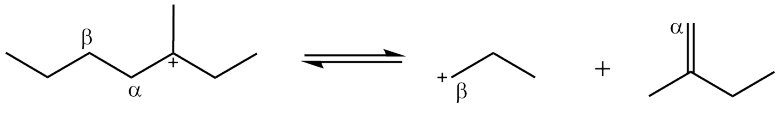

(4.2)

In the transition state, the scission of the α C - β C bond has started and the alkene fragment and cation fragment begin to form. Both the α C in the isobutene fragment

and the β C in the 1-butyl fragment are already reorganized to the sp^2 hybridization state. The positive charge has shifted to the β C atom, such that a primary cation is formed. It is coordinated towards the π-bond of the alkene fragment. This is the case for all transition states in this chapter. For this particular reaction, it is coordinated towards the exterior C atom of the double bond with a distance of 2.49 Å and towards the interior C atom with a distance of 2.84 Å. It is also stabilized by coordination with the framework oxygen at a distance of 2.25 Å(see Figure 4.5).

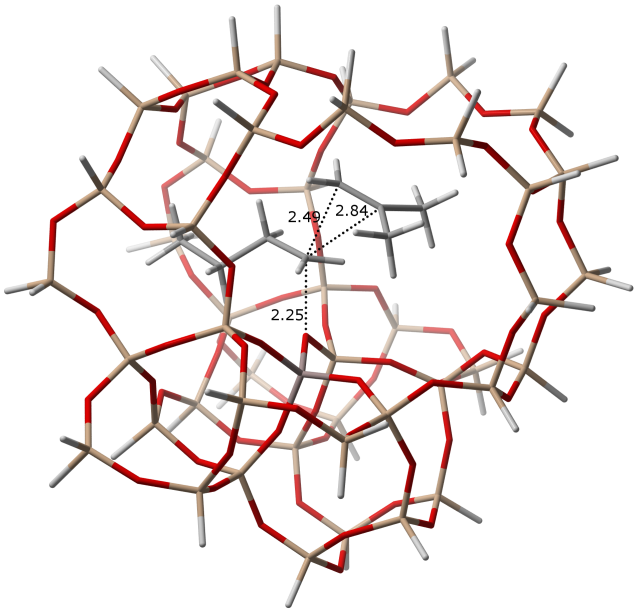

Figure 4.5: Transition state geometry of Reaction (4.1)

In contrast, the tertiary cation in the reactant state is more stabilized on itself by inductive and hyperconjugative interactions in addition to dispersion interactions with the zeolite wall. Furthermore, electrostatic repulsive interactions with the framework are important for this tertiary branched structure. Therefore, it shows less interaction with the framework oxygens, at a distance between 4.73 and 5.29 Å.

During product optimization, the distance between the two fragments (α C - β C) elongate to 3.72 Å. The isobutene fragment moves into the straight channel, while the cationic fragment settles in the sinusoidal channel of the catalyst. The 1-butyl cation binds to a framework oxygen, forming a stable 1-butoxide species.

Kinetic and thermodynamic parameters are given in Table 4.3 and Table 4.4 respectively. Note that the activation energy for Reaction (4.1) is quite high, while Reaction (4.2) has a high but acceptable activation barrier. Consequently, the rate coefficient for Reaction

Table 4.3: Intrinsic kinetic parameters at 833 K for the bimolecular tertiary - primary cracking (LOT : ωB97X-D/6-31+g(d,p)//ONIOM(B3LYP/6-31+g(d,p):pm3))

No.	Forward reaction		
	A	E_a	k_{fwd} $(833K)$
	s^{-1}	$kJ\ mol^{-1}$	s^{-1}
(4.1)	6.2 10^{12}	121.9	1.4 10^{5}
(4.2)	1.6 10^{14}	85.1	7.0 10^{8}

(4.1) is much lower than the one for Reaction (4.2). This is also reflected in the activation enthalpy barrier, which is very high for both reactions as a result of the charge shift from a tertiary carbon to a primary carbon in the transition state. The activation entropy is small resulting in high free energy barriers. Based on the reaction free energy, cracking into C_4 species is slightly disfavored, while cracking into a C_3 and C_5 species is strongly favored. This can be attributed in the first place to a larger entropy increase for Reaction (4.2) and in second place to the enhanced stability of the primary alkoxide of Reaction (4.2) (lower ΔH_r). The reaction entropy is much larger for Reaction (4.2), which may be due to the fact that only 3 carbon atoms (instead of 4 for Reaction (4.1)) are bound to the catalyst framework. The number of degrees of freedom will hence be larger.

Table 4.4: Thermodynamic parameters at 833 K for bimolecular tertiary - primary cracking (LOT : ωB97X-D/6-31+g(d,p)//ONIOM(B3LYP/6-31+g(d,p):pm3))

No.	$\Delta H^{\ddagger}$	$\Delta S^{\ddagger}$	$\Delta G^{\ddagger}$	ΔH_r	ΔS_r	ΔG_r
	$kJ\ mol^{-1}$	$J\ mol^{-1}K^{-1}$	$kJ\ mol^{-1}$	$kJ\ mol^{-1}$	$J\ mol^{-1}K^{-1}$	$kJ\ mol^{-1}$
(4.1)	114.97	-16.84	128.99	16.48	18.23	1.29
(4.2)	78.60	10.25	70.06	-17.12	52.22	-60.62

Two factors are at play within this class of reactions. First, it can be expected that the stable tertiary octyl cations will be present at relatively high concentrations at the catalyst surface. However, the activation energy of these reactions is still quite high.

Secondary - primary transitions

Within the class of secondary - primary transitions, cracking of following carbenium ions are considered: the 3-octyl carbenium ion, yielding 1-butene and a 1-butyl cation (Reaction (4.3)), the 2-octyl carbenium ion yielding propene and a 1-pentyl cation (Reaction (4.4)). Secondly, cracking of two branched carbenium ions are studied: the 3,5-dimethyl-2-hexyl carbenium yielding 2-butene and an isobutyl cation (Reaction (4.5)) and the 5-methyl-2-heptyl carbenium ion yielding propene and a 2-methyl-1-butyl cation (Reaction (4.6)). Thirdly, cracking of the 4-octyl carbenium ion into either 1-pentene and a 1-propyl cation (Reaction (4.7)) or 1-hexene and an ethyl cation (Reaction (4.8)) is investigated.

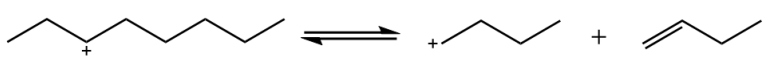

(4.3)

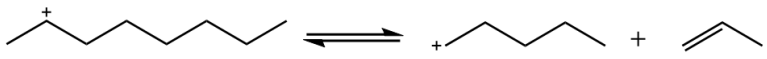

(4.4)

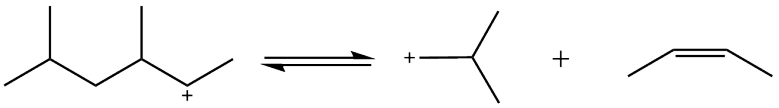

(4.5)

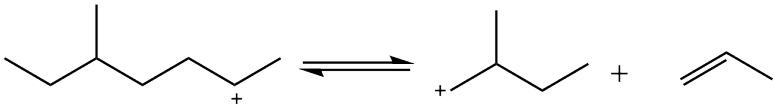

(4.6)

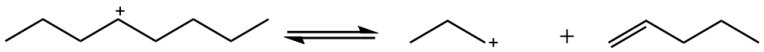

(4.7)

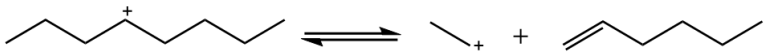

(4.8)

Geometrical aspects within this class of β - scission reactions are transferable are largely similar to the tertiary - primary reaction class. A main point of difference is the lower $^{+}C{-}O$ distance between the positively charged carbon and the central framework oxygen in the reactant state (dashed line in Figure 4.6). Reduced steric repulsion combined with lower inductive stabilization of the secondary ion allows the reactant species to show a closer interaction with the acid site, resulting in a lower $^{+}C-O$ distance in comparison with a tertiary carbenium ion reactant.

The β $C-O$ bond distance appears to be a little more elongated in the transition state for the branched species. This can possibly be attributed to the larger bulkiness of these

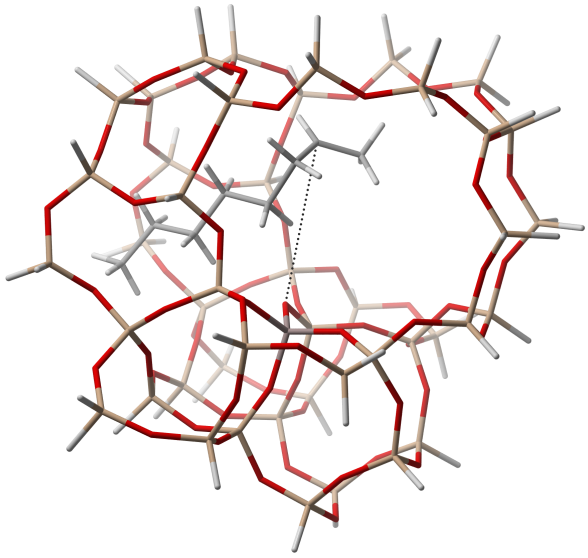

Figure 4.6: Reactant state geometry of Reaction (4.4)

ions compared to their linear homologues. Steric constraints prohibit the reactant to come closer to the framework. An analogous effect is seen for the $^{+}C-O$ bond in the reactant state. These considerations indicate that the transition state for β - scissions of linear species has already a higher degree of advancement (reflected in the bond breaking distance) than for branched species, in accordance with the Hammond-Leffler postulate.[43] This theory thus confirms the higher stability of the branched reactant, relative to the linear reactant species.

Kinetic and thermodynamic parameters are given in Table 4.5 and Table 4.6, respectively. A first observation from the kinetic parameters for Reaction (4.3) through Reaction (4.6) is that cracking towards C_4 species is higher activated than cracking towards C_3 and C_5 species, indicating that propene and 1-pentoxide are more easily formed than butene and 1-butoxide or i-butoxide. Linked to this observation, the reaction free energies indicate that upon comparison of the similar Reactions (4.3) and (4.4) or similar Reactions (4.5) and (4.6), the C_3 and C_5 products are also more stable than the C_4 products. A second observation from the thermodynamic parameters is that cracking of branched species has a higher enthalpic barrier than cracking of linear species, which reflects the larger stability of branched components. However, this enhanced stability effect is partially compensated by a lower ΔS between the branched reactant species and the reactant of Reaction (4.1) than between linear reactant species and the reactant of Reaction (4.1)

Table 4.5: Intrinsic kinetic parameters at 833 K for the bimolecular secondary - primary cracking (LOT : ωB97X-D/6-31+g(d,p)//ONIOM(B3LYP/6-31+g(d,p):pm3))

No.	Forward reaction		
	A	E_a	k_{fwd} $(833K)$
	s^{-1}	$kJ\ mol^{-1}$	s^{-1}
(4.3)	2.7 10^{12}	68.9	1.3 10^{8}
(4.4)	5.4 10^{13}	55.8	1.7 10^{10}
(4.5)	3.3 10^{14}	87.4	1.1 10^{9}
(4.6)	2.4 10^{13}	57.9	5.5 10^{9}
(4.7)	8.3 10^{12}	97.8	6.1 10^{6}
(4.8)	2.1 10^{12}	73.3	5.4 10^{7}

(see Table A.3 in Appendix A), implying that branched carbenium ions have in general a lower mobility in the 10-ring channels of H-ZSM-5 (see also Chapter 5). For Reaction (4.5), this is translated in a more positive entropy barrier, $\Delta S^{ddagger}$. Both effects are combined in the free energy barriers, from which no clear trend can be recognized.

Two exceptions from the above tendencies can also be found in Table 4.5. For Reaction (4.7), the activation energy is much higher than for the comparable Reaction (4.4). This is caused by the enhanced stability (lower enthalpy) of the 4-octyl carbenium rotational conformer compared to the 2-octyl carbenium ion rotational conformer (see Table A.3 in Appendix A), while there is little difference in the transition state stabilities (or enthalpies). Secondly the activation energy for Reaction (4.8) is also quite high, which can possibly be attributed to the higher unstability of the transition state structure, more specifically the ethyl cation. Indeed, there is little difference between the reactant state stabilities of the 4-octyl cation and the 2-octyl cation.

The reaction Gibbs free energy is negative for all reactions, indicating that the reaction products (alkene and primary alkoxide) are more stable than the reactants. Also, the reaction enthalpies show that all investigated reactions are exothermic. This may seem surprising at first sight since we are talking about secondary - primary transitions. However, the primary cation forms a primary alkoxide, which is the most stable class of alkoxides. Consequently, the inverse reaction, dimerization will be endothermic and higher activated (see Table A.1 in Appendix A). Instead of two stable molecules, dimerization will yield a (stabilized) cation.

Table 4.6: Thermodynamic parameters at 833 K for bimolecular secondary - primary cracking (LOT : ωB97X-D/6-31+g(d,p)//ONIOM(B3LYP/6-31+g(d,p):pm3))

No.	$\Delta H^{\ddagger}$ $kJ\ mol^{-1}$	$\Delta S^{\ddagger}$ $J\ mol^{-1}K^{-1}$	$\Delta G^{\ddagger}$ $kJ\ mol^{-1}$	ΔH_r $kJ\ mol^{-1}$	ΔS_r $J\ mol^{-1}K^{-1}$	ΔG_r $kJ\ mol^{-1}$
(4.3)	62.1	-23.6	81.7	-41.1	17.2	-55.4
(4.4)	49.0	1.2	48.0	-54.4	12.5	-64.8
(4.5)	80.5	16.3	66.9	-32.2	69.6	-90.1
(4.6)	51.0	-5.8	55.8	-88.6	57.3	-136.3
(4.7)	90.9	-14.5	102.9	-18.5	22.8	-37.5
(4.8)	66.3	-25.8	87.9	-32.5	8.8	-39.8

All reactions have a positive entropy of reaction and the smallest value has been found for Reaction (4.8). This may be a result of the strongly adsorbed ethoxide that reduces the number of degrees of freedom. The reaction entropy is much more positive for cracking of branched species. In the zeolite pores, a branched species has less rotational freedom compared to narrow linear species. A primary alkoxide partially limits the freedom of movement, but since it is only bound at a terminal carbon atom, the remainder of the alkoxide species still has some rotational freedom.

The linear reactant species within this reaction class can be formed via 1,2-hydride shifts of a direct dimer of 1-butene. However, information about the dynamic behavior of these species is still lacking. To this end, molecular dynamics simulations need to be performed (see Chapter 5).

Tertiary - secondary transitions

As reference reactions from the tertiary - secondary transition class, the 2,4-dimethyl-2-hexyl carbenium ion cracking into a 2-butyl cation and isobutene (Reaction (4.9)) and the 2,4-dimetyl-4-hexyl carbenium ion cracking into a 2-propyl cation and 2-methyl-1-butene (Reaction (4.10)) are considered. Both reactions have again very similar geometrical features, therefore only Reaction (4.9) will be discussed in detail.

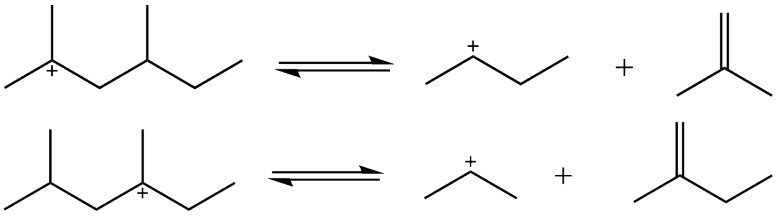

(4.9)

(4.10)

In the transition state the isobutene fragment and the 2-butyl cation fragment are already formed. Both the α C and β C are perfectly sp^2 hybridized. The distance between the broken bond C atoms is 2.74 Å, while the $C-O$ distance with the central framework oxygen is 2.34 Å (see Figure 4.7). In the product optimization, the two product fragments drift further away to a distance of 3.55 Å. The cation fragment binds to the framework, forming an alkoxide species with $C-O$ distance of 1.53 Å. The alkene fragment settles in the straight channel, while the alkoxide fragment remains in the sinusoidal channel.

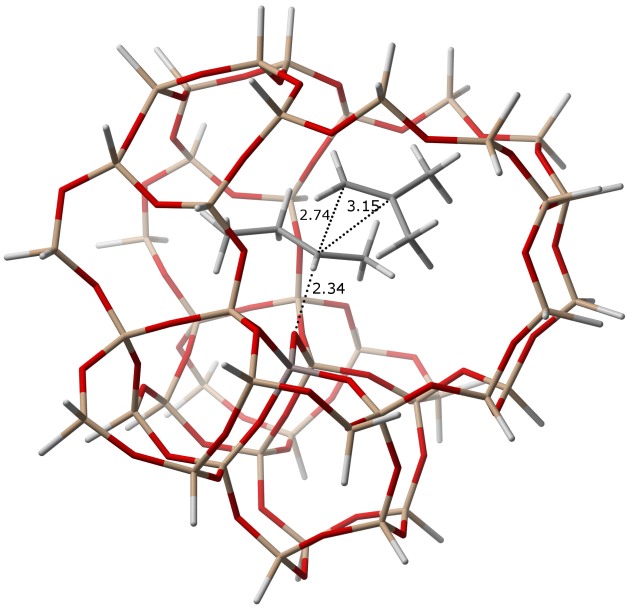

Figure 4.7: Transition state geometry of Reaction (4.9)

Kinetic and thermodynamic parameters are given in Table 4.7 and Table 4.8. The rate coefficient of both reactions lies within the same order of magnitude, which is not surprising since the geometries are comparable. The activation energy for both reactions is equal and relatively high, but nor insurmountable. Entropy contributions are limited: The reactant is a highly branched bulky molecule with few degrees of freedom,

Table 4.7: Intrinsic kinetic parameters at 833 K for the bimolecular tertiary - secondary cracking (LOT : ωB97X-D/6-31+g(d,p)//ONIOM(B3LYP/6-31+g(d,p):pm3))

No.	Forward reaction		
	A	E_a	k_{fwd} $(833K)$
	s^{-1}	$kJ\ mol^{-1}$	s^{-1}
(4.9)	1.5 10^{14}	88.9	4.1 10^{8}
(4.10)	9.9 10^{13}	89.3	2.5 10^{8}

while in the product (and transition) state, the rotational freedom is limited by alkoxide formation. The reaction entropy is more positive for the scission towards 2-propoxide and 2-methyl-1-butene, probably because only three carbon atoms are bonded to the surface instead of four. On the other hand, the endothermicity of the reaction is more pronounced for Reaction (4.9). Consequently, the reaction free energy is negative for Reaction (4.10), while positive for Reaction (4.9).

Table 4.8: Thermodynamic parameters at 833 K for bimolecular tertiary - secondary cracking (LOT : ωB97X-D/6-31+g(d,p)//ONIOM(B3LYP/6-31+g(d,p):pm3))

No.	$\Delta H^{\ddagger}$	$\Delta S^{\ddagger}$	$\Delta G^{\ddagger}$	ΔH_r	ΔS_r	ΔG_r
	$kJ\ mol^{-1}$	$J\ mol^{-1}K^{-1}$	$kJ\ mol^{-1}$	$kJ\ mol^{-1}$	$J\ mol^{-1}K^{-1}$	$kJ\ mol^{-1}$
(4.9)	82.0	9.8	73.8	16.8	9.1	9.3
(4.10)	82.4	6.2	77.2	6.7	19.9	-9.9

The question if these species occur and how they behave dynamically in the zeolite environment can be answered with MD simulations (see Chapter 5).

Secondary - secondary transitions

Within the class of secondary - secondary transitions, two scissions are considered: cracking of a 3,4-dimethyl-2-hexyl carbenium ion into 2-butene and a 2-butyl cation (Reaction (4.11)) and cracking of a 2,5-dimethyl-3-hexyl carbenium ion into 3-methyl-1-butene and a 2-propyl cation (Reaction (4.12)).

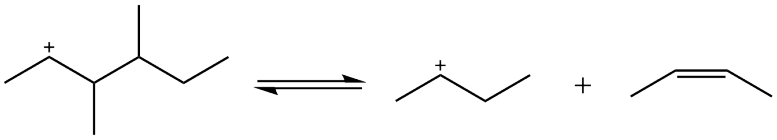

(4.11)

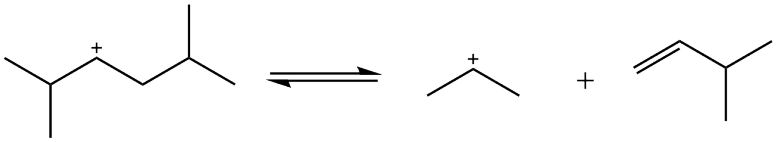

(4.12)

Transition state (shown in Figure 4.8) and product geometries are similar to the class of tertiary - secondary transitions. The secondary cationic reactant state, however, has a closer interaction with the framework acid sites. The fragments in the product state also tend to move a little further away from each other compared to the tertiary - secondary transition class and certainly compared to the secondary - primary transitions (see also Table A.4 in Appendix A).

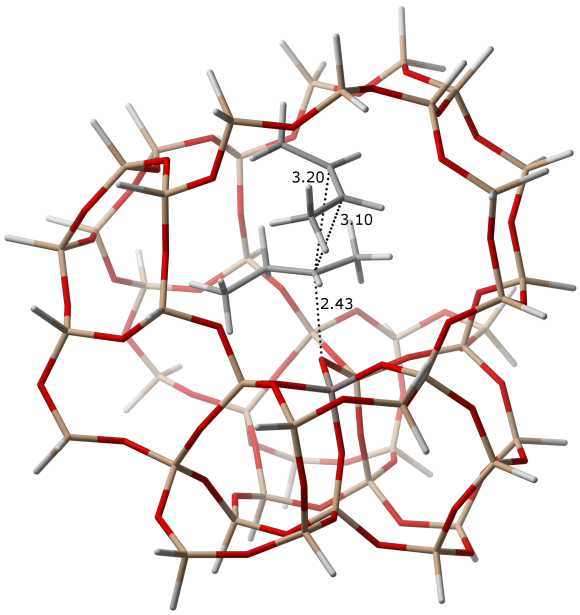

Figure 4.8: Transition state geometry of Reaction (4.11)

Kinetic and thermodynamic parameters are listed in Table 4.9 and Table 4.10. Since there is no particular difference in the degree of stabilization from reactant to transtition state for secondary - secondary reactions, the resulting forward activation energies are quite low. The activation energy for Reaction (4.11) is significantly higher than for Reaction (4.12), which is confirmed by the larger reactant stabilization for Reaction

(4.11), cfr. a lower ΔH between the reactants of Reaction (4.11) and Reaction (4.1) (84.6 kJ/mol) than between the reactants of Reaction (4.12) and Reaction (4.1) (119.4 kJ/mol) (see Table A.3 in Appendix A). The difference is magnified in the free-energy barriers due to the larger entropic contribution for Reaction (4.12), a scission to C_3 and C_5 species. Both reactions are strongly exothermic, resulting in high activation energies for the reverse dimerizations (see Table A.1 in Appendix A).

Table 4.9: Intrinsic kinetic parameters at 833 K for the bimolecular tertiary - secondary cracking (LOT : ωB97X-D/6-31+g(d,p)//ONIOM(B3LYP/6-31+g(d,p):pm3))

No.	Forward reaction		
	A	E_a	k_{fwd} $(833K)$
	s^{-1}	$kJ\ mol^{-1}$	s^{-1}
(4.11)	7.0 10^{14}	66.5	4.7 10^{10}
(4.12)	3.7 10^{15}	46.9	4.2 10^{12}

Table 4.10: Thermodynamic parameters at 833 K for bimolecular tertiary - secondary cracking (LOT : ωB97X-D/6-31+g(d,p)//ONIOM(B3LYP/6-31+g(d,p):pm3))

No.	$\Delta H^{\ddagger}$	$\Delta S^{\ddagger}$	$\Delta G^{\ddagger}$	ΔH_r	ΔS_r	ΔG_r
	$kJ\ mol^{-1}$	$J\ mol^{-1}K^{-1}$	$kJ\ mol^{-1}$	$kJ\ mol^{-1}$	$J\ mol^{-1}K^{-1}$	$kJ\ mol^{-1}$
(4.11)	59.6	22.4	40.9	-35.6	20.4	-52.6
(4.12)	40.0	36.3	9.8	-81.2	46.3	-119.7

Tertiary - tertiary transitions

Only one possible tertiary - tertiary transition can be written down: 2,4,4-trimethyl-2-pentyl carbenium ion cracking into isobutene and a t-butyl cation (Reaction (4.13)). In the transition state geometry, the α C - β C breaking bond distance is 2.27 Å. The C - O bond distance is with 4.93 Å quite elongated. Unlike the previous reactions, the α C and β C are very close but not yet perfectly sp^2 hybridized (see Figure 4.9).

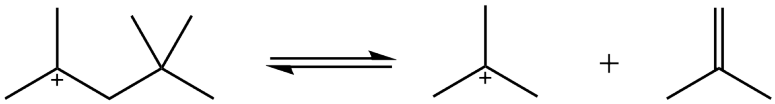

(4.13)

Table 4.11: Intrinsic kinetic parameters at 833 K for the bimolecular tertiary - tertiary cracking (LOT : ωB97X-D/6-31+g(d,p)//ONIOM(B3LYP/6-31+g(d,p):pm3))

No.	Forward reaction		
	A	E_a	k_{fwd} $(833K)$
	s^{-1}	$kJ\ mol^{-1}$	s^{-1}
(4.13)	3.1 10^{15}	46.7	3.6 10^{12}

In contrast to the previously discussed results, the product optimization does not result in a tertiary butoxide fragment, bound to a framework oxygen. Instead, a t-butyl cation is found to be a stable minimum on the PES and may exist as reaction product in the zeolite channels even though the proton affinity of isobutene has been estimated at only 802 kJ/mol.[123] These results are in agreement with other studies on isobutene protonation.[86,89] However, the existence of the t-butyl carbenium ion has only very limited experimental evidence.[82]

Unlike for secondary or primary products, the t-butyl carbenium ion is not perfectly oriented to one of the basic oxygens. At distances of 3.52 Å and 4.04 Å from two basic oxygens, there is barely interaction with the framework acid site. The highly branched structure provides sufficient stabilization on its own so the electrostatic stabilization contribution is less important. Furthermore, steric repulsion with the zeolite wall prohibits the formation of a tertiary butoxide.

In the transition state, the distance between the t-butyl fragment and the framework is large compared to previous classes due to steric repulsion. Consequently, there is only limited space in the zeolite channel for the two highly branched cracking products. As a result, the isobutene fragment moves further away during product optimization. Due to the limited size of the 46T-cluster model, the electrostatic interactions with the zeolite wall are not accurately described. Dispersion interactions are also not taken into account in the geometry optimization. As a consequence, the isobutene fragment moves out of the model and the acquired data for the reverse reaction are thus not reliable. The optimized reactant geometry also fits barely inside the cage, rendering the forward

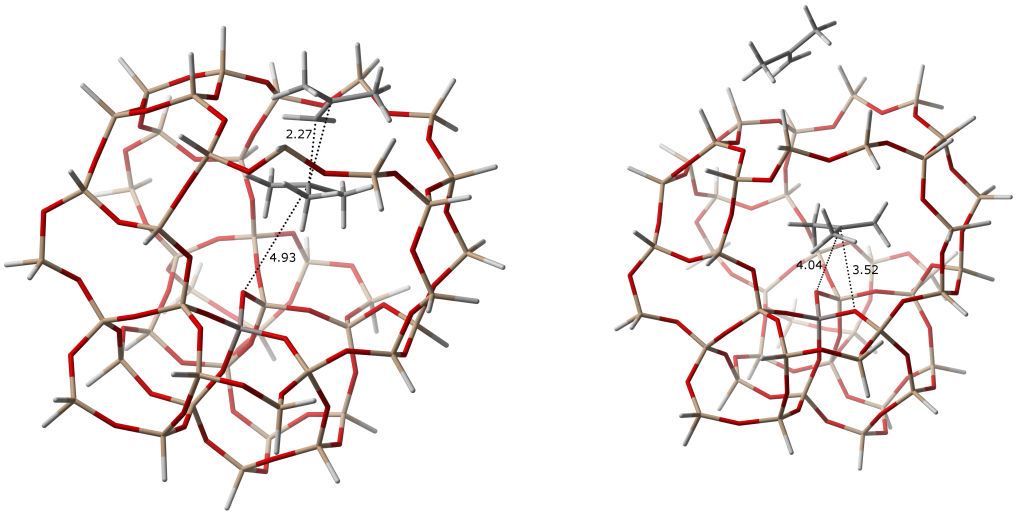

(a) Transition state (b) Product state

Figure 4.9: Transition and product state geometries of Reaction (4.13)

reaction data only little more reliable.

Table 4.12: Thermodynamic parameters at 833 K for bimolecular tertiary - tertiary cracking (LOT : ωB97X-D/6-31+g(d,p)//ONIOM(B3LYP/6-31+g(d,p):pm3))

No.	$\Delta H^{\ddagger}$ $kJ\ mol^{-1}$	$\Delta S^{\ddagger}$ $J\ mol^{-1}K^{-1}$	$\Delta G^{\ddagger}$ $kJ\ mol^{-1}$	ΔH_r $kJ\ mol^{-1}$	ΔS_r $J\ mol^{-1}K^{-1}$	ΔG_r $kJ\ mol^{-1}$
(4.13)	39.8	34.8	10.8	4.0	131.9	-105.9

Kinetic and thermodynamic parameters are listed in Table 4.11 and Table 4.12. The accuracy of the reaction parameters can be questioned as stated previously. It is however noteworthy that the difference between reactant and product stability is almost negligible (low ΔH_r), reflecting in a low activation energy for this reaction. The entropy difference between the activated complex and the reactant is also remarkable, which may be explained due to the little number of degrees of freedom of this bulky reactant inside the cluster. Also, the alkene fragment is partially outside the cage, giving it more rotational freedom than expected in reality.

Secondary - tertiary transitions

Secondary - tertiary transitions that are investigated are the 3,4,4-trimethyl-2-pentyl carbenium ion cracking into 2-butene and a t-butyl cation (Reaction (4.14)) and secondly, the 4,4-dimethyl-2-hexyl carbenium ion cracking into propene and a 2-methyl-2-butyl cation (Reaction (4.15)).

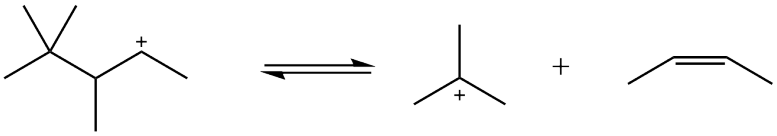

(4.14)

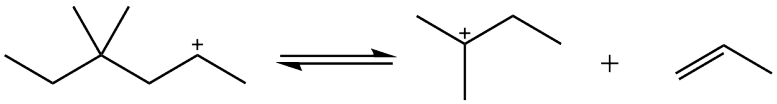

(4.15)

The transition state and product state geometries of these reactions are very similar to Reaction (4.13). Electrostatic repulsion between the voluminous tertiary fragments results causes the alkene fragment to (partially) drift outside the zeolite cage. Dispersion interactions cannot be described accurately and the numerical values of the resulting parameters are not reliable. The reactant state however, is a secondary cation that shows less repulsion with the surrounding framework than for a tertiary cation. Therefore $^{+}C-O$ distances are smaller compared to tertiary - tertiary transitions. Due to the formation of a tertiary fragment as product, steric hindrance is still larger compared to secondary - secondary transitions, resulting in a longer $^{+}C-O$ interaction distance.

Table 4.13: Intrinsic kinetic parameters at 833 K for the bimolecular tertiary - tertiary cracking (LOT : ωB97X-D/6-31+g(d,p)//ONIOM(B3LYP/6-31+g(d,p):pm3))

No.	Forward reaction		
	A	E_a	k_{fwd} $(833K)$
	s^{-1}	$kJ\ mol^{-1}$	s^{-1}
(4.14)	1.3 10^{13}	-8.1	1.4 10^{13}
(4.15)	9.6 10^{15}	-8.8	3.4 10^{16}

Kinetic and thermodynamic reaction parameters are summarized in Table 4.13 and Table 4.14. Quite remarkably, negative activation energies are calculated with the applied level of theory, which makes physically no sense. The kinetic and thermodynamic data are

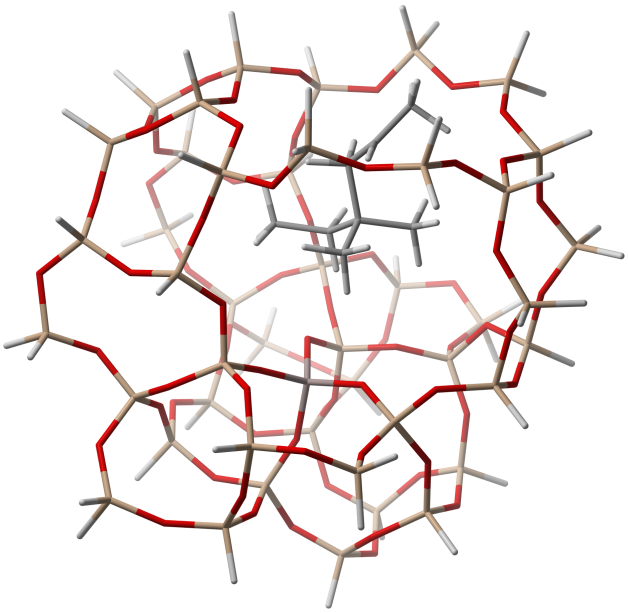

(a) Reactant

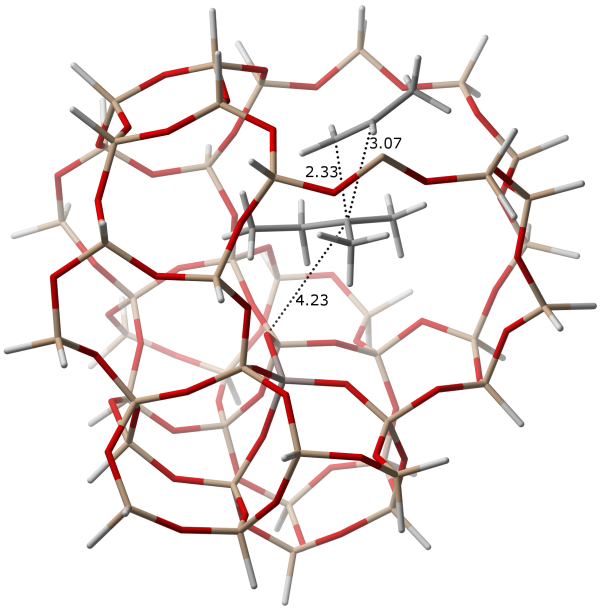

(b) Transition state

Figure 4.10: Reactant and transition state geometry of Reaction (4.15)

thus not representative for the investigated reactions. Although, the electronic barriers at ONIOM level for Reaction (4.14) and Reaction (4.15), respectively 32.14 kJ/mol and

53.24 kJ/mol, do lie in a realistic range. This is a sign that the potential energy surfaces before and after the energy refinement are not parallel with each other. The activation energies for the backward reaction were also found to take unrealistic values, indicating that the problem may be caused by the (partial) drift of the transition state fragments out of the zeolite model. The applied cluster model is suspected to be too small for an accurate description of the interactions at hand within this reaction class.

Table 4.14: Thermodynamic parameters at 833 K for bimolecular tertiary - tertiary cracking (LOT : ωB97X-D/6-31+g(d,p)//ONIOM(B3LYP/6-31+g(d,p):pm3))

No.	$\Delta H^{\ddagger}$ $kJ\ mol^{-1}$	$\Delta S^{\ddagger}$ $J\ mol^{-1}K^{-1}$	$\Delta G^{\ddagger}$ $kJ\ mol^{-1}$	ΔH_r $kJ\ mol^{-1}$	ΔS_r $J\ mol^{-1}K^{-1}$	ΔG_r $kJ\ mol^{-1}$
(4.14)	-7.6	-10.9	1.5	-2.0	33.9	-30.2
(4.15)	-15.7	44.3	-52.6	29.5	107.8	-60.3

4.3 General trends and model evaluation

A link to the kinetic model

It is interesting to compare the different reaction classes with each other to evaluate global trends. Figure 4.11 plots the free energy barriers, grouped per transition class for the investigated reactions. In Figure 4.12, the enthalpic barriers of the same reactions are shown.

A general trend can be recognized for the free energy barriers in both tertiary and secondary transitions. Starting from a tertiary reactant cation, the barriers follow a decreasing trend in the order: tertiary - primary > tertiary - secondary > tertiary - tertiary. Analogously, starting from a secondary reactant cation, the barriers decrease in the order: secondary - primary > secondary - secondary. This sequence is a consequence of the carbenium ion stability order in the transition state. The activation energy for formation of a primary carbenium ion in the transition state will be higher than formation of a secondary carbenium ion, which will be higher than formation of a tertiary carbenium ion. An exception to this trend is the difference between tertiary - primary Reaction (4.2) and tertiary - secondary Reaction (4.10).

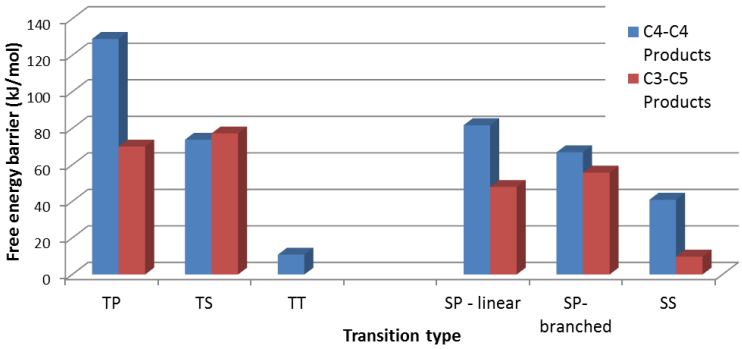

Figure 4.11: Free energy barriers at 560 °C for the β - scissions towards two C_4 products (blue) and towards a C_3 and C_5 product (red), grouped by transition type (TP = tertiary - primary, TS = tertiary - secondary, TT = tertiary - tertiary, SP-linear = secondary - primary with linear reactant, SP-branched = secondary - primary with branched reactant, SS = secondary - secondary) (LOT : ωB97X-D/6-31+g(d,p)//ONIOM(B3LYP/6-31+g(d,p):pm3))

Furthermore, the free energy barrier is generally lower for transitions with secondary reactants than for transitions with tertiary reactants. This may be attributed to a higher difference in enthalpic stabilization, i.e., higher enthalpic barriers, in a transition from tertiary to primary carbenium ions than in a transition from secondary to primary carbenium ions, while it can also be seen from Figures 4.11 and 4.12 that this is not significantly affected by entropic contributions. The reactivity will thus be higher for secondary carbenium ions compared to tertiary carbenium ions.

Mazar et al. found that the activation energies are primarily determined by the degree of substitution of the carbocationic atom in the transition state and to a secondary extent by the degree of substitution of the charge-carrying carbon atom in the reactant state.[70] Our results are comparable for the dependency on the transition state, however an opposite influence was found for the reactant state. Note that entropic contributions were taken into account and that IRC calculations were performed, while Mazar et al. started from alkoxides as initial guesses to optimize reactant geometries.

In general, the β -scission elementary steps leading to two C_4 products are also found to have a higher free energy barrier than those leading to a C_3 and C_5 species. Although this trend is visible in the enthalpic barriers, it is intensified by the entropic effect for most reactions. Intrinsic carbenium ion stability is insufficient to explain this behavior since most reactants are comparable. The solvatation of the cation in the zeolite channel

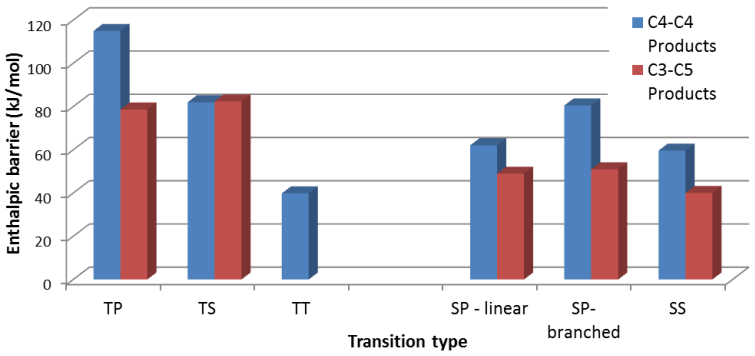

Figure 4.12: Enthalpic barriers at 560 °C for the β - scissions towards two C_4 products (blue) and towards a C_3 and C_5 product (red), grouped by transition type (TP = tertiary - primary, TS = tertiary - secondary, TT = tertiary - tertiary, SP-linear = secondary - primary with linear reactant, SP-branched = secondary - primary with branched reactant, SS = secondary - secondary) (LOT : ωB97X-D/6-31+g(d,p)//ONIOM(B3LYP/6-31+g(d,p):pm3))

also contributes to a large extent to the reactant enthalpy and entropy. However, due to the limitation of considering only a single conformer within static calculations, a large difference exists in the stabilization of different species. Consequently, the difference in resulting reactant enthalpies shows a large variation.

As an implication of this trend, the product yield of propene (and pentene) will be higher than the yield of butenes, which is in agreement with the expected cracking product distribution. One exception to this rule are the tertiary - secondary transitions, which have very similar geometries and hence comparable enthalpic and free energetic barriers.

Tertiary - primary transitions can be predicted to play a minor role due to the high free energy barriers, although the reactants are among the most stable of all considered reactions. Tertiary - secondary and secondary - primary transitions are energetically not the most favorable path but due to the high stability of the reactant, these reactions can be expected to be important. Tertiary - tertiary and secondary - tertiary transitions involve the formation of a highly branched reactant, which is rather unstable and which can be sterically hindered. If the reactant species can be formed, a scission will probably occur, but this family will presumably not be the most important. Secondary - secondary transitions show an ideal balance between stability and thus concentration of the reactant and the rate coefficient. Based on the rate coefficients from static calculations, this reaction class can be considered to be one of the prominent routes.

Two aspects regarding the reaction rate need to be considered in order to determine which type of reaction will occur dominantly and to link the results with the expected product distribution of a butene cracking process: the intrinsic kinetics and the probability that the considered carbenium ion reactants will be formed inside the zeolite channels. Clearly, the free energy barrier will determine to a large extent if the reaction pathway is accessible. However, from the investigated reactions, those with the lowest barrier correspond typically to those with least stable reactant configuration and consequently those with the lowest concentration in the zeolite pores. Once they are formed, rapid rearrangements to a more stable configuration are plausible. Due to the large variety of species and conformers that can be formed, the second aspect is difficult to describe statically, therefore, molecular dynamics simulations are performed to investigate if the considered carbenium ions are likely to be formed in the zeolite environment (see Chapter 5).

Model limitations

For some of the studied reactions, limitations of the applied model and methodology emerged. First, for modeling certain reactions with large species, like an octyl carbenium ion, the 46T-cluster model is too small to ensure an appropriate description of interactions with the zeolite wall even if dispersion correcting functionals are used. Due to the lack of an accurate description of both stabilizing (e.g. London forces) and repulsive (e.g. steric), both electrostatic and dispersion interactions in the geometry optimization, the scission product geometries may settle at the boundaries of the model or even move outside the model. If the stabilization by the framework of the ionic species in reactant and transition state is not accurately described, this will result in wrong estimations of the activation barriers.

A second shortcoming is related to the applied level of theory. For certain reactions with extended structures, like secondary - tertiary transitions, a deformation can be observed between the potential energy surface from geometry optimization calculations and the PES from energy refinement calculations. In these situations, the different level of theories that are used are not compatible with each other. As a result, the kinetic parameters can take unrealistic values, for example negative activation energies.

Thirdly, a general limitation of static cluster calculations is that only a single point on the PES is considered within the harmonic oscillator (HO) approximation. Kinetic (and thermodynamic) parameters are determined at an actual cracking temperature, 560 °C, which gives the species sufficient thermal energy to allow them to rearrange to other configurations. At high temperatures, anharmonic effects are more likely to occur. Also, the entropy effect is in some reactions far from negligible, indicating that the HO approximation is no longer valid and other conformers should be taken into account. It

is reasonable to assume that both reactant and product state can quickly rearrange from their pre- and post-reactive complex to a more stable state or that the ionic reactant species will access a less stable configuration to allow β - scission reactions more easily.

Finally, static calculations yield a narrow view on the complex potential energy surface, although a number of different configurations exist for transition states of the same reaction. A small perturbation of the reactant position or a change in the framework conformation (e.g., different Al-O-Al angles, elongated Al-O bonds,...). Also, the cluster is only allowed to relax in a limited way, but for this extended system, the actual flexibility of the framework is not correctly accounted for. A static 46T-cluster calculations enlightens a single geometry of configuration of the many possiblities. Furthermore, it cannot be prevented that during geometry optimizations from several reactions, different framework conformations are found. The energies that are calculated based on these geometries will therefore differ, making a direct comparison hard.

Combining these four considerations leads to the conclusion that the limitations of the cluster approach prevent the calculation of reliable (within standard error margins of quantum chemical calculations) numerical values for the kinetic and thermodynamic reaction parameters. These shortcomings can be solved using extended cluster models or periodic models, combined with metadynamics simulations to obtain more accurate values for the reaction kinetics.

Chapter 5

Molecular dynamics simulations of carbenium ions

In this chapter, the dynamic behaviour of different carbenium ion species from Chapter 4 in the zeolite environment is investigated in order to determine if these carbocations may exist as stable, long-lived species reactants for the cracking reactions from the previous chapter. First, a 2-butyl species is simulated. Secondly, several C_8 carbenium ions with different degrees of branching are studied: a linear chain, a single, double and triple branched chain. The aim is to link the results to experimental product distributions.

Molecular dynamics simulations using the NPT ensemble on a periodically repeated H-ZSM-5 unit cell are performed. Analogously to the 46T-cluster, the active site is placed at the T12 position, at the intersection of the straight and sinusoidal channel. The CSVR thermostat is set at a temperature of 560 °C, the barostat at a pressure of 1 bar. In all simulations, an equilibration run of 5 ps is performed, followed by a production run of variable length.

5.1 The 2-butyl cation

From static calculations on monomolecular cracking (see 4), it appeared that no primary carbenium ion could be detected as a minimum on the PES. A barrierless rearrangement occurred to a secondary butyl carbenium ion. Although this is clearly a local minimum, a 2-butyl cation is still not very stable. It is reasonable to assume that this species will transform to a more stable state, like a π - complex or butoxide (see Paragraph 4.1). Static calculations lack information about the dynamic behavior of the reactant species on the potential energy surface, therefore the behavior of a 2-butyl species as reactant intermediate is simulated.

An MD run of 40 ps is simulated. Figure C.1 in Appendix C.1 displays the energy (conserved quantity), instantaneous and average temperature and pressure evolution. Figure C.2 in Appendix C.1 shows the evolution of the cell lengths and cell angles in the three dimensions. Note that during the simulation, the total energy or conserved quantity is not strictly constant, but show a drift due to numerical integration artifacts in CP2K. The energy drift, which is a measure for the quality of the simulation, is rather high (0.0014 % of the potential energy), but still acceptable. After 5 ps, the average temperature remains oscillating within 10°C variation from the setpoint temperature. It is therefore jusitified to start the production run after 5 ps equilibration time. Due to the very large pressure fluctuations, the average pressure still shows a strong deviation after 5 ps (approximately -50 bar) and is even not yet converged at a simulation time of 35 ps. In Figure 5.1, an overview of the discussed reaction pathways for the 2-butyl cation is given.

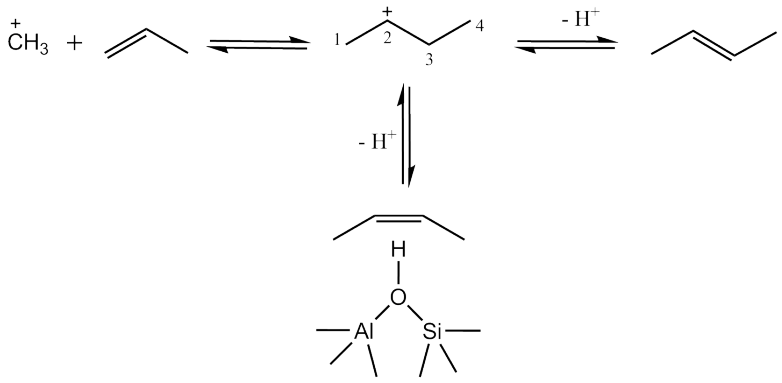

Figure 5.1: Overview of sampled states for a 2-butyl carbenium ion and the accompanying cracking routes

In order for the monomolecular cracking route to be a feasible route for ethene production, a sufficient concentration of 2-butyl species is required. The simulation results reveal that there appears to be a transition from the secondary 2-butyl carbenium ion to the physisorbed 2-butene π - complex. Once, a deprotonation (shown in Figure 5.2) has occurred, the butene molecule is not reprotonated again, hence the equilibrium can be expected to lie strongly towards 2-butene. Three independent simulations with different starting geometries yield the same result, indicating that the observations are not simply a statistical event. A 2-butyl cation species is thus a short-lived intermediate with probably a low concentration in the zeolite environment and combined with the high activation energy for β - scission, it can be concluded that monomolecular cracking is indeed not a feasible pathway.

Deprotonation to the framework active site occurs between 5 and 10 ps in the simulations.

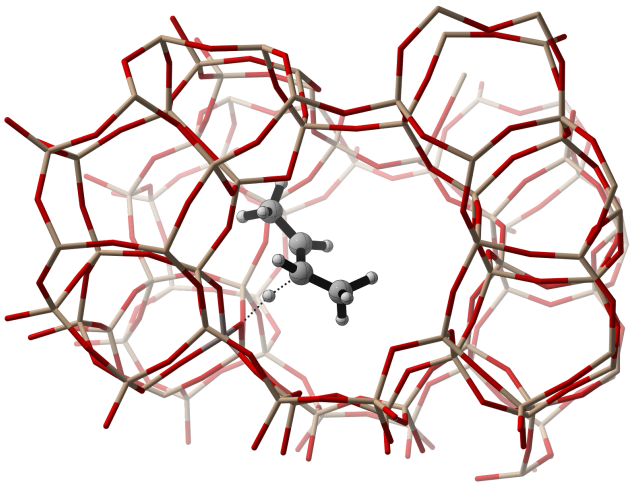

Figure 5.2: Snapshot of a frame showing a deprotonation from the linear butyl chain to the framework

Figure 5.3(a) displays the $Al - O$ bond distance during the simulation, while in figure 5.3(b) the $O - H$ (bond) distance is shown. The moment of deprotonation is clearly recognizable as the point where the distance between the proton and the framework oxygen drops to about 1 Å. Except from the thermal vibrations, no transfer of the proton back to the butene molecule occurs. Note that at the instant of deprotonation, the average $Al-O$ bond distance jumps from 1.8 Åto about 2.0 Å. Indeed, the protonated framework oxygen gets a partial positive charge, while Al bears a partial negative charge. The electrons of this dative bond are transferred closer to the oxygen, hence the bond distance becomes larger.

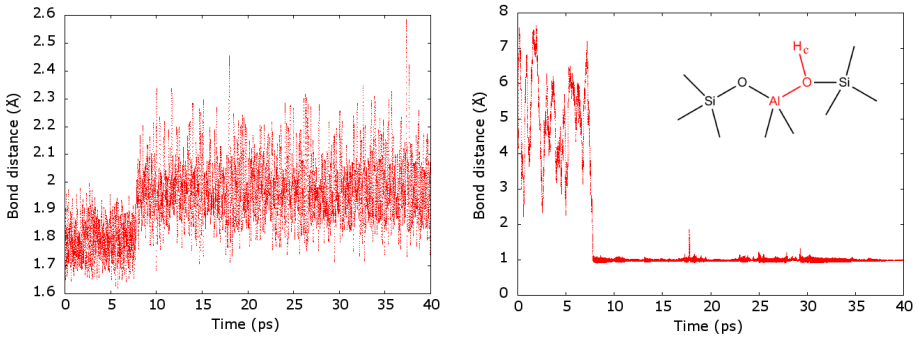

(a) Al-O bond distance (b) O-H bond distance

Figure 5.3: Framework Al-O and O-H bond distance as a function of simulation time

Figure 5.4 pictures the evolution of the three initial $C - H$ bond distances from the two

central carbon atoms. The hydrogen atom that was initially bonded to the positively charged carbon appears to be the one that is transferred to the framework (see rising bond distance in Figure 5.4(a)). This implies that the other protons of the cation travel between the carbon atoms during the simulation. During the carbenium ion sampling (0 - 8 ps), it can be observed that the bond distances sometimes jump from 1.1 Å to about 2.2 Å, indicating that the proton shifts to a neighboring carbon atom. 1,2-hydrogen shifts are found to have a very low activation barrier and during the protonated state of 2-butene, frequent proton shifts occur between the two central carbon atoms. The terminal carbon atoms bear no charge at any point in the simulation.

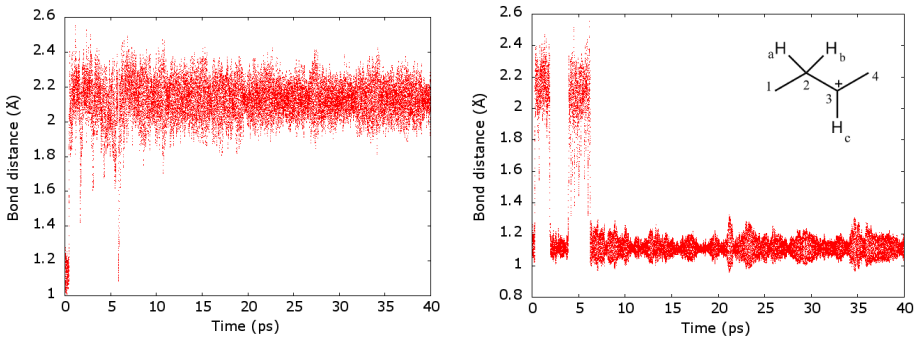

(a) C_2-H_a bond distance

(b) C_2-H_b bond distance

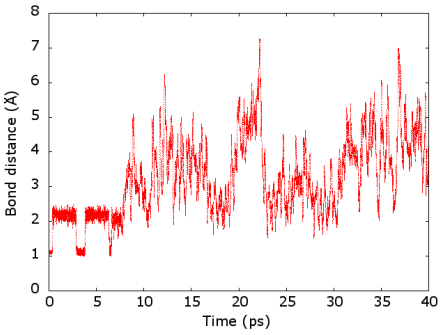

(c) C_3-H_c bond distance

Figure 5.4: Evolution of the central C-H bond distances of the initial 2-butyl cation

Theoretically, two isomers can be formed from deprotonation of a 2-butyl carbenium ion: cis-2-butene and trans-2-butene. Our simulations show that both are possible reaction products. Two simulations yielded the cis isomer, while the other ended up with the trans isomer. The trans-2-butene product is expected to be more stable. If the simulation would have be repeated a sufficient number of times to obtain significant statistical data, this should be reflected in a ratio of simulations ending up with a cis isomer to the ones ending up with a trans isomer smaller than one. In practice, this is not achievable due to the large number of simulations that is required.

5.2 A linear octyl chain

One of the direct ways to form a n-butene dimer, is the attack of a 1-butyl cation on the terminal position of 1-butene, yielding the linear 3-octyl cation. It is interesting to observe the behavior of a linear octyl backbone in order to determine if these linear cations are possible cracking reactants for Reactions (4.3), (4.4), (4.7) and (4.8) in Chapter 4 and if this can be linked to the relative rates of the reaction steps and hence the product distribution. A 2-octyl carbenium ion was used as initial geometry. During the equilibration run, it isomerized to a 4-octyl carbenium ion, which is the starting structure of the production run of 77.95 ps. After a simulation time of 35 ps, a sharp increase in the conserved quantity was observed, therefore the simulation was restarted with new random initial velocities. The same problem was encountered after 65 ps and the simulation was again continued with randomly assigned velocities. In Figure 5.5, the sampled isomers are shown together with the feasible cracking pathways: from top to bottom Reaction (4.4), Reaction (4.3), Reaction (4.7) and Reaction (4.8).

In contrast to the 2-butyl species, the equilibrium between the physisorbed octene π - complex and the octyl carbenium ion appears to lie much more towards the ionic state. Furthermore, deprotonation occurs on a shorter timescale since reprotonation of the octene product has been observed during the simulation. Larger inductive and hyperconjugative stabilization explain why an octyl cation is indeed more stable than a butyl cation. It has been stated earlier that the stability of the protonated alkene is linked with the proton affinity of the alkene and that the proton affinity increases with increasing carbon number.[86,87]

In total, during 20.4 % of the simulation time, the carbenium ion is deprotonated to the framework oxygens, neighboring the *Al* atom. Based on this time fraction, which can be seen as the probability p for that state, the free energy difference and equilibrium coefficient at 560 °C between the physisorbed π - complex (A) and the carbenium ion (B) can be calculated.

$$A \rightleftharpoons B$$

$$C_nH_{2n} \rightleftharpoons C_nH_{2n+1}^+$$

$$\Delta G_{AB} = -RTln\frac{p(B)}{p(A)} = -9.4\ kJ/mol \tag{5.1}$$

$$K = e^{-\frac{\Delta G_{AB}}{RT}} = 3.903 \tag{5.2}$$

A small stability difference exists between the deprotonated alkene and the carbenium ion with a slight advantage for the protonated state, which is translated in an equilibrium coefficient that is shifted a little towards the secondary octyl carbenium ion. These

numerical values should however be considered a rough estimate since multiple independent simulations with sufficient proton transitions are required to obtain a significant statistical average. At one point, alkoxide formation is sampled however it desorbs immediately. Clearly, an alkoxide is not the most stable configuration for this species, which can possibly explained by steric constraints of the extended chain with the framework.

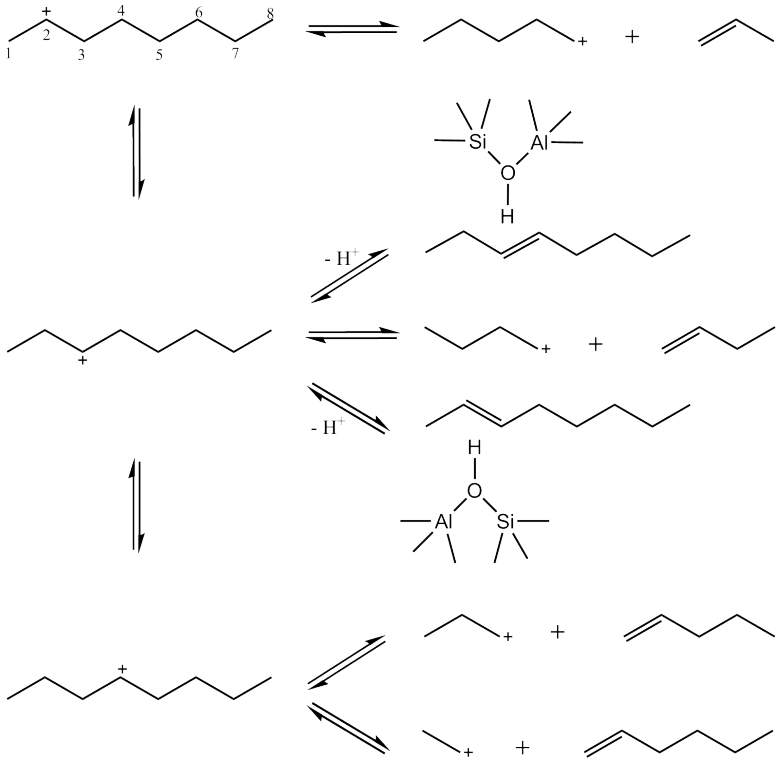

Figure 5.5: Overview of sampled isomers and deprotonation reactions for a 2-octyl carbenium ion, together with the possible cracking pathways

One of the main characteristics of a linear chain is that it consists primarily of secondary carbon atoms. Only if the charge would be transferred to one of the terminal carbon positions, a primary carbenium ion could be formed. However, primary carbenium ions are less stable than secondary ones, and therefore not observed in the MD simulation. The activation barrier for isomerization to a primary ion is clearly too high to sample. In Chapter 4,the importance of primary carbenium ions was assumed to be negligible. These molecular dynamics simulations confirm this premise.

Analogous to the 2-butyl species, proton shifts between the inner secondary carbon atoms take place frequently. During the production run, the positive charge resides on all carbon atoms, from the second to the seventh position. Three different ways for isomerization between these linear carbenium ions are observed (see Figure 5.6). The

first and most straightforward possibility is a proton hop between two neighboring carbon atoms or the 1,2-hydride shift. Secondly, a proton hop can occur between the first next nearest neighbour carbon atom and the protonated carbon, also called the 1,3-hydride shift. The ease of this transition can be understood, given that the carbon chain occurs often in a trans configuration. A third option is a 1,5-hydride shift, which is only an option if the positive charge is not situated at the center of the chain and if the chain has a high mobility, which is the case for a linear chain. This requires a local folding of the chain, enabling a transition over a 6-ring transition state.

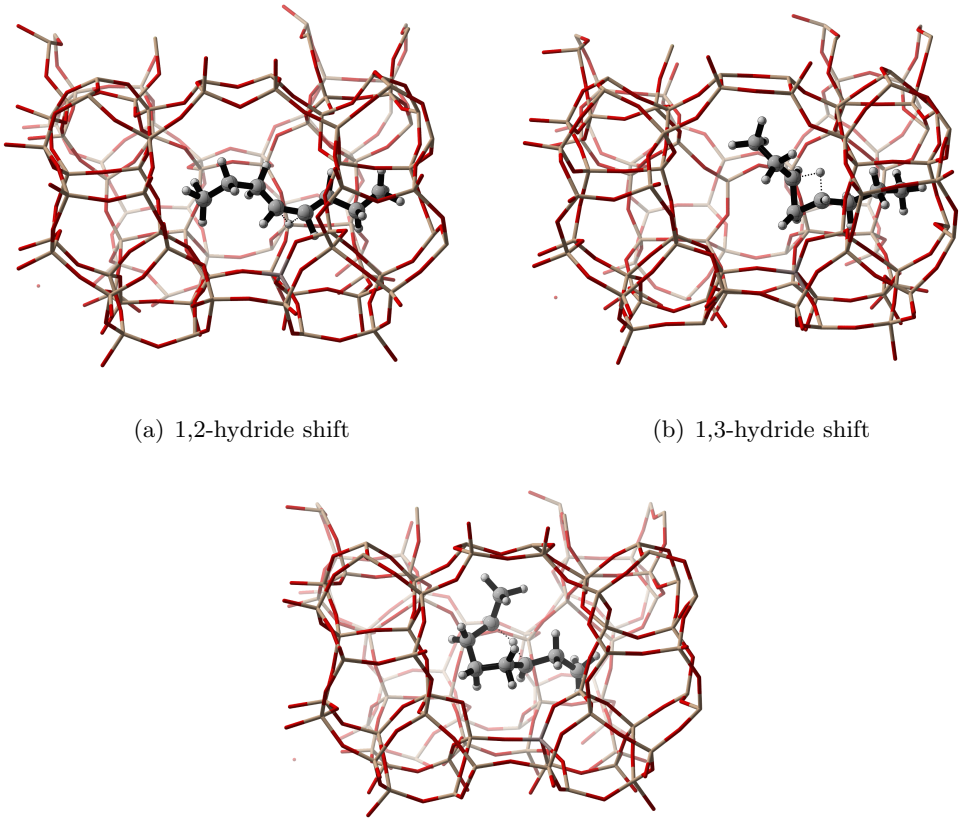

(a) 1,2-hydride shift

(b) 1,3-hydride shift

(c) 1,5-hydride shift

Figure 5.6: Snapshots of frames showing the three types of isomerization for the linear octyl chain

A first qualitative impression of the number of proton transitions can be obtained by plotting the evolution of the initial $C-H$ bond distances for atom C_2 to C_7, as shown in Figure 5.7 and Appendix C.2. Apparently, a lot of hydride transfers occur over the course of the production run. Most changes are situated at the central hydrogen atoms on C_4, C_5 and C_6, while only few transitions take place at C_2 and C_3. Figure 5.7(c) shows that H_c on the third carbon atom even lacks a single transition. Figure 5.7(d) shows

that the hydrogen, initially situated at the central, positively charged carbon undergoes only transitions of about 1.0 Å, i.e., to a neighboring carbon atom. In contrast, some transitions of about 3.0 Å take place in Figure 5.7(b), corresponding to a 1,3-hydride shift transition, while in Figure 5.7(a) even jumps of about 5.0 Å are observed, corresponding to the cyclic 1,5-hydride transfers.

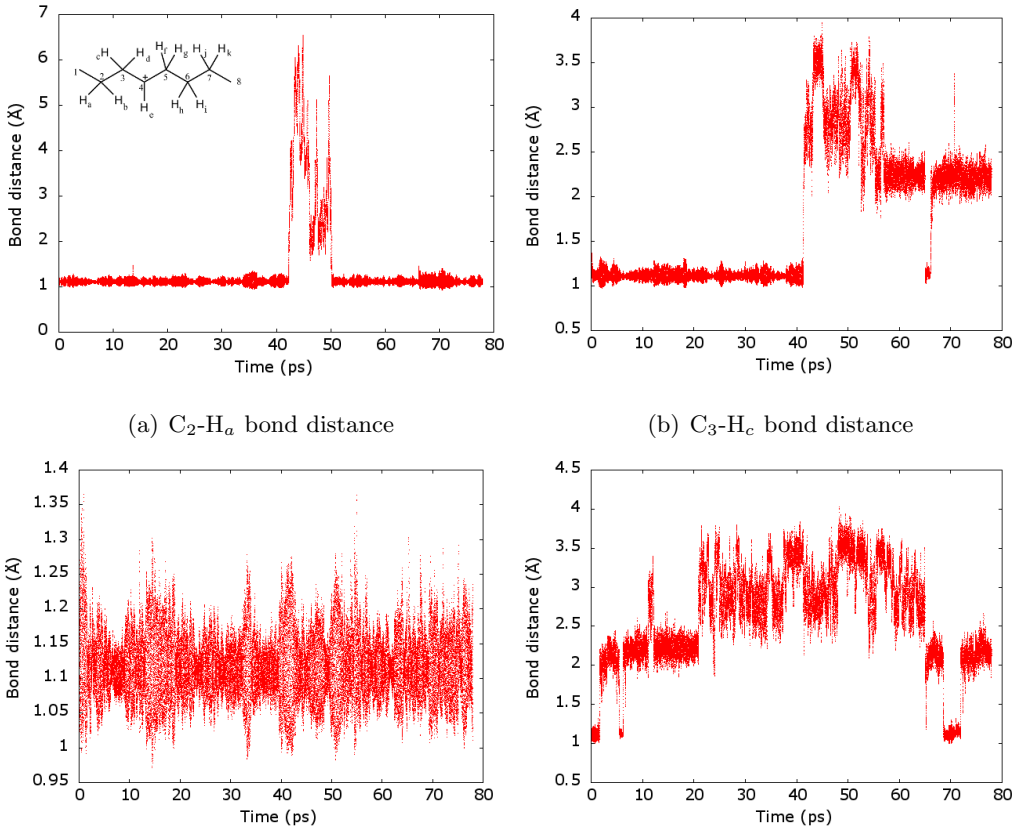

(a) C_2-H_a bond distance

(b) C_3-H_c bond distance

(c) C_3-H_d bond distance

(d) C_4-H_e bond distance

Figure 5.7: Evolution of the initial $C-H$ bond distances for C_2 to C_6 on the 2-octyl cation

To quantitatively determine at which chain position the charge is situated at each instant, the following methodology is used. For each frame, the number of hydrogen atoms bonded to each carbon atom is checked. A bond is defined by a cut-off distance of 1.37 Å, which allows sufficient relaxation of the bond due to thermal vibrations. However, for the frames in which the proton is transferring, it is possible that the proton is closer than the cut-off distance to two carbon atoms or that is further away than the cut-off distance from two carbon atoms. Therefore, these frames need to be eliminated from calculating the average position of the charge. Also, deprotonated frames need to be skipped. These frames are recognized by analyzing the distance between the framework oxygens (at the active site) and the hydrogen atoms and counting the number of frames

in which a bond exist with a cut-off distance of 1.23 Å. During this simulation, the alkene exists in its protonated state for 69.8 % of the time and in its deprotonated state during 20.4 % of the time, while it undergoes proton transitions during 9.8 % of the time.

Figure 5.8 is a point plot of the charge position (carbon number) during the simulation. Proton transfer and deprotonated states are indicated as 0. The different transitions as discussed above can be recognized on this graph. For each carbon atom, Table 5.1 shows the fraction of time that the atom bears a positive charge. If only linear carbenium ions would be present in the zeolite pores, this can be translated to molar fractions of the corresponding carbenium ion. Again, a sufficient sampling of the different states is required to draw significant conclusions about the carbenium ion distribution. To this end, the convergence of the fractions with increasing simulation time must be checked. Convergence is achieved if the fractions between two sample points do not differ more than 0.1 %. The evolution of the different carbenium ion fractions is shown in Figure 5.9. For some carbenium ions, the variation between the last two sample points has the same order of magnitude as the fraction of a less prominent carbenium ion, therefore, the sampling time may still be too short to draw definitive conclusions.

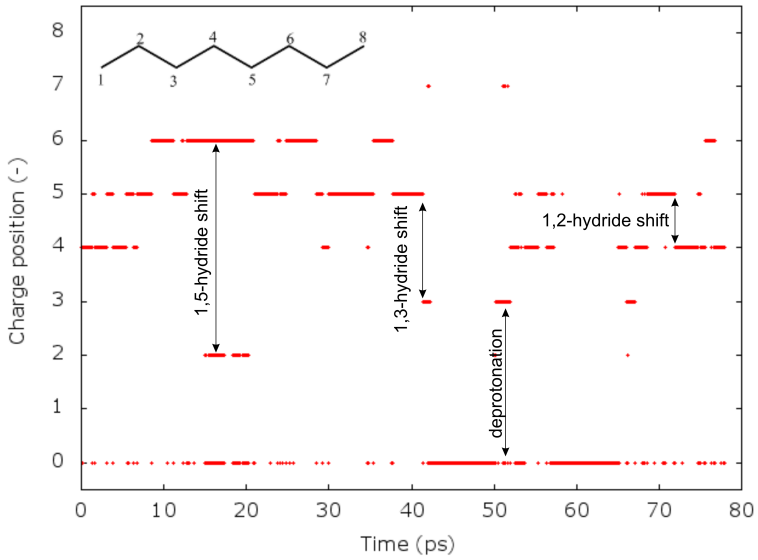

Figure 5.8: Evolution of the positive charge position (carbon number 1 to 8; 0 is a proton transfer or deprotonated state)

Despite the fact that all positions in the chain are secondary carbons, carbenium ion stability appears to differ between the positions. Due to the symmetry of the molecule, the number of chemically different positions reduces to 4. Intuitively, a 4-octyl carbenium

Table 5.1: Fraction of the carbenium ion time frames that the positive charge is situated at each position after a production run of 77.95 ps

Carbon number	Time percentage
C_1	0.00
C_2	1.75
C_3	5.54
C_4	26.63
C_5	39.19
C_6	26.45
C_7	0.44
C_8	0.00
$C_1 + C_8$	0.00
$C_2 + C_7$	2.19
$C_3 + C_6$	31.99
$C_4 + C_5$	65.82

ion is expected to be more stable than a 2-octyl carbenium since the hyperconjugative interactions with both sides of the chain are enhanced. Static 46T-cluster calculations (see Chapter 4) indicated that the 4-octyl carbenium ion is 21 kJ/mol more stable than the 3-octyl carbenium ion, which is in turn 15 kJ/mol more stable than the 2-octyl carbenium ion. Since the difference between the stabilities of the corresponding transition states of β - scission is limited to maximum 10 kJ/mol, the difference in intrinsic activation energy for the different cracking reactions can be attributed to this difference in reactant stability. These observations are also reflected into the calculated carbenium ion fractions, which follow the order $C_4 > C_3 > C_2$.

Figure 5.10 and Appendix C.2 display the evolution of the central $C-C$ bond distances during the production run. From the drop in bond distance, the deprotonated state around 45 ps can be recognized to be 2-octene, while the deprotonated state around 60 ps can be recognized to be 4-octene. The C_3 - C_4 bond shows a lot of peaks, reflecting the vibration towards formation of the β - scission transition state if the positive charge is situated at the C_5 position. This phenomenon is also observed for the C_4 - C_5 distance

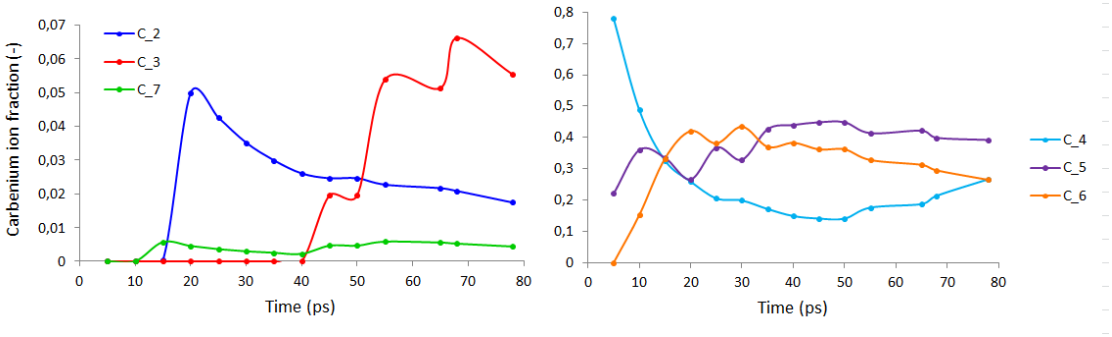

Figure 5.9: Evolution of the time percentage (or molar fraction) of the different possible secondary carbenium ions during the simulation

at instants that the positive charge is either at C_3 or at C_6 situated. Although the charge resides on C_4 for a large fraction of the production run, the peak amplitude is lower compared with the previous examples, which again indicates the higher stability of a C_4 carbocation.

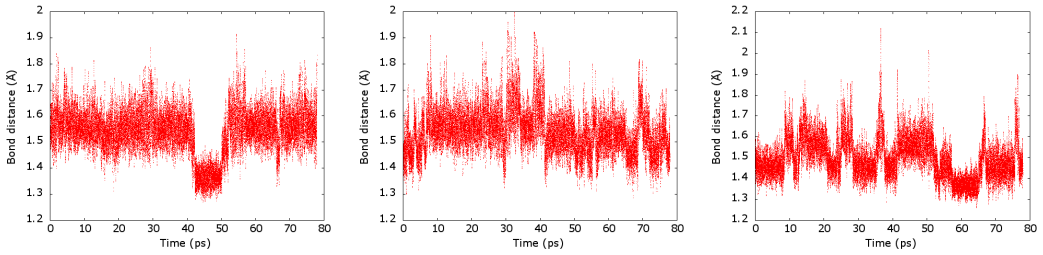

(a) C_2-C_3 bond distance (b) C_3-C_4 bond distance (c) C_4-C_5 bond distance

Figure 5.10: Evolution of the inner $C-C$ bond distances of the 2-octyl cation

If the difference between the initial length of the breaking bond and the final length of the breaking bond is called τ , and the difference of the breaking bond length at the current instant and the initial length is called σ , the degree of advancement of the reaction can be expressed as the ratio $\frac{\sigma}{\tau}$. Static calculations for cracking of a 2-octyl carbenium ion (see Chapter 4) have shown that at the transition state, the reaction has a degree of advancement of 36.3 %, which can be seen as an early transition state according to Hammond's postulate.[43] Analogous results for the other linear carbenium ions leads to the assumption that the stability difference is linked to the product distribution of these reactions. Cracking of the least stable cation will have the lowest activation barrier.

From dynamic simulations on the other hand, it is observed that the 2-octyl carbenium ion will have a much lower molar fraction compared to the 3- and 4-octyl carbenium ion, implying that the the 4-octyl carbenium ion can be expected to have the highest concen-

tration of all isomers. These results are in agreement with the stability order obtained from Chapter 4. To obtain an accurate distinction between the different pathways for linear octyl cation cracking, reaction rates r_i of cation β - scissions must be compared.

$$r_i(T) = k(T) y_i \frac{p_{tot}}{RT}$$

with y_i the molar fraction of carbenium ion with positive charge at carbon i. Clearly, this method requires converged carbenium ion fractions and reliable rate coefficients from static calculations. Nevertheless, based on our static and dynamic simulations, a rough estimate of the product composition can be made.

Cracking of the 4-octyl carbenium ion yields either propene and pentene or ethene and hexene, cracking of the 3-octyl carbenium ion yields two butene species and cracking of the 2-butyl cation yields propene and pentene. For each time scission of the 3-octyl carbenium ion occurs, scission of the 2-octyl carbenium ion occurs approximately 9 times, while scission of the 4-octyl carbenium ion occurs only 0.1 times with a propene and pentene as product and 0.8 times with an ethene and hexene product. These preliminary calculations indicate that cracking of a linear octyl chain will result in higher propene than butene yields, in agreement with experimental results.[30,125,127] It should also be noted that in reality a mixture of differently branched chains will be present in the zeolite pores.

5.3 An octyl chain with a single methyl branch

Another straightforward path for butene dimerization is the reaction of a 2-butyl cation with 1-butene, forming a single branched 5-methyl-3-heptyl cation. In Chapter 4, we studied the cracking of an isomer, 5-methyl-2-heptyl cation (Reaction (4.6)), which has the same carbon skeleton. To observe the occurence of this cation, it was also chosen as initial geometry for a molecular dynamics simulation. Figure 5.11 summarizes the simulated chain configurations, isomerizations and the most important corresponding cracking pathways. In Chapter 4, cracking of the 3-methyl-3-heptyl cation (Reaction 4.1), which has the same backbone structure, has also been investigated. During the equilibration run, a deprotonation occurs to the 5-methyl-2-heptene species and a protonated framework (see Figure 5.12), which is the start of a production run of 44.52 ps.

Figure 5.13 shows bond distances between two different framework oxygens and hydrogens. After about 4 ps, reprotonation of the alkene takes place, followed by proton hops between the two secondary carbon atoms, C_2 and C_3 with a preference for the more stable C_3 position. However these atomic positions are not the most stable positions in the chain and a relatively fast deprotonation to a different framework oxygen occurs,

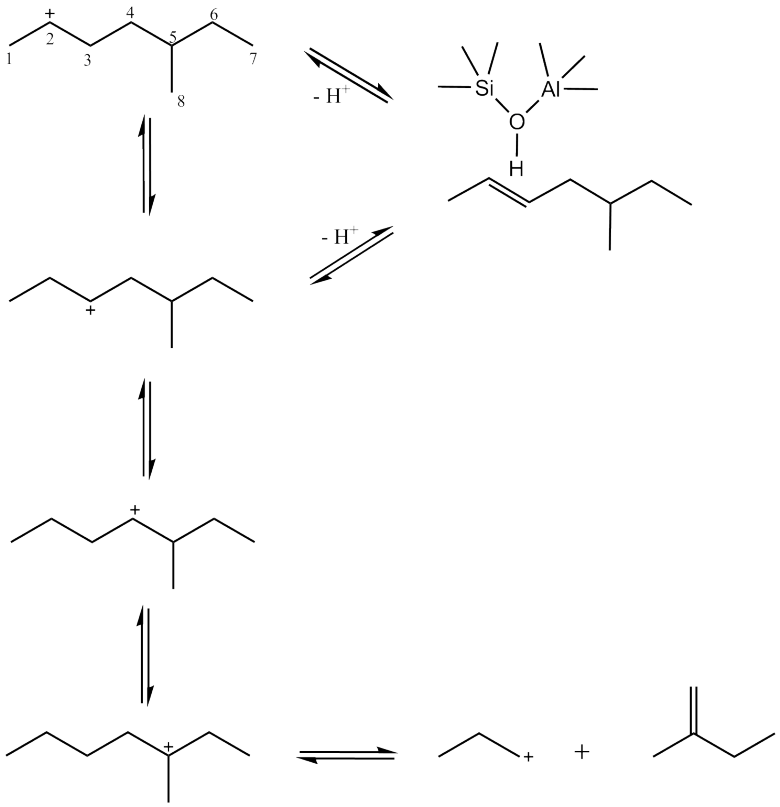

Figure 5.11: Overview of sampled isomers and deprotonation reactions, together with feasible cracking reactions for a 5-methyl-2-heptyl carbenium ion

forming again a 5-methyl-2-heptene π -complex (see Figure 5.12). During the remainder of the production run, the alkene remains deprotonated, which can be understood since protonation is usually an activated process [88] and the barrier will be higher to form a secondary cation at the C_3 position compared to the C_4 position for example. Longer sampling times are required to observe sufficient transitions to determine the equilibrium between the π -complex and the carbenium ion state.

A tertiary carbenium ion is expected to be more stable than a secondary one, hence the question remains if the proton hops allow the positive charge to find the tertiary carbon atom before deprotonation will occur. Therefore a second production run with reinitialized velocities and a length of 18.05 ps is performed. Although this simulation is too short to draw decisive conclusions, it is interesting to analyze the results qualitatively. Note that proton transfers take place relatively fast as can be seen from some $C - H$ bond distances in Figure 5.14. Once the positive charge has shifted to the tertiary C_5 position, no proton shifts to neighboring nor deprotonation occurs. Apparently, a second way, next to alkene formation, is possible to rearrange the secondary carbenium to a stable minimum on the potential energy surface, i.e. by hydride shift isomerization

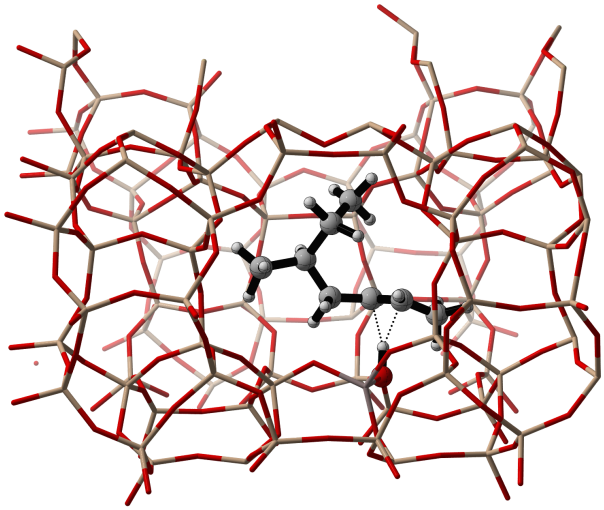

Figure 5.12: Snapshot of a frame showing the π - complex state of the 5-methyl-2-heptyl chain

to a tertiary carbenium ion.

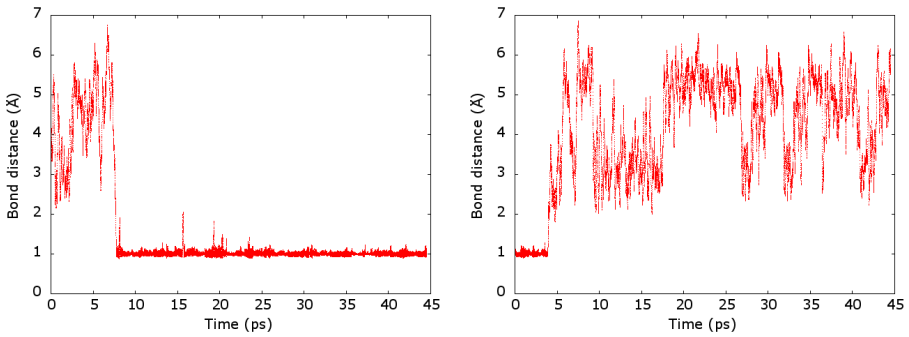

(a) O-H bond distance 1 (b) O-H bond distance 2

Figure 5.13: Evolution of two bond distances between a central hydrogen of the 5-methyl-2-heptyl cation and a framework oxygen during the first production run

Since a methyl branch is present in the chain, methyl shifts might also be expected to be sampled next to hydride shifts. However, the activation barrier for these type of isomerizations is clearly too high to be observed on the timescale of these production runs.

If the two runs are placed after each other, an evolution of the positive charge position through the chain can be plotted (see Figure 5.15). The primary carbon positions C_1, C_7 and C_8 bear no charge at any point during the production runs. The secondary C_6 position is also bonded to two hydrogen atoms during the entire simulation. Further-

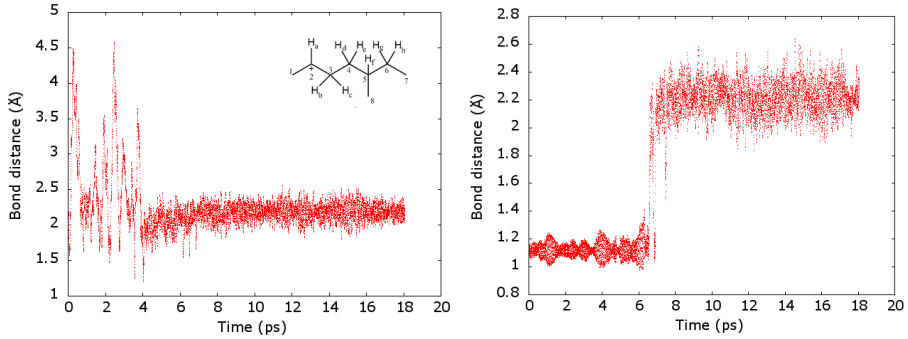

(a) C_3-H_c bond distance (b) C_4-H_e bond distance

Figure 5.14: Evolution of some initial, inner $C-H$ bond distances of the 5-methyl-2-heptyl cation during the second production run

more, the difference in stability between the other secondary carbenium ions and the tertiary carbenium ion or the deprotonated alkene is apparently so large, it will almost spontaneously rearrange to one of the more stable minima, from which it cannot escape anymore.

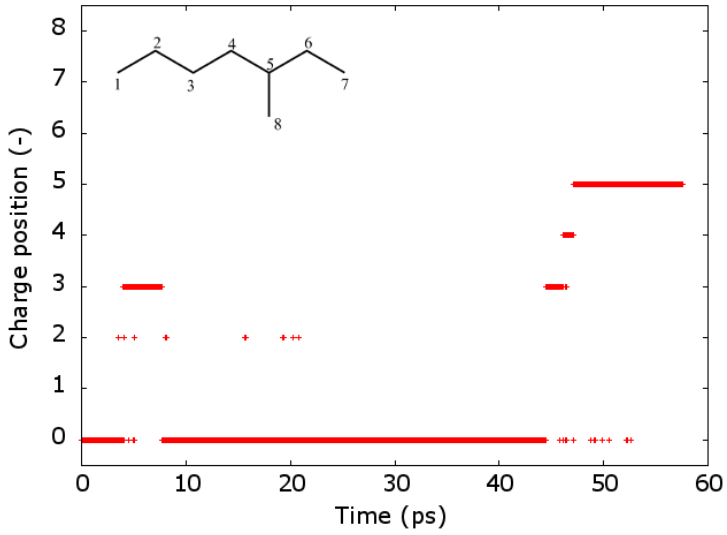

Figure 5.15: Evolution of the positive charge position (carbon number 1 to 5; 0 is a proton transfer or deprotonated state)

If it is assumed that Figure 5.15 gives an accurate view of a real situation, it can be concluded that in contrast to a linear octyl chain, secondary carbenium ions will only exist for a short time as transition carbenium ions to a more stable state. Once these minima on the PES are reached, there is little to no tendency to rearrange further, hence

the only feasible, long-lived reactant for β - scission for this chain is the 3-methyl-3-heptyl carbenium ion, which forms 2-methyl-1-pentene and propene (upon desorption) as products. The simulation time achieved for these species is however too short for statistical significance and hence for calculation of reaction rates. Based on our results with this relatively short simulation length, cracking of the tertiary species (Reaction (4.1)), yielding propene and pentene can be expected to have a high contribution for this carbon skeleton.

5.4 An octyl chain with two methyl branches

As example component for the double branched backbone species, a 2,5-dimethyl-3-hexyl cation was selected. This isomer can in theory be formed via a 1,2-hydrogen shift of a 2,5-dimethyl-2-heyxl carbenium ion, a dimer from 2 isobutene species. Cracking of this isomer corresponds to Reaction (4.12) and has been investigated in Chapter 4. A molecular dynamics simulation has been performed with a production run of 40 ps to observe the behavior and occurrence of this ion. Figure 5.16 gives an overview of the sampled states with the most important cracking pathway.

During the equilibration run, a fast isomerization occurs to a 2,5-dimethyl-2-hexyl carbenium ion. The enhanced stability of tertiary carbenium ions seems to suggest that the charge distribution will be tilted towards the tertiary ion. The results show that the charge remains located on the tertiary carbon atom during the entire production run. A single attempt for a proton transfer to a neighboring secondary carbon atom is immediately followed by shifting the proton back to the tertiary position. This indicates that the tertiary ion is indeed more stable than a secondary cation and that either the barrier for a proton shift to a secondary carbon will be too high to simulate or that the simulation time was insufficient for a statistical significant sampling.

Again transitions between the protonated alkene and the corresponding π - complex are simulated. Although theoretically the alkene can either be formed by proton transfer from two primary carbon atoms resulting in an alkene with a terminal double bond or by transfer form one secondary carbon atom resulting in a 2-alkene, the simulation run will only sample transitions from the latter type, which is in agreement with the higher expected stability of a 2-alkene. Figures 5.17(a) and 5.17(b) display the distances between the framework oxygen and the two secondary hydrogens. On a regular basis, there is a tendency towards deprotonation and both hydrogen atoms are transferred to the framework during the run, respectively around 10 ps and 30 ps with a total time interval of the deprotonated state is 4.1 ps. The equilibrium is thus shifted towards the tertiary carbenium ion and at a temperature of 560 °C, the equilibrium coefficient can be estimated at 8.84, the free energy difference at -15.1 kJ/mol. Clearly, the tertiary

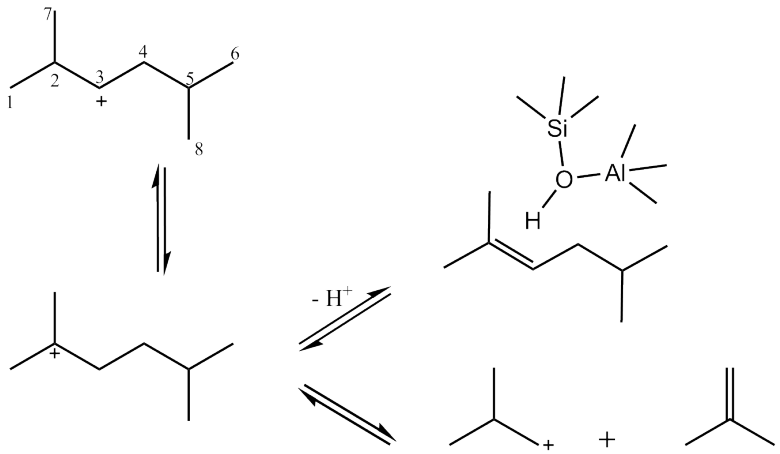

Figure 5.16: Overview of sampled isomers and deprotonation reactions next to feasible β - scission reactions for a 2,5-dimethyl-2-hexyl carbenium ion

carbenium ion is more stable than the alkene state, which is translated in a reaction equilibrium that is shifted to the cationic species.

In contrast with the previously discussed backbone structure, there is only one feasible pathway for cracking due to the symmetry of the structure: β - scission of a 2,5-dimethyl-2-hexyl carbenium ion into isobutene and an isobutyl cation. Figure 5.17(c) shows the α C - β C bond distance evolution. Bond elongations towards the transition state geometry can be recognized. Apparently, this species will barely produce propene (or ethene), therefore this species is unlikely to be the most abundant cracking reactant in the zeolite pores.

Other chain configuration with two methyl branches are more prone to light olefin formation upon cracking. As an example, the 2,4-dimethyl-4-hexyl carbenium ion has been simulated (see Figure 5.18). In Chapter 4, Reaction (4.5), Reaction (4.9) and Reaction (4.10), with the same backbone structure, have been studied. Only the latter is indicated on Figure 5.18. During a production run of 35 ps, the positive charge remains at its initial, tertiary position. The stability of this species is clearly rather high, hence making β scission of this carbenium ion a feasible pathway for the production of propene (and 2-methyl-1-pentene).

Theoretically, two different cracking reactions are possible for the 2,4-dimethyl-4-hexyl carbenium ion: β - scission of the central α C - βC bond or β - scission of the terminal α C - βC bond. The latter path is however less probable since it involves formation of a methyl cation in the transition state. The premise that it could practically be neglected is confirmed by Figure 5.19, displaying both bond distances. The vibration amplitude and consequently the bond elongation is much less pronounced for the terminal bond

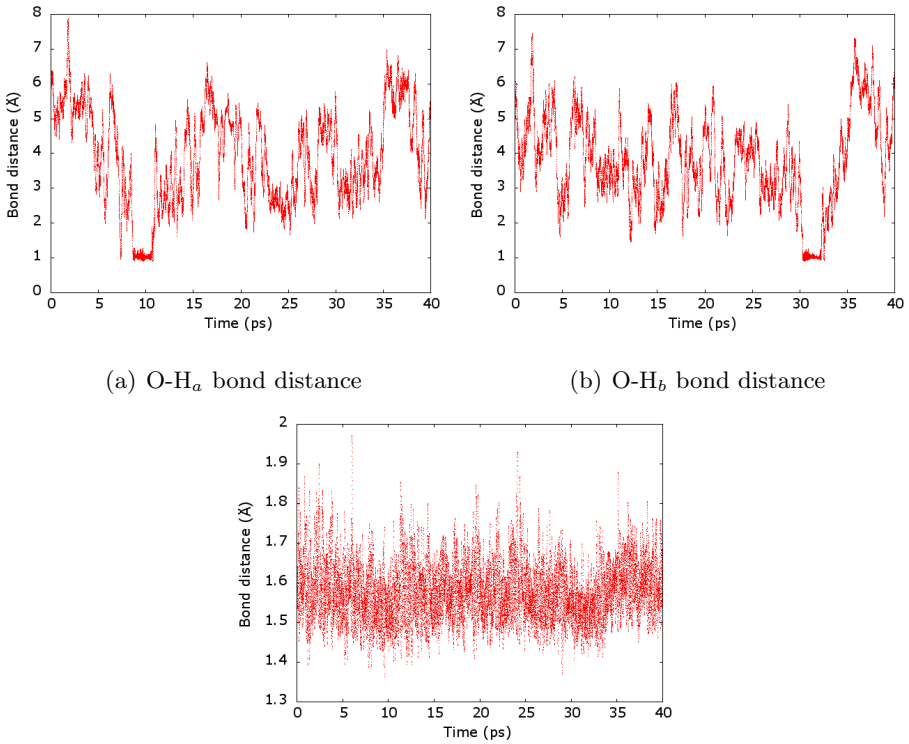

(a) O-H_a bond distance

(b) O-H_b bond distance

(c) α C - β C bond distance

Figure 5.17: Evolution of the framework O-H bond distances and of the α C - β C bond distance with respect to the tertiary carbon on the 2,5-dimethyl-2-hexyl cation

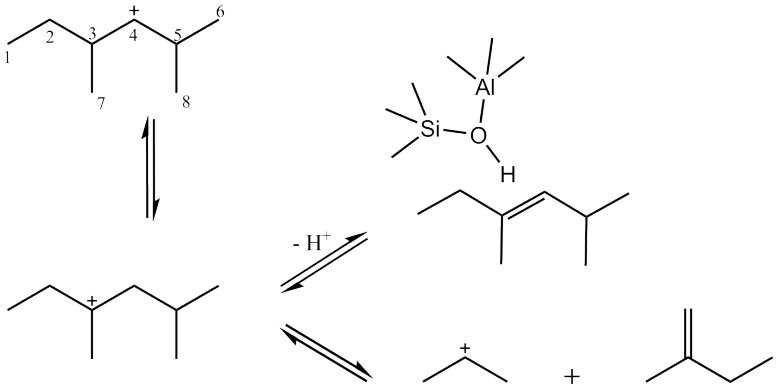

Figure 5.18: Overview of sampled isomer states, deprotonation reactions and feasible cracking pathways for a 2,4-dimethyl-2-hexyl carbenium ion

than for the central bond, indicating that the latter bond elongations are closer to the transition state and that he activation energy will be lower for the central β - scission.

Analogously to the previous carbenium ion species, transitions between the protonated

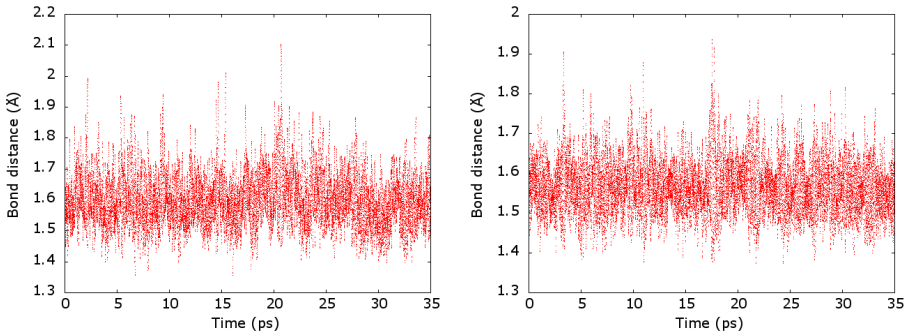

(a) central α C - β C bond distance (b) terminal α C - β C bond distance

Figure 5.19: Evolution of the α C - β C bond distances with respect to the tertiary carbon on the 2,4-dimethyl-4-hexyl cation

alkene and the deprotonated (physisorbed) alkene are simulated. The physisorbed alkene exists for about 1.15 ps of the production run. From Figure 5.19(a), the deprotonated state around 30 ps can be recognized from the local decrease in the bond length since a C - C π - bond is formed. An equilibrium coefficient value of 29.54 and free energy difference of -23.4 kJ/mol can be estimated based on this single run. These results are comparable to the 2,5-dimethyl-2-hexyl cation. Note that, in comparison to the octyl cation (Section 5.3), the equilibrium is shifted more towards the protonated state, a reflection of the higher stability for tertiary carbenium ions.

5.5 An octyl chain with three methyl branches

Only one triple branched octyl species was studied with static calculations: a 2,4,4-trimethyl-2-pentyl cation. Cracking of this C_8 isomer has been studied in Chapter 4 as Reaction (4.13). A molecular dynamics simulation has been performed to observe the behavior of this highly branched molecule. A production run of 40 ps has been simulated. The simulated isomers for this chain, together with deprotonation and possible cracking reactions are given in Figure 5.20.

Compared to previous cationic species (with the exception of the 2,5-dimethyl-2-hexyl carbenium ion), the current simulation indicates that the chain moves more slowly through the zeolite channels and remains most of the time at the same position. Probably, the number of degrees of freedom is strongly reduced due to the high branching degree of this chain, which shows steric repulsion with the walls of the zeolite channel. This entropy reduction is known as the confinement effect of the zeolite catalyst (H-ZSM-5). In large pore zeolites, a different mobility effect can be expected. Consequently, (un)folding of the carbon skeleton is prohibited, resulting in a reduced flexibility

of these species.

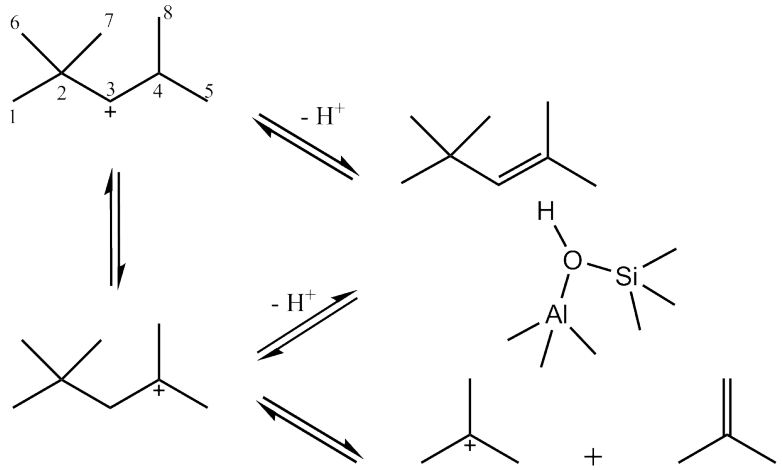

Figure 5.20: Overview of sampled isomer states, deprotonation and reaction pathways for a 2,2,4-trimethyl-4-pentyl carbenium ion

The possibilities for hydride shifts within this carbenium ion are very limited. The molecule possesses four primary carbon atoms. It was previously established that the positive charge will never reside on a primary carbon during the simulations. The quaternary carbon atom also cannot bear a positive charge since no methyl shifts are simulated. This leaves only two positions for the charge, i.e., the tertiary carbon atom C_t or the neighboring secondary carbon atom C_s. Only the two protons, initially bonded to the C_s atom may undergo proton shifts to the C_t atom and vice versa, as shown in Figure 5.21.

Again, a transition between the physisorbed 2,4,4-trimethyl-2-pentene and its corresponding carbenium ion is simulated. A highly branched alkene has a larger proton affinity, hence the stability of the protonated species increases compared to the π - complex and an equilibrium that is shifted towards the carbenium ion state, can be expected. Simulation results confirm this hypothesis since only during 0.331 ps the carbenium ion is deprotonated to the framework. Figure 5.22(a) shows the distance between the framework oxygen and the transferred hydrogen. Only in a short time interval around 28 ps, the bond distance is approximately 1 Å, corresponding to a protonated zeolite. From these results, the equilibrium coefficient at 560 °C is estimated to be 119.85 and the corresponding free energy difference at -33.1 kJ/mol. Due to the compact structure of the tertiary cationic species, the stability difference is quite large, which causes the equilibrium of the reaction shifted strongly towards the protonated state.

The stability order of the carbenium ions indicates that the positive charge will prefer

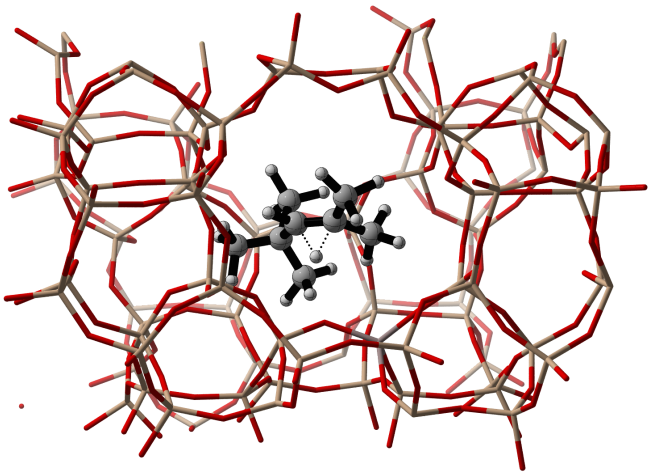

Figure 5.21: Snapshot of a frame showing the 1,2-hydride shift between a C_t and C_s position on the 2,4,4-trimethyl-2-pentyl chain

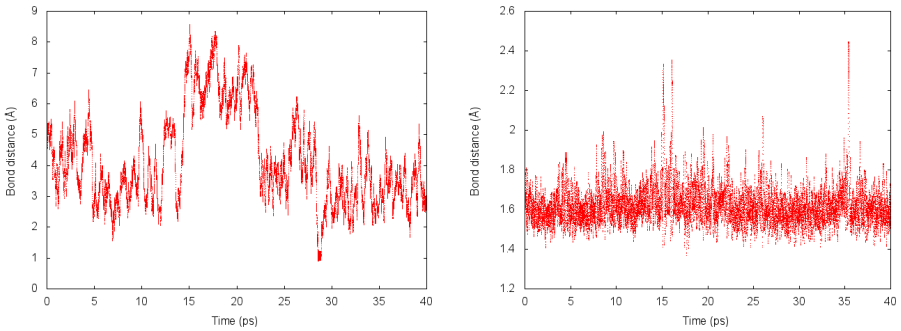

(a) O-H bond distance

(b) α C - β C bond distance

Figure 5.22: Evolution of the framework O-H bond distance and of the α C - β C bond distance with respect to the tertiary carbon on the 2,4,4-trimethyl-2-pentyl cation

the tertiary carbon atom over the secondary carbon atom. This is confirmed by our simulations. Figure 5.23 displays the distance between the secondary carbon atoms and the two hopping protons. From time to time, a small peak in the distance, corresponding to a proton transfer can be observed. However, these proton hops are rare and once a proton has left the C_s to the C_t position, it almost instantaneously returns to its original state. The higher stability of a tertiary cation is thus so distinct, almost no secondary cations will occur. Furthermore, the bond distance does not double at these transfers, indicating that the state with the proton at the C_t position is not fully relaxed before the proton shifts back to the C_s position. Also note that the large peak around 28 ps

corresponds to the deprotonated state.

Figure 5.22(b) shows the distance between the α C and β C in this configuration. Clearly, the average bond distance is higher than a normal $C-C$ bond distance of 1.54 Å. Some peaks in the oscillations indicate that the bond may be elongated to about 2.5 Å. The bond vibrations show that at certain moments, a motion upwards the potential hill, towards the cracking transition state, occurs, indicating the ease for β - scission of this 2,4,4-trimethyl-2-pentyl species.

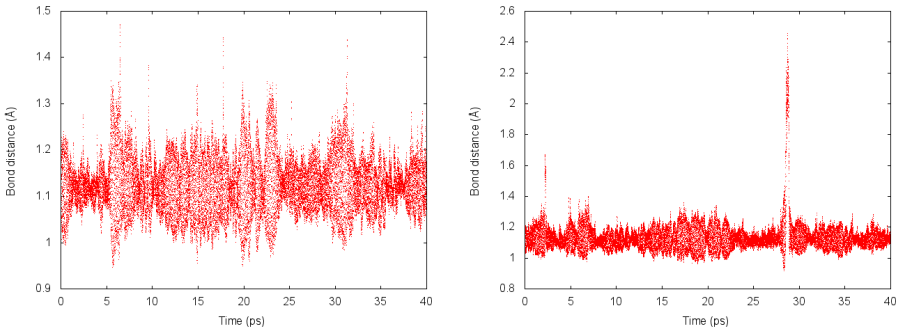

(a) C_s-H_a bond distance (b) C_s-H_b bond distance

Figure 5.23: Evolution of the secondary C-H bond distances on the 2,4,4-trimethyl-2-pentyl cation

The relative molar fractions of the two possible carbenium ions can be calculated using the statistical averaging methodology from section 5.2. During 1.2 % of the time, proton transfer occurs. At the end of the production run of 40 ps, it is estimated that 99.8 % of the time, the charge is located at the C_t postion, while only 0.2 % at the C_s position. From Figure 5.24, showing the evolution of the molar fractions of secondary and tertiary carbenium ions during the production run, it can be seen that the absolute figures are almost converged. Clearly, the positive charge resides at the tertiary carbon atom for the majority of the time.

If the charge would be situated at the secondary position, all possible cracking routes involve formation of a CH_3^+ cation, hence these are no feasible reaction pathways and the existence of this species is almost irrelevant to the product distribution. If the tertiary carbenium ion undergoes β - scission a t-butyl cation and isobutene species are formed. Since experimental product distributions [30,125,127] indicate a lot of propene formation, this species will again probably not have the highest concentration in the zeolite pores. A combination of the confinement effect, the low mobility of the highly branched species and the small number of possible isomers leads to the conclusion that the 2,4,4-trimethyl-2-pentyl cation will not be part of the most feasible pathways for

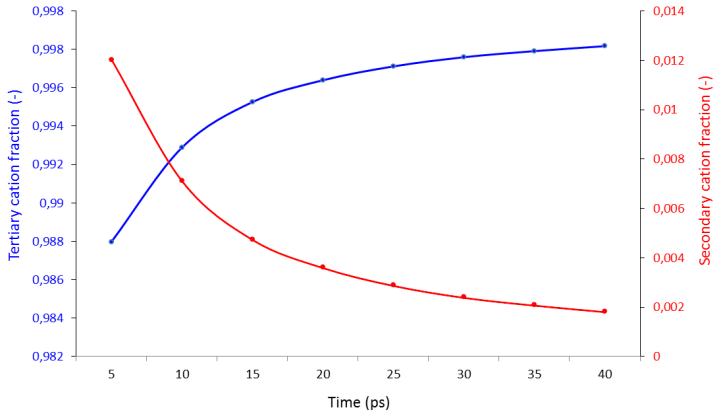

Figure 5.24: Evolution of the time percentage (or molar fraction) of the tertiary carbenium ion (blue) and the secondary carbenium ion (red) during the simulation.

butene cracking, despite its high stability.

5.6 Conclusion

MD simulations provide insights in the intermediates, present in the zeolite pores. Combined with static calculations, information can be extracted about the relative importance of different cracking pathways. Since butyl cations can only survive during a very short time period and the barrier for cracking is quite high, direct β - scission of these species can almost be excluded. Regarding octyl carbenium ions with different branching degrees, transitions between the protonated and deprotonated states are sampled. If stable tertiary cations can be formed, which is the case for the species with a higher degree of branching, the equilibrium of the deprotonation reaction is typically shifted towards the protonated state. Frequent proton hops are observed between the different chain positions. After elimination of the frames in which the hydride shifts occur, the molar fractions of each positive charge position can be determined. If tertiary carbon atoms are present, the positive charge will reside most of the time on this position, reflecting the higher stability of tertiary carbenium ions. If only secondary carbon atoms are present, the positive charge will most likely reside on the central carbon atoms, resulting in the most stable intermediates.

Chapter 6

Conclusions and future outlook

Over the past decades, the light olefin demand has steadily increased due to the expanding polymer industry. The lion's share of ethene and propene production is based on traditional steam pyrolysis and catalytic cracking of crude oil or natural gas derivatives. However, chemical industry will be faced with two major challenges in the near future. First, the potentially dangerous impact of climate change needs to be addressed by reducing greenhouse gas emissions, using renewable feedstock and maximizing energy efficiency of processes. The transition to a 'green' chemistry and the search for alternative feedstocks is reinforced by the depletion of the oil reserves. Secondly, the recent discovery and exploitation of shale gas in the USA has given a boost to natural gas based technologies. In the Middle East, large ethane crackers have become operational. However, cracking ethane from natural gas or shale gas as feedstock produces mainly ethene, what resulted in a propene shortage, causing the propene price to overtake the ethene price. To meet the annually increasing propene demand, several on-purpose technologies can be expected to become economically interesting.

One of the most promising alternative technologies is the methanol-to-olefins (MTO) technology. Methanol can be synthesized from feedstocks varying from coal over natural gas to biomass. A second advantage of this process is the large range in which the propene to ethene yields can be tuned. Another on-purpose technology is the cracking of olefins in the C_4 - C_{10} cut. Olefin cracking plays an important role in both these upcoming technologies as well as in the traditional fluid catalytic cracking. In all these industrial processes, the H-ZSM-5 zeolite, characterized by its shape selectivity, is one of the most used catalysts.

In this dissertation, cracking of butene as a model component on H-ZSM-5 is studied using computational modeling. Catalytic cracking of butene is a complex process involving isomerization, oligomerization and cracking reactions. In the literature, a carbenium ion based cracking mechanism has been proposed. A single butene molecule can either

undergo immediate β - scission, following the so-called monomolecular cracking path or can first dimerize before undergoing β - scission, the so-called bimolecular cracking path. The latter has been suggested to be the most prominent route. Experimental studies have shown that the product distribution consists mainly of propene, followed by butenes. Furthermore, theoretical studies have indicated that scissions towards propene have typically higher rates compared to scissions towards ethene.

Although, the carbenium ion mechanism is generally accepted in the literature, there is still a lot of discussion about the exact nature of the reaction intermediates. A key question is whether carbocations are long-lived species in the zeolite pores or will quickly rearrange to a more stable structure like framework-bound alkoxides. Due to the difficult experimental validation of the existence of simple alkyl carbenium ions, molecular modeling can be applied to elucidate this issue. In theoretical studies, carbenium ion stability was found to be influenced by two main factors: stabilizing electronic effects and destabilizing steric constraints.

To determine which reaction pathways are feasible routes for light olefin production, several cracking reactions have been modeled with static calculations on a 46T-cluster model of H-ZSM-5. A two-layer ONIOM(B3LYP/6-31+g(d,p):pm3) scheme has been used for geometry optimizations. A single point energy calculation has been performed at the ωB97X-D level of theory, including dispersion interactions, to obtain reliable energies. Kinetic coefficients were determined from transition state theory. To obtain insights in the behavior of the intermediate species in the zeolite environment, ab initio molecular dynamics simulations have been carried out on a periodic model at the revPBE level of theory. The NPT ensemble has been sampled in simulations between 40 and 80 ps with a sampling period of 0.5 ps.

First, the monomolecular cracking pathway has been investigated. Only a single cracking reaction belongs to this class: β - scission of a 1-butyl cation to ethylene and an ethyl cation. Formation of the unstable ethyl cation in the transition state results in rather high activation barriers. A 'free' ethyl cation is not a stable minimum on the potential energy surface; it spontaneously rearranges to an ethoxide species during product optimization. The 1-butyl cation appears also not to be a stable species since it rearranges via a barrierless transition to a 2-butyl cation during reactant optimization. In general, primary carbenium ions are not found as stable minima on the PES. Molecular dynamics simulations confirm that even the secondary butyl carbenium is unstable and will be short-lived in the zeolite environment.

Since the monomolecular cracking pathway is a rather high-barrier route towards ethene production and cannot be invoked to explain propene production, bimolecular cracking routes have been investigated. Assuming that isomerizations occur on a smaller time

scale than cracking reactions, an organic pool with a broad range of C_8 isomers will exist inside the zeolite pores. To get a systematic view on this complex reaction system, the possible β - scissions have been grouped first by the class of products (two C_4, a C_5 and C_3 or a C_6 and C_2 alkene) and secondly by the carbenium transition type (e.g. tertiary - primary, secondary - primary). Based on the observations for the butyl carbenium ions, primary octyl carbenium ions were also assumed to be unstable, therefore only transitions starting from secondary and tertiary carbocations have been studied. This assumption was further validated by the MD simulations. The most notable insights are listed:

- The cationic type of the transition state (and product state) is the main factor determining the free energy barriers, following a decreasing trend in the order: primary > secondary > tertiary products.
- A second factor determining the free energy barriers is the stabilization of the reactant state with the barriers for cracking of secondary reactants being typically lower than for cracking of tertiary reactants.
- Cracking reactions towards a C_3 and C_5 species appear to be lower activated than reactions towards two C_4 species. This trend is primarily determined by enthalpy differences and is magnified if entropic contributions are taken into account.
- Tertiary carbenium ion products are found to be local minima on the potential energy surface during product optimization, while primary or secondary cation products will stabilize by forming a framework bound alkoxide.

The calculations also show that the 46T-cluster model reaches its limits and is no longer sufficient to accurately describe the interactions with large adsorbates such as some octyl cations. Furthermore, the inability to account for different framework configurations may affect the numerical data of the kinetic parameters.

Next to the intrinsic kinetic coefficients, the ability to form the carbenium ion reactants plays an important role in the determination of the most prominent reaction pathways. Molecular dynamics under typical operating conditions (560 °C) have been carried out on several octyl carbenium ions with different branching degrees to observe their behavior in the zeolite environment and to answer the question if these species are fleeting intermediates or long-living and can be considered as cracking reactants. The confinement effect of the zeolite pores and the stability of the carbenium ions are two crucial factors influencing the nature of the intermediates. The most important conclusions are again summarized:

- In contrast with linear butyl carbenium ion species, octyl cationic species are long-lived in the zeolite environment. No rearrangements to alkoxide species are observed. Transitions between the carbenium ion and the stable alkene are sampled.

- Non-branching isomerizations (e.g. 1,2-hydride shifts) can readily occur, while branching isomerization (e.g. 1,2-methyl shifts) barriers appear to be too high to be sampled at 560 °C.

- If a tertiary carbon atom is present in the chain, which is the case for branched species, the positive charge will mainly reside on this atom. The high stability of tertiary carbenium ions results in an equilibrium that is shifted to the protonated alkene. For a linear chain, frequent hydride shifts occur between the carbon atom positions. In the most stable configurations, the charge is situated at the central positions.

- For highly branched species, the confinement effect of H-ZSM-5 becomes important. The higher the branching degree of the molecule, the lower its mobility appears to be in the zeolite channel.

Highly branched reactants have rather low mobility in the zeolite pores and their corresponding transitions only show limited possibilities for β - scissions. Probably, these species will thus not be the most important. Static calculations suggest that transitions with secondary carbenium ion reactants have the highest rate coefficients, which can be explained by the relative unstability of the reactant state. These results are confirmed by MD simulations, in which tertiary reactants appear to be the most prominent in the zeolite pores. This is not surprising given the higher stability of tertiary cations compared to secondary cations. Transitions leading to primary products are typically highly activated due to the formation of unstable species in the transition state. Based on these considerations, a major contribution to the cracking products by secondary - secondary and tertiary - secondary transitions can be expected, although this requires further investigation.

MD simulations allowed to calculate relative concentrations for linear octyl carbenium ion species and combined with the rate coefficients obtained from static calculations, relative β - scission rates have been compared. Preliminary calculations have shown that the propene production rate is higher than the butene or ethene production rate, in agreement with the expected product distribution. However, in reality the organic pool will exist of a broad range of C_8 isomers with different branching degrees. To draw accurate conclusions from the relative reaction rates, the global composition of all C_8 species inside the zeolite pores should be known and the question how fast branching isomerizations (methyl shifts) will occur and what the contribution of the species with different branching degrees will be, need to be answered. Currently this piece of the

puzzle is still lacking. Advancements in molecular modeling can allow to take on this challenge at a higher level and to elaborate this study further. An extended cluster model or metadynamics simulations can be used to increase the accuracy of the calculated activation barriers. Via a combination of the latter with the distribution of the organic species as obtained by MD simulations, reaction rates can be calculated and used to make a further discrimination between different reaction paths.

Other questions related to the alkene cracking process also remain unanswered. What is the importance of secondary reactions to the cracking product distribution? Which differences exist between cracking of butene or pentene and cracking of larger olefins? What is the effect of the zeolite composition and topology and how can this be used to tune the P/E ratio? Answering these and other questions will require extensive additional studies combining the efforts of experimental and theoretical researchers.

Appendix A

Bimolecular cracking results

In this appendix, an overview of the bimolecular cracking results is given. Table A.1 summarizes the kinetic parameters of the forward and backward reactions. In Table A.2, the thermodynamic parameters (activation barriers, activation entropy, reaction energies and reaction entropy) are listed. The enthalpies and entropies of reactant, transition state and product complexes are given in Table A.3 with reference to the species of Reaction (4.1). Finally, Table A.4 contains the geometric parameters of the optimized reactant, transition and product states. Below, an overview of the investigated reactions is given.

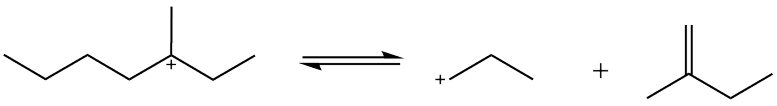

(4.1)

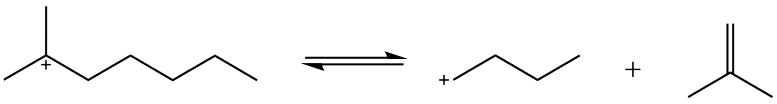

(4.2)

(4.3)

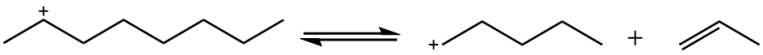

(4.4)

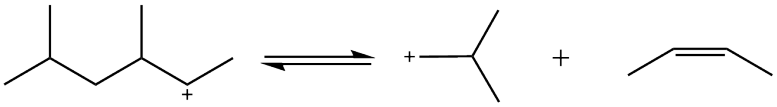

(4.5)

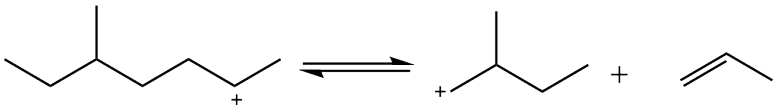

(4.6)

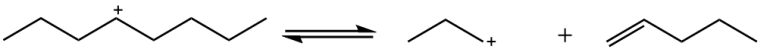

(4.7)

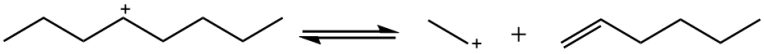

(4.8)

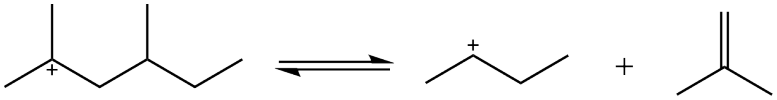

(4.9)

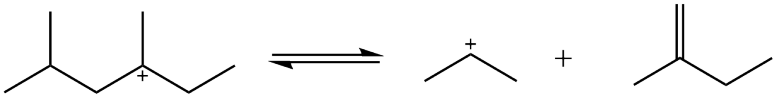

(4.10)

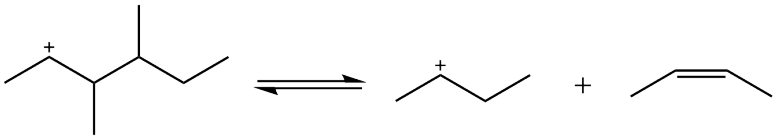

(4.11)

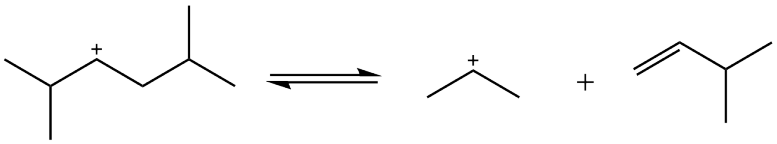

(4.12)

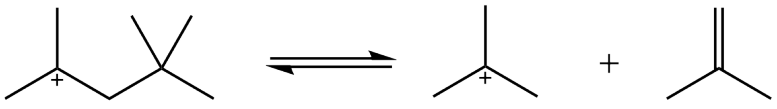

(4.13)

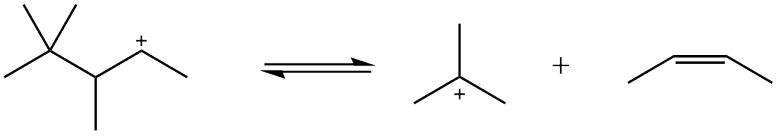

(4.14)

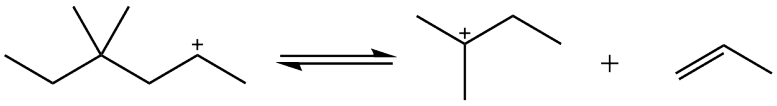

(4.15)

Table A.1: Intrinsic kinetic parameters at 833 K for the bimolecular cracking reactions (LOT : ωB97X-D/6-31+g(d,p)//ONIOM(B3LYP/6-31+g(d,p):pm3))

No.	Forward reaction			Backward reaction		
	A	E_a	k_{fwd} $(833K)$	A	E_a	k_{bwd} $(833\ K)$
	s^{-1}	$kJ\ mol^{-1}$	s^{-1}	s^{-1}	$kJ\ mol^{-1}$	s^{-1}
(4.1)	6.21E+12	121.87	1.42E+05	6.92E+11	105.38	1.70E+05
(4.2)	1.61E+14	85.14	7.02E+08	3.02E+11	102.61	1.11E+05
(4.3)	2.74E+12	68.94	1.30E+08	3.47E+11	110.03	4.36E+04
(4.4)	5.42E+13	55.83	1.71E+10	1.19E+13	110.15	1.47E+06
(4.5)	3.32E+14	87.38	1.10E+09	7.75E+10	119.85	2.46E+03
(4.6)	2.35E+13	57.86	5.52E+09	2.39E+00	146.44	1.57E+01
(4.7)	8.27E+12	97.76	6.12E+06	5.35E+11	116.27	2.73E+04
(4.8)	2.12E+12	73.28	5.38E+07	7.35E+11	105.78	1.71E+05
(4.9)	1.53E+14	88.87	4.08E+08	5.14E+13	72.04	1.56E+09
(4.10)	9.89E+13	89.27	2.49E+08	9.08E+12	82.60	6.00E+07
(4.11)	6.97E+14	66.50	4.71E+10	5.98E+13	102.14	2.35E+07
(4.12)	3.70E+15	46.92	4.23E+12	1.43E+13	128.1	1.32E+05
(4.13)	3.09E+15	46.71	3.63E+12	4.01E+08	42.81	8.29E+05
(4.14)	1.27E+13	-8.09	1.41E+13	2.17E+11	1.34	1.78E+11
(4.15)	9.64E+15	-8.81	3.44E+16	2.26E+10	-38.3	5.69E+12

Table A.2: Thermodynamic reaction parameters at 833 K for bimolecular cracking (LOT : ωB97X-D/6-31+g(d,p)//ONIOM(B3LYP/6-31+g(d,p):pm3))

No.	$\Delta H^{\ddagger}$ $kJ\ mol^{-1}$	$\Delta S^{\ddagger}$ $J\ mol^{-1}K^{-1}$	$\Delta G^{\ddagger}$ $kJ\ mol^{-1}$	ΔH_r $kJ\ mol^{-1}$	ΔS_r $J\ mol^{-1}K^{-1}$	ΔG_r $kJ\ mol^{-1}$
(4.1)	114.97	-16.84	128.99	16.48	18.23	1.29
(4.2)	78.60	10.25	70.06	-17.12	52.22	-60.62
(4.3)	62.05	-23.64	81.74	-41.09	17.19	-55.41
(4.4)	48.93	1.18	47.95	-54.38	12.53	-64.82
(4.5)	80.49	16.26	66.94	-32.19	69.55	-90.12
(4.6)	50.95	-5.78	55.77	-88.58	57.278	-136.29
(4.7)	90.87	-14.45	102.91	-18.51	22.76	-37.48
(4.8)	66.34	-25.78	87.85	-32.50	8.80	-39.83
(4.9)	81.98	9.80	73.81	16.83	9.05	9.29
(4.10)	82.38	6.18	77.23	6.68	19.86	-9.86
(4.11)	59.61	22.42	40.94	-35.63	20.41	-52.64
(4.12)	40.03	36.31	9.78	-81.15	46.25	-119.69
(4.13)	39.82	34.79	10.84	3.96	131.90	-105.91
(4.14)	-7.61	-10.89	1.46	-2.02	33.88	-30.24
(4.15)	-15.71	44.26	-52.57	29.53	107.84	-60.30

Table A.3: Enthalpies and entropies of the reactant (rea), transition state (TS) and product (pro) species at 833 K for the bimolecular cracking reactions with the species of Reaction (4.1) as reference level (LOT : ωB97X-D/6-31+g(d,p)//ONIOM(B3LYP/6-31+g(d,p):pm3))

No.	Enthalpy			Entropy		
	H_{rea}	H_{TS}	H_{pro}	S_{rea}	S_{TS}	S_{pro}
	$kJ\ mol^{-1}$	$kJ\ mol^{-1}$	$kJ\ mol^{-1}$	$J\ mol^{-1}K^{-1}$	$J\ mol^{-1}K^{-1}$	$J\ mol^{-1}K^{-1}$
(4.1)	0.0	0.0	0.0	0.0	0.0	0.0
(4.2)	40.8	4.5	7.2	-44.6	-17.5	-10.6
(4.3)	75.2	22.3	17.6	-12.1	-18.9	-13.1
(4.4)	89.7	23.7	18.9	-31.7	-13.7	-37.4
(4.5)	46.8	12.4	-1.8	-55.9	-22.8	-4.6
(4.6)	166.2	102.2	61.1	-75.7	-64.7	-36.7
(4.7)	54.4	30.3	19.4	-26.1	-23.7	-21.6
(4.8)	88.3	39.7	39.3	-13.2	-22.2	-22.6
(4.9)	18.4	-14.6	18.7	-39.2	-12.5	-48.4
(4.10)	64.2	31.6	54.4	-68.7	-45.6	-67.0
(4.11)	84.6	29.2	32.5	-45.0	-5.8	-42.9
(4.12)	119.4	44.4	21.7	-71.2	-18.0	-43.1
(4.13)	139.5	64.3	127.0	-70.9	-19.3	42.8
(4.14)	143.2	20.7	124.7	-61.5	-55.5	-45.8
(4.15)	119.1	-11.6	132.2	-57.5	3.6	32.1

Table A.4: Geometry parameters (bond distances) for the bimolecular cracking reactions (LOT : ONIOM(B3LYP/6-31+g(d,p):pm3))

No.	Reactant	Transition state		Product	
	$^{+}C-O$	$C_\alpha - C_\beta$	$C_\beta - O$	$C_\alpha - C_\beta$	$C_\beta - O$
	$\mathring{A}$	$\mathring{A}$	$\mathring{A}$	$\mathring{A}$	$\mathring{A}$
(4.1)	4.73	2.49	2.25	3.72	1.50
(4.2)	5.29	2.81	2.23	3.64	1.50
(4.3)	4.75	2.47	2.28	3.64	1.50
(4.4)	4.44	2.46	2.29	3.77	1.51
(4.5)	4.71	2.53	2.35	3.78	1.50
(4.6)	4.92	2.37	2.32	3.88	1.49
(4.7)	4.85	2.49	2.29	3.76	1.50
(4.8)	4.63	2.46	2.20	3.82	1.49
(4.9)	5.24	2.74	2.34	3.55	1.53
(4.10)	5.41	2.63	2.25	3.27	1.54
(4.11)	5.40	2.43	3.10	4.77	1.53
(4.12)	4.79	2.87	2.32	5.05	1.54
(4.13)	7.41	2.27	4.93	7.40	4.04
(4.14)	6.13	2.47	3.67	2.87	3.58
(4.15)	6.82	2.33	4.23	8.66	3.91

Appendix B

Bimolecular cracking transition state geometries

In this appendix, the optimized transition state geometries of all investigated bimolecular cracking reactions are shown.

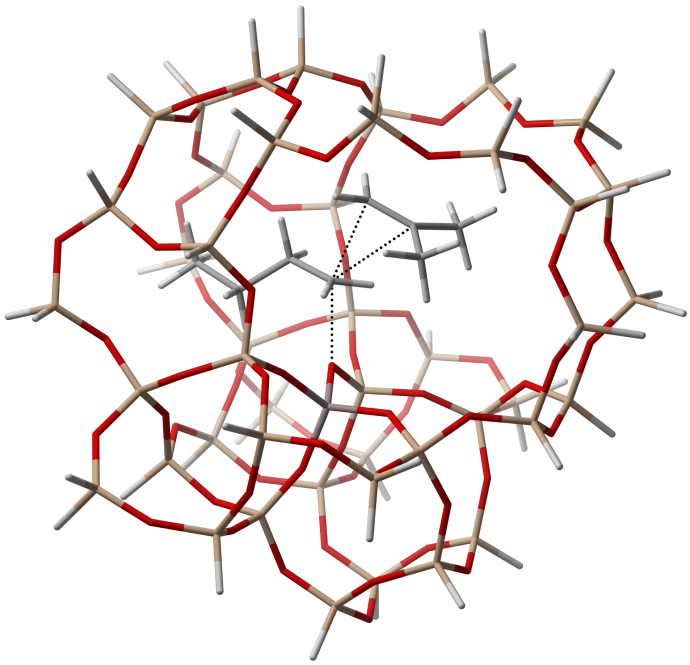

Figure B.1: Optimized transition state geometry of Reaction (4.1)

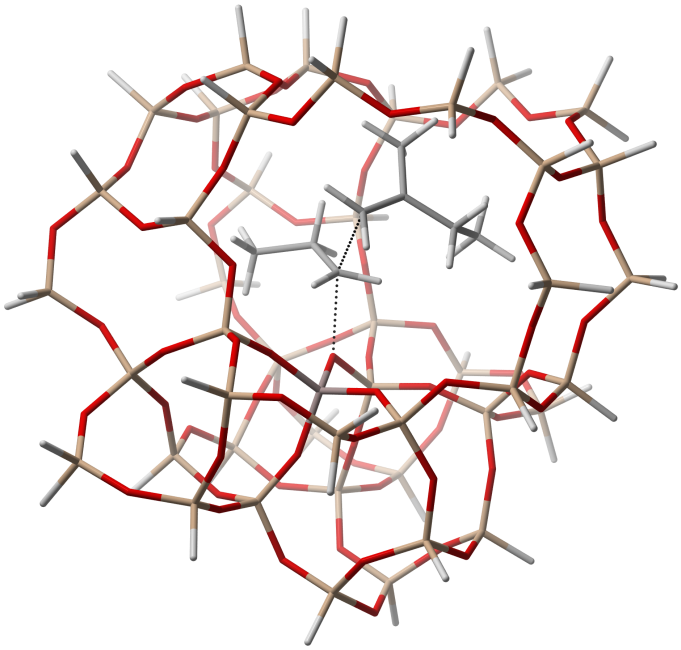

Figure B.2: Optimized transition state geometry of Reaction (4.2)

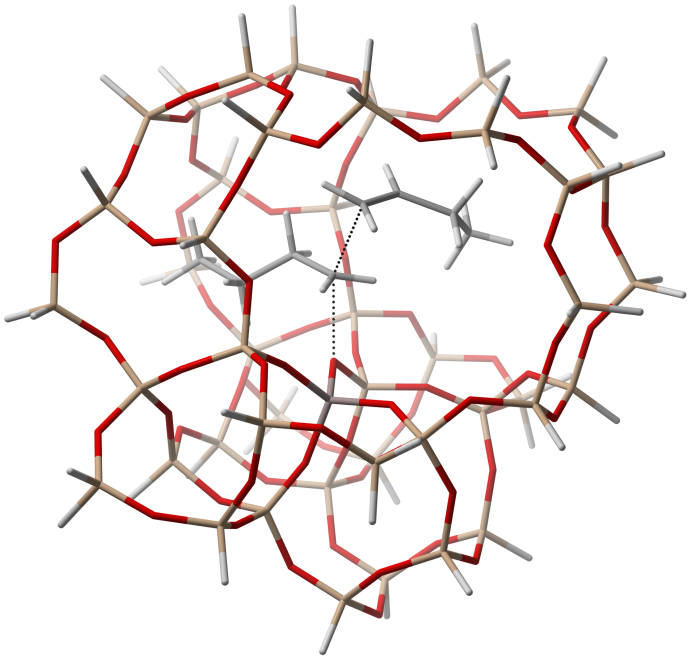

Figure B.3: Optimized transition state geometry of Reaction (4.3)

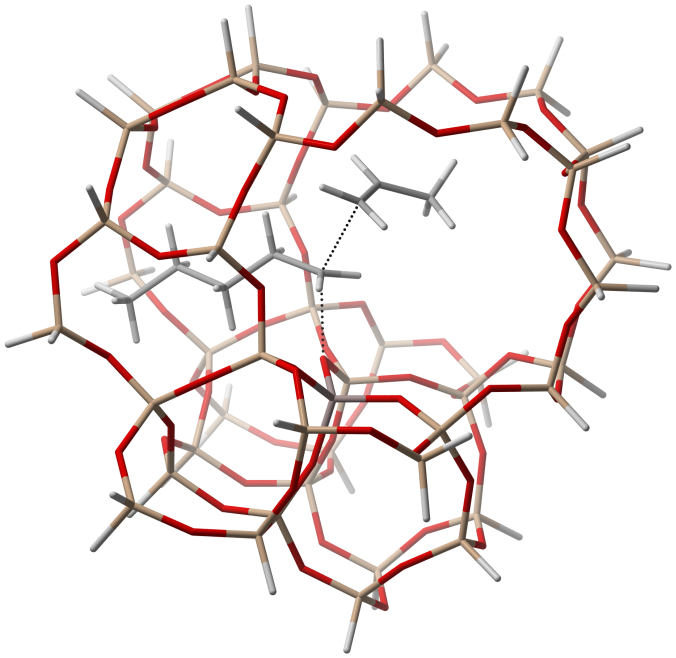

Figure B.4: Optimized transition state geometry of Reaction (4.4)

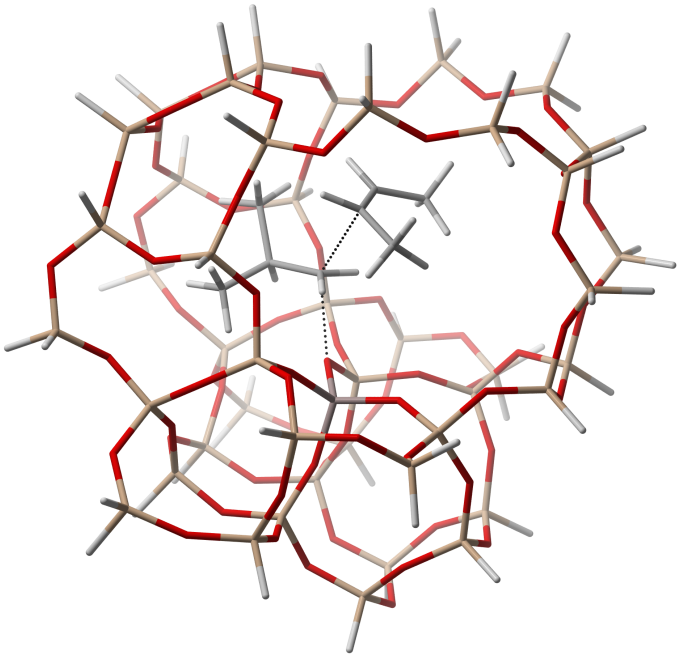

Figure B.5: Optimized transition state geometry of Reaction (4.5)

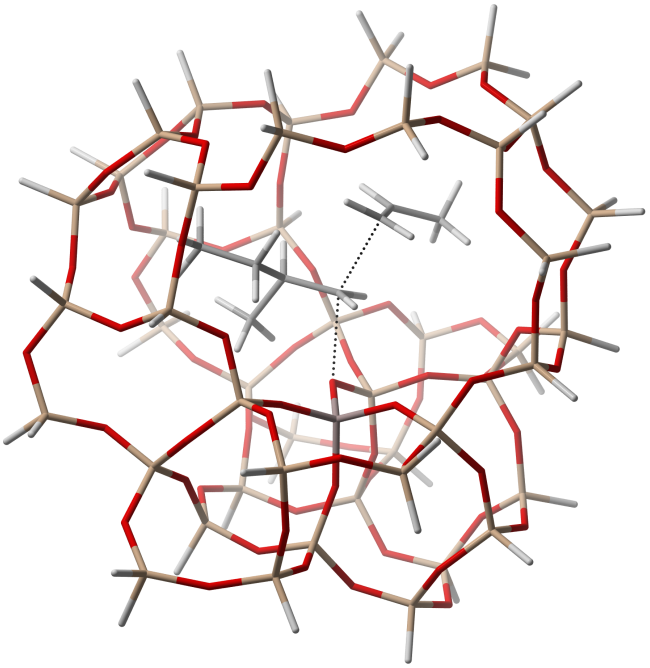

Figure B.6: Optimized transition state geometry of Reaction (4.6)

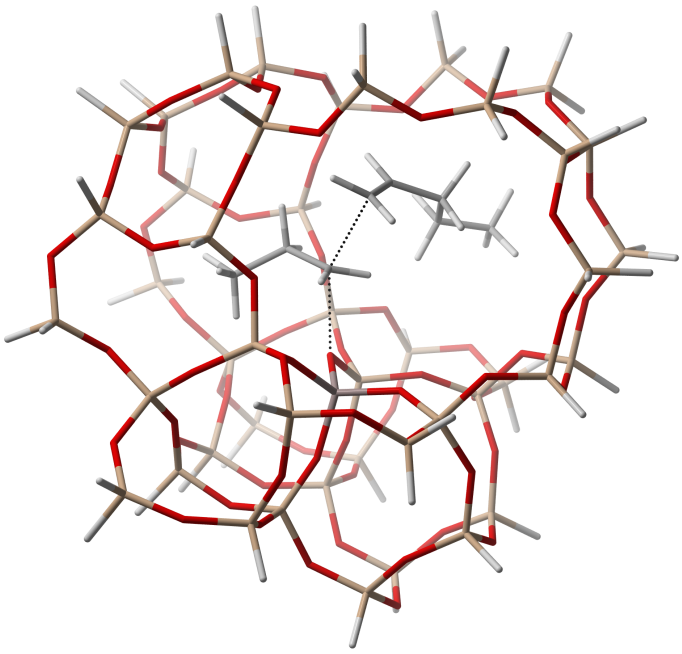

Figure B.7: Optimized transition state geometry of Reaction (4.7)

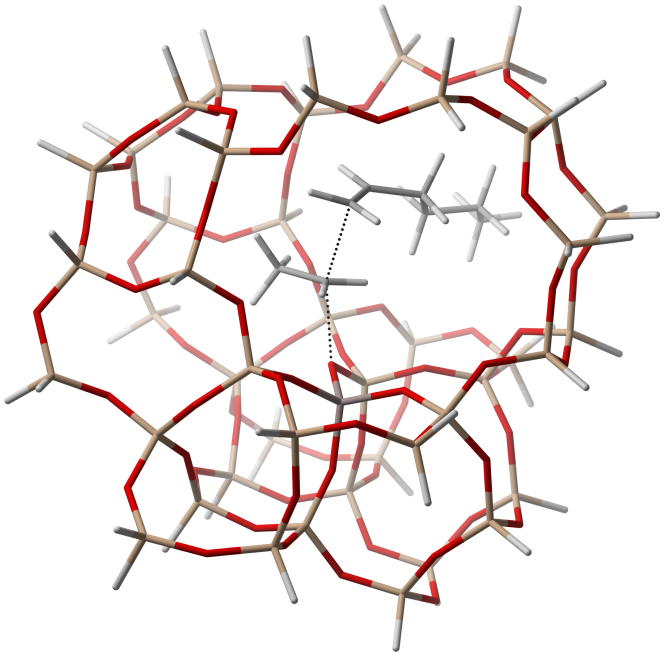

Figure B.8: Optimized transition state geometry of Reaction (4.8)

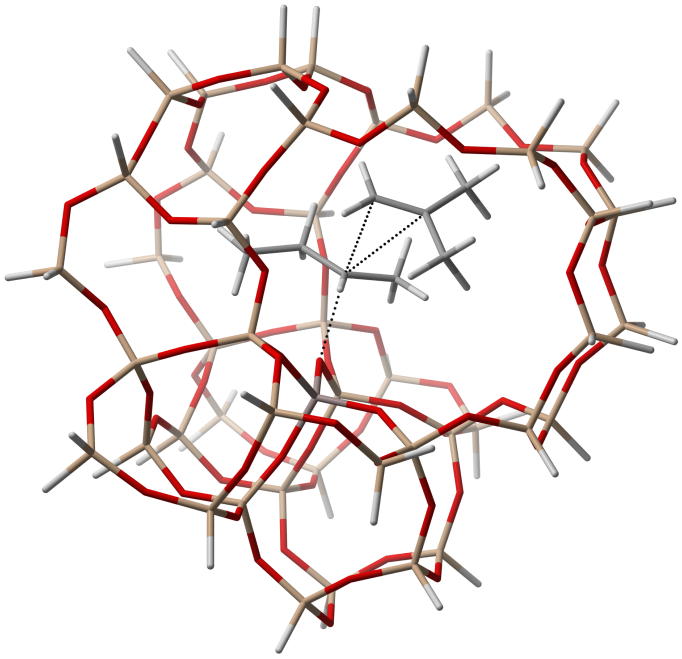

Figure B.9: Optimized transition state geometry of Reaction (4.9)

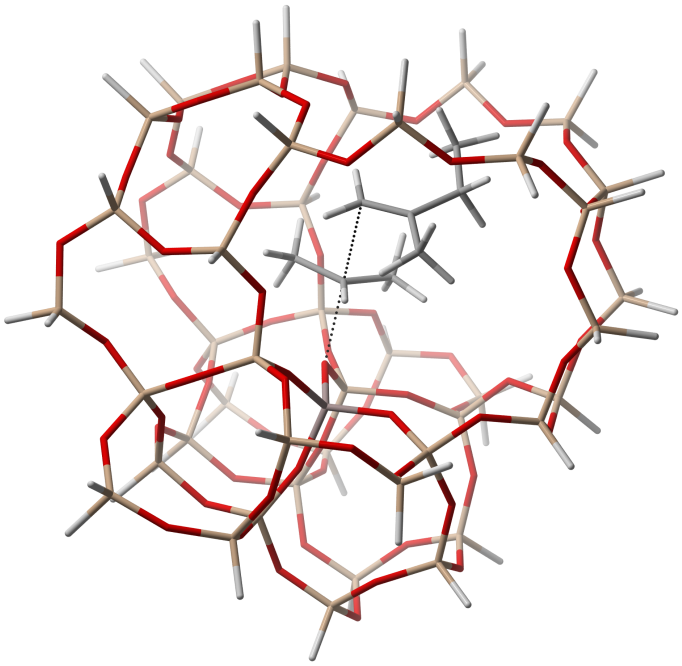

Figure B.10: Optimized transition state geometry of Reaction (4.10)

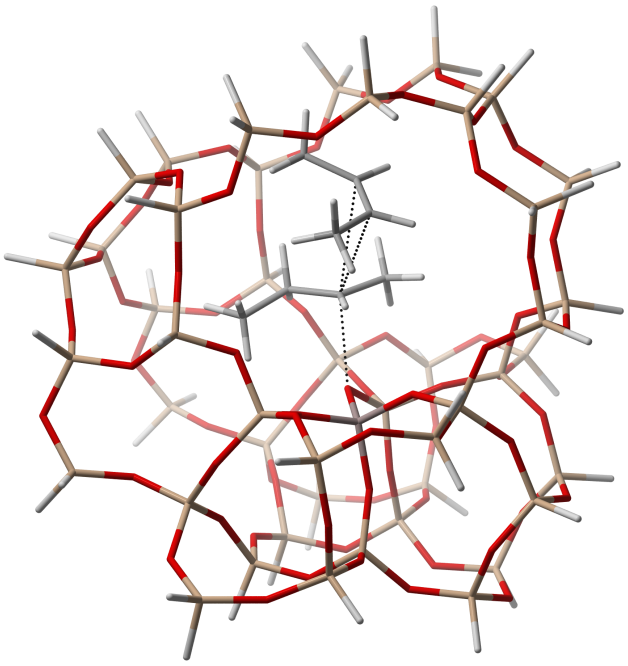

Figure B.11: Optimized transition state geometry of Reaction (4.11)

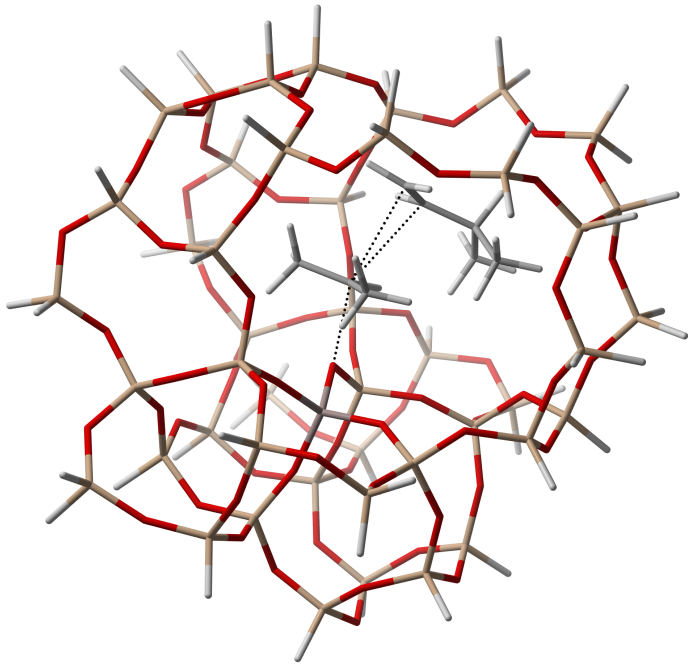

Figure B.12: Optimized transition state geometry of Reaction (4.12)

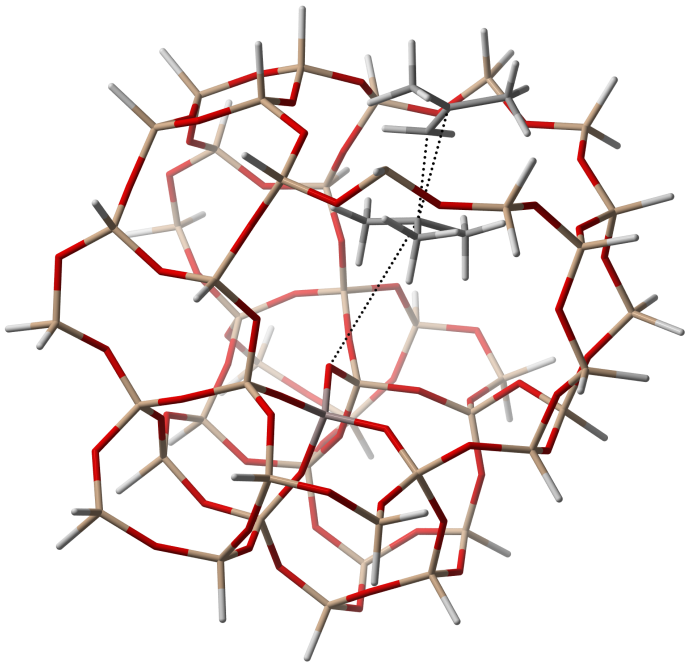

Figure B.13: Optimized transition state geometry of Reaction (4.13)

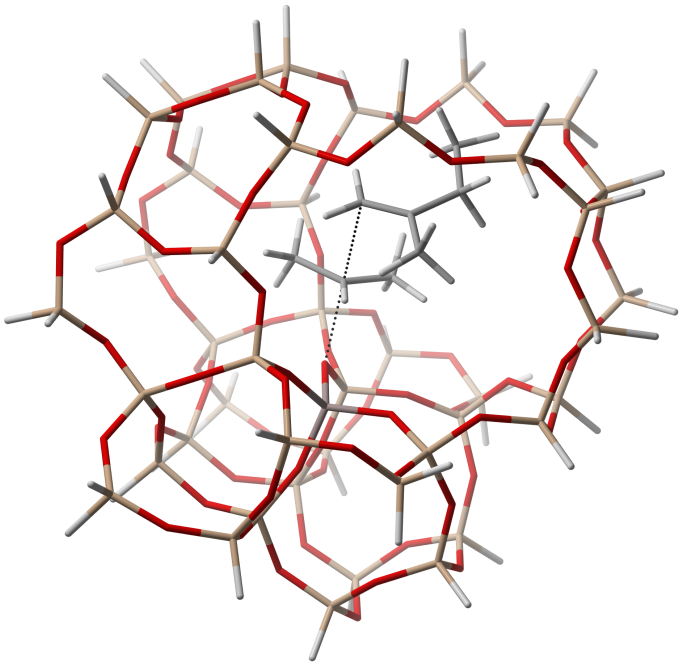

Figure B.14: Optimized transition state geometry of Reaction (4.14)

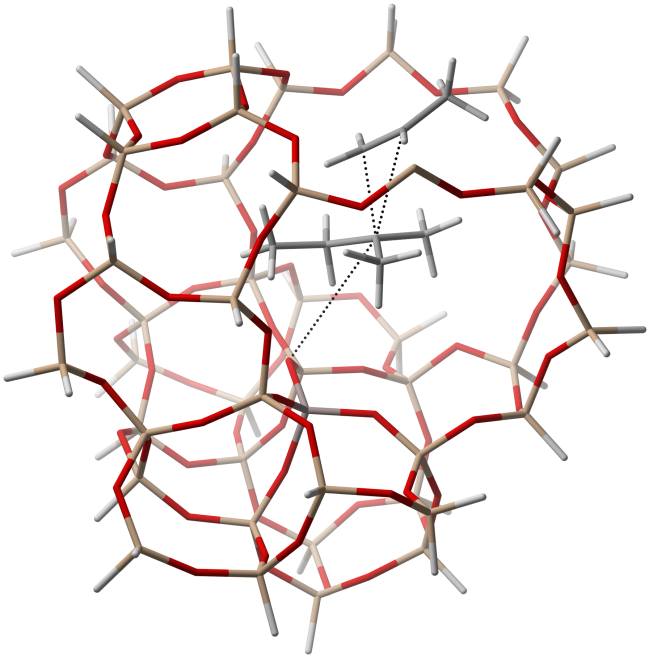

Figure B.15: Optimized transition state geometry of Reaction (4.15)

Appendix C

Molecular dynamics simulation results

In this appendix, first, the evolution of conserved quantity, temperature, pressure and cell parameters for the 2-butyl cation simulation are shown in Figure C.1 and Figure C.2. Secondly the evolution of the initial $C-H$ bond distances are pictured in Figure C.3 for the 2-octyl cation and the evolution of the $C-C$ bond distances is plotted in Figure C.4. In Figure C.5, the evolution of the initial $C-H$ bond distances for the 2-methyl-5-heptyl cation are shown.

C.1 2-butyl simulation analysis

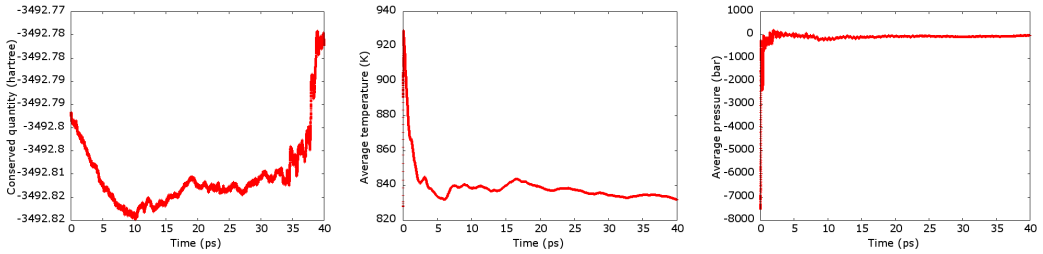

(a) Conserved quantity

(b) Average temperature

(c) Average pressure

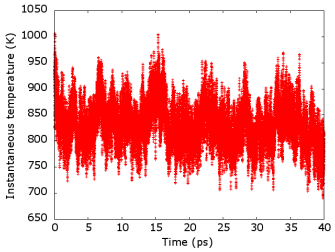

(d) Instantaneous temperature

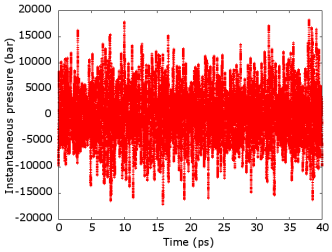

(e) Instantaneous pressure

Figure C.1: Conserved quantity, temperature and pressure as a function of simulation time

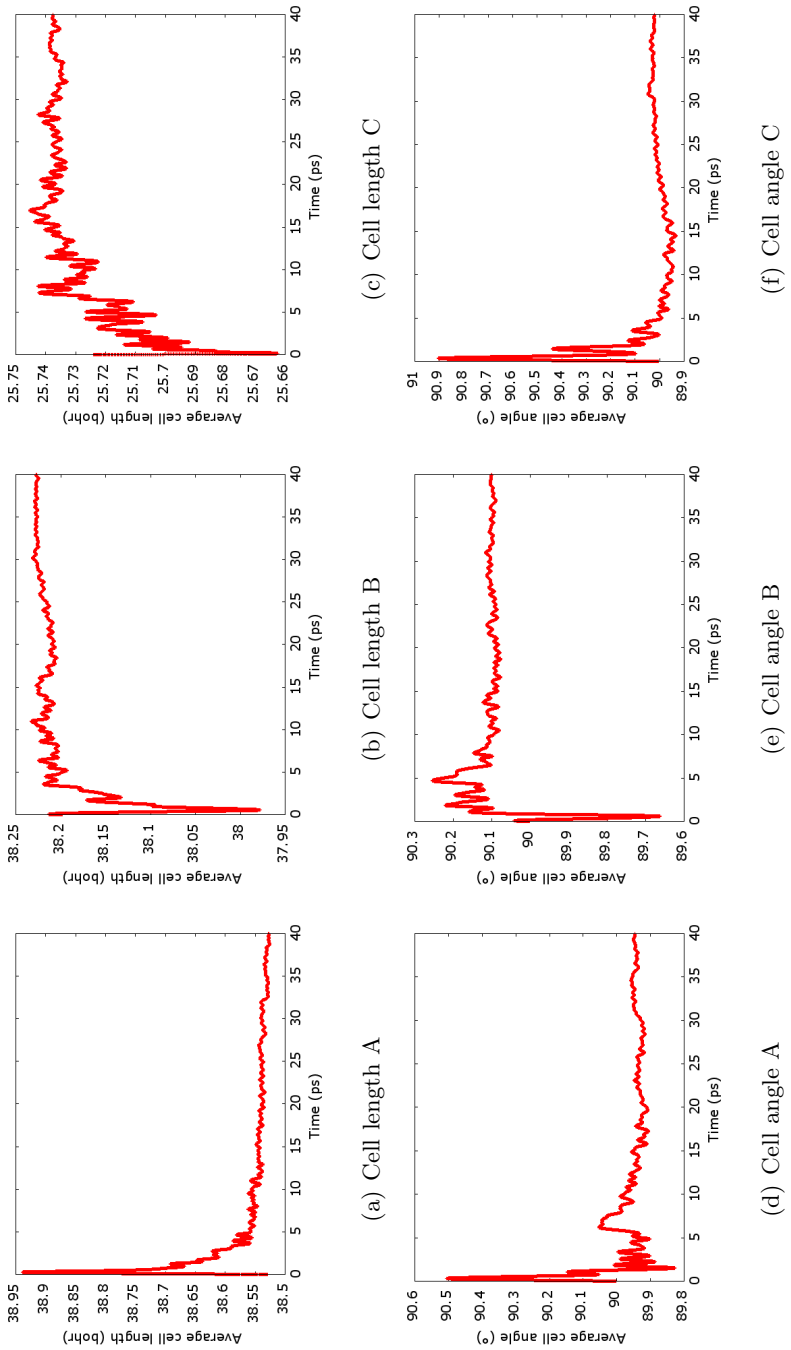

(a) Cell length A (b) Cell length B (c) Cell length C

(d) Cell angle A (e) Cell angle B (f) Cell angle C

Figure C.2: Average cell parameters as a function of the simulation time

C.2 2-octyl bond distances

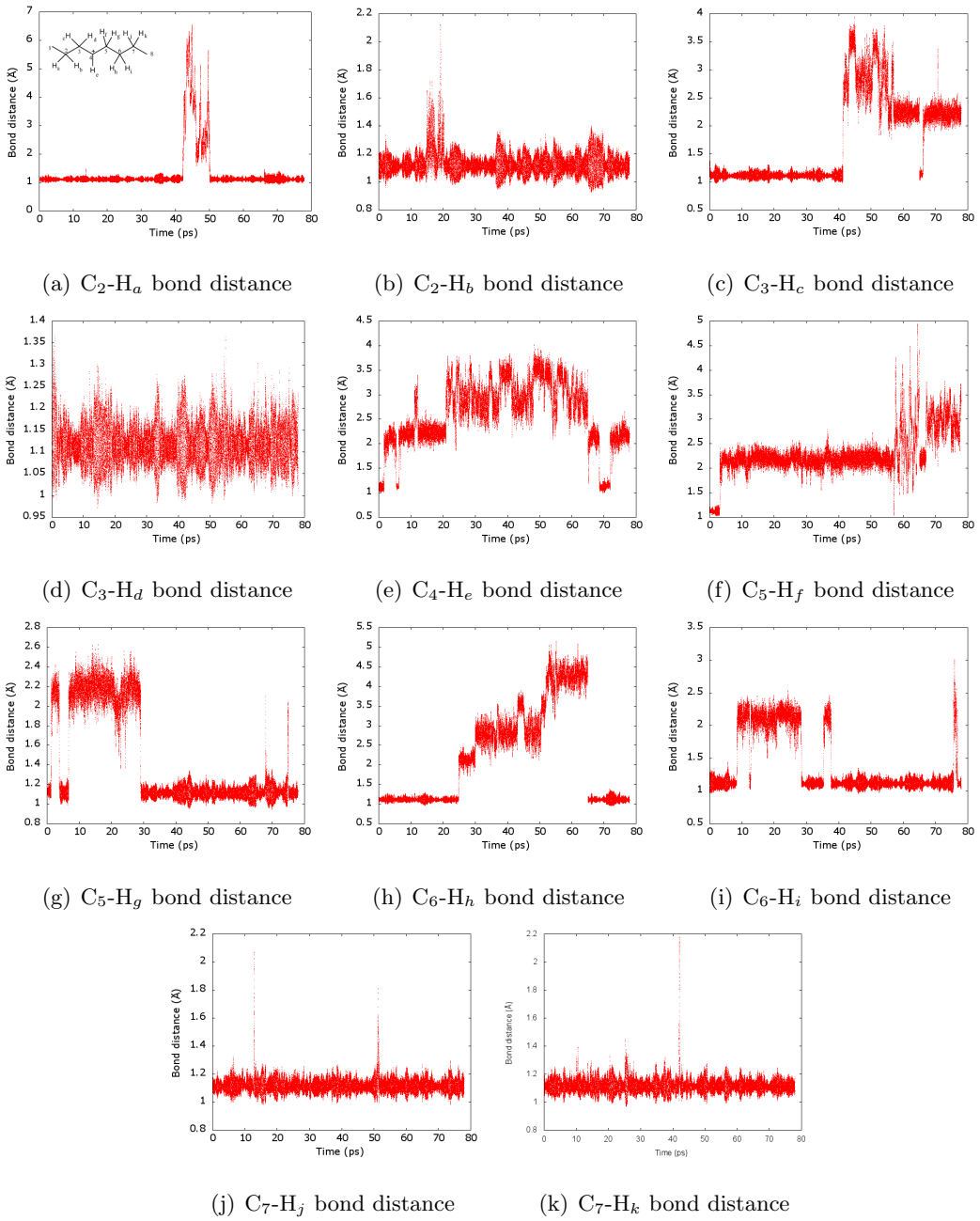

(a) C_2-H_a bond distance (b) C_2-H_b bond distance (c) C_3-H_c bond distance

(d) C_3-H_d bond distance (e) C_4-H_e bond distance (f) C_5-H_f bond distance

(g) C_5-H_g bond distance (h) C_6-H_h bond distance (i) C_6-H_i bond distance

(j) C_7-H_j bond distance (k) C_7-H_k bond distance

Figure C.3: Evolution of the initial $C-H$ bond distances for C_2 to C_7 on the 2-octyl cation

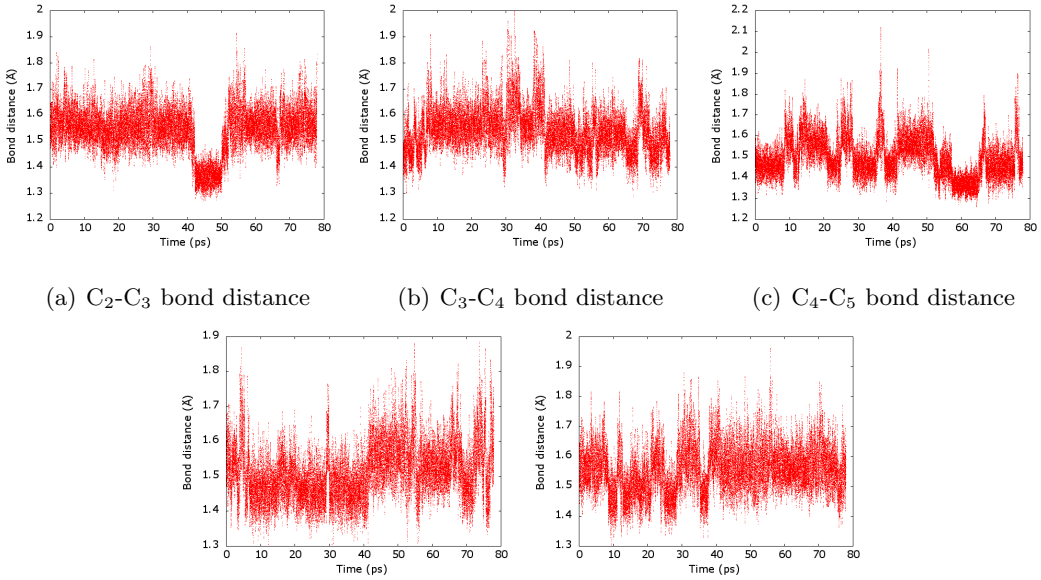

(a) C_2-C_3 bond distance (b) C_3-C_4 bond distance (c) C_4-C_5 bond distance

(d) C_5-C_6 bond distance (e) C_6-C_7 bond distance

Figure C.4: Evolution of the inner $C-C$ bond distances of the 2-octyl cation

C.3 5-methyl-2-heptyl bond distances

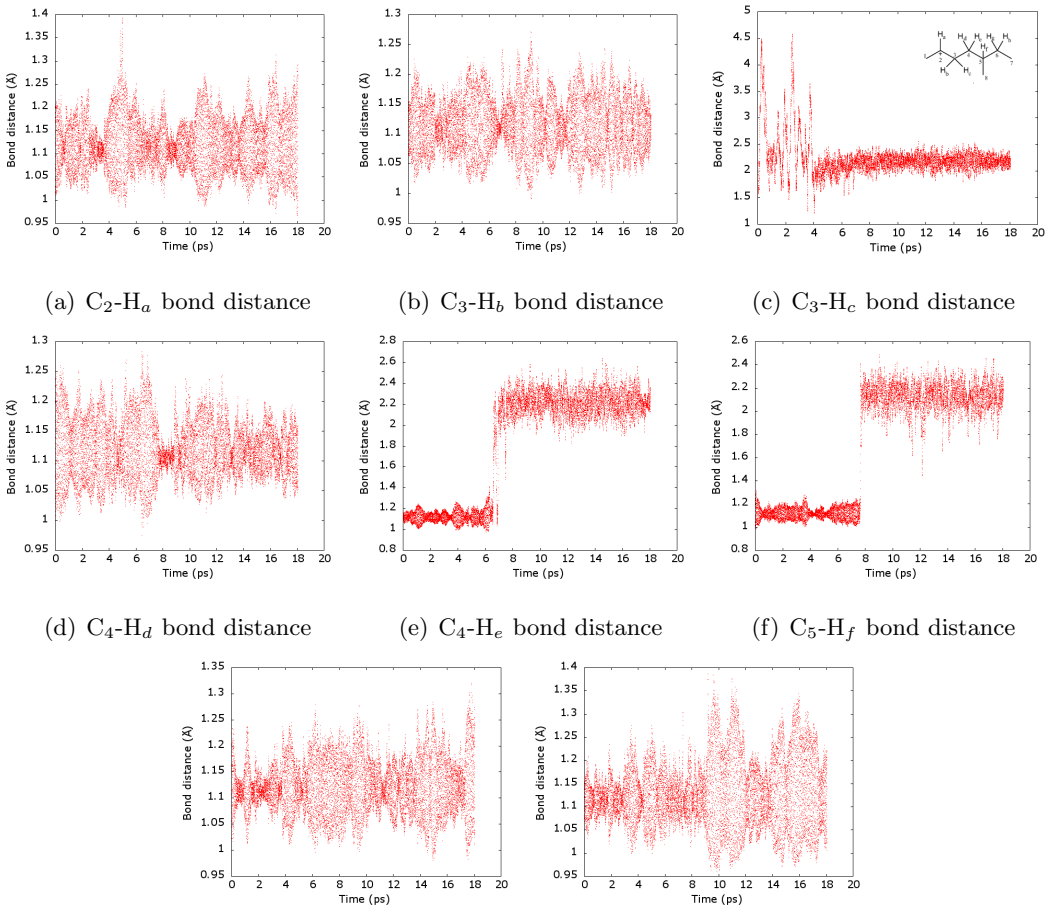

(a) C_2-H_a bond distance (b) C_3-H_b bond distance (c) C_3-H_c bond distance

(d) C_4-H_d bond distance (e) C_4-H_e bond distance (f) C_5-H_f bond distance

(g) C_6-H_g bond distance (h) C_6-H_h bond distance

Figure C.5: Evolution of some initial, inner $C-H$ bond distances of the 5-methyl-2-heptyl cation during the second production run

Appendix D

NCCC Poster

This appendix contains a small version of the poster that was presented on March the 11th, 2014 at NCCC XV (XVth Netherlands' Catalysis and Chemistry Conference), March 10-12, 2014, Noordwijkerhout (NL).

First principle kinetic study of butene cracking on H-ZSM-5

Pieter Cnudde, Jeroen Van der Mynsbrugge, Kristof De Wispelaere,
Karen Hemelsoet, Veronique Van Speybroeck

Center for Molecular Modeling, Ghent University, Technologiepark 903, 9052 Zwijnaarde, Belgium

Industrial relevance

Methanol-to-olefins (MTO)

- dual cycle mechanism in ZSM-5
- alkene methylation + cracking in alkene cycle [1]

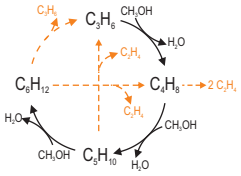

Olefin Cracking Process (OCP)

- ZSM-5 catalyst
- goal: increase propene yield
- highly olefinic feed (> 70 wt% butenes) [2]

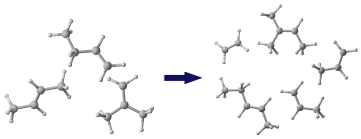

Comparison of zeolite performances

varying zeolite catalyst

Decreasing cage diameter

Zeolite	Butene conversion	$C_2^=$ / $C_3^=$ selectivity	C_2 / C_3 selectivity	Stability
Y	*****	*	*****	*
Beta	****	*	*****	**
MCM-22	****	**	****	****
ZSM-5	****	***	***	*****
ZSM-22	*	****	*	**
ZSM-35	***	****	**	**
ZSM-23	**	****	**	***
SAPO-34	*	*****	**	*

ZSM-5 has an optimal balance between conversion, selectivity and coking stability [3]

varying Si/Al$_2$ ratio for ZSM-5

Decreasing acid site density

Si/Al$_2$ ratio	Butene conversion	$C_2^=$ / $C_3^=$ selectivity	C_2 / C_3 selectivity	Stability
50	*****	*	*****	*
108	****	**	****	**
166	***	***	***	***
230	**	****	**	****
366	*	*****	*	*****

Optimal Si/Al$_2$ ratio ranges between 200 and 400 [4]

Reaction network

Catalytic cracking of a mixture of butenes proceeds via a complex network of reactions [5,6]

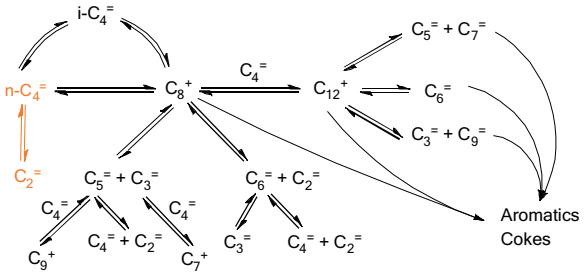

Cracking mechanism

Cracking through β-scission of carbenium ion intermediates

e.g. monomolecular cracking

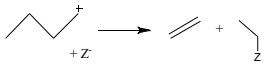

Objectives

- Determine feasible reaction pathways for butene cracking
- Link to product yields
- Study temperature dependence of cracking mechanism
- Investigate nature of pre-activated complexes (chemisorption vs physisorption)

Computational details

finite cluster model

- 46T H-ZSM-5 zeolite cluster
- single Bronsted acid site
- dangling bonds saturated with hydrogen
- two layer ONIOM scheme 8T:46T

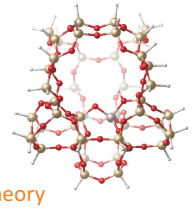

level of theory

- geometry optimization:
  ONIOM (B3LYP/6-31+g(d,p):PM3)
- energy refinement:
  ωB97X-D/6-31+g(d,p)
  ⇨ including dispersion interactions

kinetics

- based on transition state theory
- unimolecular/bimolecular

Monomolecular cracking: energy diagram

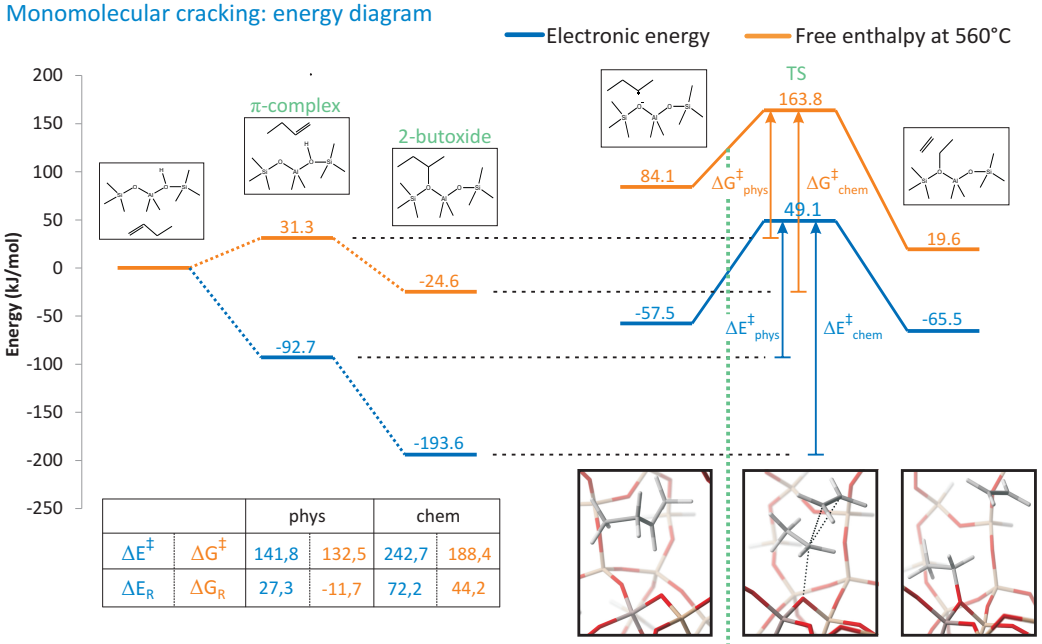

		phys		chem	
$\Delta E^{\ddagger}$	$\Delta G^{\ddagger}$	141,8	132,5	242,7	188,4
ΔE_R	ΔG_R	27,3	-11,7	72,2	44,2

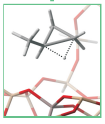

No stable primary butyl carbenium ion can be found. It isomerizes spontaneously to a secondary ion over a cyclopropyl intermediate

Conclusions & Future Work

- The free energy barrier for the monomolecular cracking of n-butene is quite high.
- Bimolecular cracking (dimerization + β scission) can involve secondary and tertiary carbenium ion transformations and may provide more feasible reaction routes.

Bimolecular cracking: reactions to investigate

Secondary carbenium ion transformations

secondary → primary

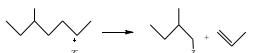

secondary → secondary

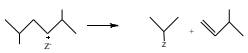

secondary → tertiary

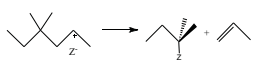

Tertiary carbenium ion transformations

tertiary → primary

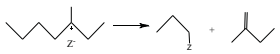

tertiary → secondary

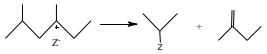

tertiary → tertiary

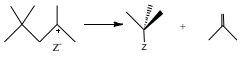

References

[1] Lesthaeghe, D. et al., ChemCatChem, 3 (2011) 208-212.
[2] Vermeiren, W. et al., Us8362183 B-229-Jan-2013.
[3] Zhu, X. et al., Appl. Catal. Gen., 288 (2005) 134-142.
[4] Zhu, X. et al., Appl. Catal. Gen., 290 (2005) 191-199.
[5] Sun, Y.-X. et al., J. Phys. Chem. C, 114 (2010) 5975-5984.
[6] Meng, X. et al., EnergyFuels, 24 (2010) 6233-6238.

List of Figures

List of Tables

Bibliography

[1] K. Van Geem, *Sustainable Chemical Production Processes. Cursus gedoceerd in 1e Master of Science: Chemical Engineering*, 2012.

[2] BP, *BP Statistical Review of World Energy*, 2013, http://www.bp.com/content/dam/bp/pdf/statistical-review.

[3] P. N. R. Vennestrøm, C. M. Osmundsen, C. H. Christensen, and Esben Taarning, "Beyond petrochemicals: The renewable chemicals industry," *Angewandte Chemie International Edition*, vol. 50, no. 45, pp. 10502–10509, 2011.

[4] Michael Ratner, P.W. Parfomak, I.F. Ferguson, and Linda Luther, *U.S. Natural Gas Exports: New Opportunities, Uncertain Outcomes*, 2013, https://www.fas.org/sgp/crs/misc/.

[5] Elaine Burridge, *Petrochemicals: Probe Economics forecasts change to propylene, butadiene pricing*, 2011, http://www.icis.com/Articles/2011/09/26/9494873/petrochemicals-probe-economics-forecasts-change-to-propylene-butadiene.html.

[6] Paul Stevens, *The Shale Gas Revolution: Developments and Changes*, 2012, http://www.chathamhouse.org/sites/default/files/public/Research/Energy, Environment and Development/.

[7] The Essential Chemical Industry, *Ethylene*, 2014, http://www.essentialchemicalindustry.org/chemicals/ethene.html.

[8] Stefano Zehnder, *Middle East Feedstocks: Are they still there?*, 2013, http://gpca.org.ae/congulf/blog/middle-east-feedstocks-are-they-still-there/.

[9] Michael J. Tallman and Curtis N. Eng, "Catalytic routes to olefins," *AIChE Paper 219c*.

[10] CB&I, *Lummus Technology*, 2011, http://www.sec.gov/Archives/edgar/containers/fix054/1027884/000095012311096816/c24376exv99w1.htm.

[11] Nazi Rahimi and Ramin Karimzadeh, "Catalytic cracking of hydrocarbons over modified ZSM-5 zeolites to produce light olefins: A review," *Applied Catalysis A: General*, vol. 398, no. 1–2, pp. 1–17, 2011.

[12] J.S Buchanan, "The chemistry of olefins production by ZSM-5 addition to catalytic cracking units," *Catalysis Today*, vol. 55, no. 3, pp. 207–212, 2000.

[13] Reza Sadeghbeigi, "Chapter 1 - process description," in *Fluid Catalytic Cracking Handbook (Third Edition)*, Reza Sadeghbeigi, Ed., pp. 1–42. Butterworth-Heinemann, Oxford, 2012.

[14] Nicolas Lambert, Ibrahim Abba, Chris Santner, Iwao Ogasawara, and Halim Redhwi, *HS-FCC for propylene: concept to commercial operation*, 2014, http://www.axens.net/news-and-events/news/307/hs-fcc-for-propylene-concept-to-commercial-operation.html.

[15] Clarence D. Chang, "Methanol conversion to light olefins," *Catalysis Reviews*, vol. 26, no. 3-4, pp. 323–345, 1984.

[16] Frerich J. Keil, "Methanol-to-hydrocarbons: process technology," *Microporous and Mesoporous Materials*, vol. 29, no. 1–2, pp. 49–66, June 1999.

[17] Unni Olsbye, Stian Svelle, Morten Bjørgen, Pablo Beato, Ton V. W. Janssens, Finn Joensen, Silvia Bordiga, and Karl Petter Lillerud, "Conversion of methanol to hydrocarbons: How zeolite cavity and pore size controls product selectivity," *Angewandte Chemie International Edition*, vol. 51, no. 24, pp. 5810–5831, 2012.

[18] John J. Senetar and Eric Romers, "Scale-up of advanced MTO technology and integrated OCP technology," *Oil & Gas Journal*, 2011.

[19] John Q. Chen, Andrea Bozzano, Bryan Glover, Terje Fuglerud, and Steinar Kvisle, "Recent advancements in ethylene and propylene production using the UOP/Hydro MTO process," *Catalysis Today*, vol. 106, no. 1–4, pp. 103–107, 2005.

[20] Harald Koempel and Waldemar Liebner, "Lurgi's methanol to propylene (MTP) report on a successful commercialisation," *Natural Gas Conversion VIII, Proceedings of the 8th Natural Gas Conversion Symposium*, vol. 167, pp. 261–267, 2007.

[21] David Lesthaeghe, Jeroen Van der Mynsbrugge, Matthias Vandichel, Michel Waroquier, and Veronique Van Speybroeck, "Full theoretical cycle for both ethene and propene formation during methanol-to-olefin conversion in H-ZSM-5," *ChemCatChem*, vol. 3, no. 1, pp. 208–212, 2011.

[22] Morten Bjørgen, Stian Svelle, Finn Joensen, Jesper Nerlov, Stein Kolboe, Francesca Bonino, Luisa Palumbo, Silvia Bordiga, and Unni Olsbye, "Conversion of methanol to hydrocarbons over zeolite H-ZSM-5: On the origin of the olefinic species," *Journal of Catalysis*, vol. 249, no. 2, pp. 195–207, July 2007.

[23] Stian Svelle, Unni Olsbye, Finn Joensen, and Morten Bjørgen, "Conversion of methanol to alkenes over medium- and large-pore acidic zeolites: Steric manipulation of the reaction intermediates governs the Ethene/Propene product selectivity," *The Journal of Physical Chemistry C*, vol. 111, no. 49, pp. 17981–17984, Dec. 2007.

[24] Karen Hemelsoet, Jeroen Van der Mynsbrugge, Kristof De Wispelaere, Michel Waroquier, and Veronique Van Speybroeck, "Unraveling the reaction mechanisms governing methanol-to-olefins catalysis by theory and experiment," *ChemPhysChem*, vol. 14, no. 8, pp. 1526–1545, 2013.

[25] Stian Svelle, Finn Joensen, Jesper Nerlov, Unni Olsbye, Karl-Petter Lillerud, Stein Kolboe, and Morten Bjørgen, "Conversion of methanol into hydrocarbons over zeolite H-ZSM-5: Ethene formation is mechanistically separated from the formation of higher alkenes," *Journal of the American Chemical Society*, vol. 128, no. 46, pp. 14770–14771, Nov. 2006.

[26] Morten Bjørgen, Finn Joensen, Karl-Petter Lillerud, Unni Olsbye, and Stian Svelle, "The mechanisms of ethene and propene formation from methanol over high silica H-ZSM-5 and H-Beta," *Catalysis Today*, vol. 142, no. 1–2, pp. 90–97, 2009.

[27] Walter Vermeiren and Nikolai Nesterenko, "MTO process based on MeAPO molecular sieves combined with an OCP process to make olefins," 2013, U.S. Classification 526/348, 585/640, 526/352, 585/638, 526/351, 585/639; International Classification C08F110/06, C08F110/02, C07C1/00, C08F210/00; Cooperative Classification C10G3/45, C10G3/49, C10G2400/20, C10G2300/802, C07C1/26, C07C2529/40, C07C4/06, C07C2529/85, C07C17/10, C07C2529/035, C07C11/04, C01B3/44, C07C11/06, C07C1/20.

[28] Todd R. Steffens and Paul K. Ladwig, "Process for selectively producing light olefins," 2002, Classificatie in de VS 585/648, 585/653, 208/120.01; Internationale classificatie C10G51/02, C10G35/06, C10G11/04, C07C4/04, C07C11/06, C07C4/06, C10G11/18, C07C11/02, C07C11/04, C10G57/02, C10G35/095, C10G35/04, C07B61/00, C10G35/02, C10G11/02, C10G51/04, C10G11/05; Coöperatieve classificatie C10G11/05, C10G57/02, C10G2400/20, C10G51/023; Europese classificatie C10G11/05, C10G57/02, C10G51/02B.

[29] Paul K. Ladwig, John Ernest Asplin, William A. Wachter, Gordon F. Stuntz, and Brian Erik Henry, "Process for selectively producing light olefins in a

fluid catalytic cracking process," 2000, Classificatie in de VS 585/648, 585/653, 585/649, 208/135, 208/72, 585/650, 585/651, 208/120.1; Internationale classificatie C10G11/05, C10G35/06, C10G35/02, C10G51/04, C10G11/04, C10G11/02, C10G35/04, C10G35/095, C07C4/06, C10G51/02, C07C4/04, C07C11/02, C10G57/02; Coöperatieve classificatie C10G57/02, C10G2400/20, C10G51/023; Europese classificatie C10G57/02, C10G51/02B.

[30] Xianghai Meng, Chunming Xu, Li Li, and Jinsen Gao, "Kinetic study of catalytic pyrolysis of C_4 hydrocarbons on a modified ZSM-5 zeolite catalyst," *Energy & Fuels*, vol. 24, no. 12, pp. 6233–6238, 2010.

[31] Rick Kempf, *Advances in Commericialization of the UOP Advanced MTO Technology, UOP LLC, a Honeywell Company.*, 2011, http://core.theenergyexchange.co.uk/agile_ assets/1547/1120H_ Rick_ Kempf_ UOP.pdf.

[32] J. Grootjans, V. Vanrysselberghe, and W. Vermeiren, "Integration of the total petrochemicals-UOP olefins conversion process into a naphtha steam cracker facility," *Catalysis Today*, vol. 106, no. 1-4, pp. 57–61, Oct. 2005.

[33] Christian Dupraz, *Axens - Refining - Petrochemical Synergies & Opportunities*, 2010, http://www.oapecorg.org/ar/Bahrain

[34] Scott M. Auerbach, Kathleen A. Carrado, and Prabir K. Dutta, *Handbook of Zeolite Science and Technology*, Marcel Dekker, Inc., New York, 2003.

[35] Jiri Cejka, Herman van Bekkum, Avelino Corma, and Ferdi Schüth, *Introduction to Zeolite Science and Practice*, Number 168 in Studies in Surface Science and Catalysis. Elsevier, Amsterdam, 2007.

[36] M. F. Reyniers, *Chemie en duurzame technologie. Cursus gedoceerd in 3e Bachelor of Science ingenieurswetenschappen: chemische technologie en materiaalkunde*, 2012.

[37] Aditya Bhan, Yogesh V. Joshi, W. Nicholas Delgass, and Kendall T. Thomson, "DFT investigation of alkoxide formation from olefins in H-ZSM-5," *The Journal of Physical Chemistry B*, vol. 107, no. 38, pp. 10476–10487, Sept. 2003.

[38] Cuong M. Nguyen, Bart A. De Moor, Marie-Franç oise Reyniers, and Guy B. Marin, "Physisorption and chemisorption of linear alkenes in zeolites: A combined QM-Pot(MP2//B3LYP:GULP)–Statistical thermodynamics study," *The Journal of Physical Chemistry C*, vol. 115, no. 48, pp. 23831–23847, 2011.

[39] Teresa Blasco, "Insights into reaction mechanisms in heterogeneous catalysis revealed by in situ NMR spectroscopy," *Chemical Society Reviews*, vol. 39, no. 12, pp. 4685–4702, Nov. 2010.

[40] Alexander G. Stepanov, Mikhail V. Luzgin, Vaycheslav N. Romannikov, and Kirill I. Zamaraev, "Carbenium ion properties of 1-octene adsorbed on zeolite H-ZSM-5," *Catalysis Letters*, vol. 24, no. 3-4, pp. 271–284, Sept. 1994.

[41] M. Boronat, P. Viruela, and A. Corma, "Theoretical study of the mechanism of zeolite-catalyzed isomerization reactions of linear butenes," *The Journal of Physical Chemistry A*, vol. 102, no. 6, pp. 982–989, Feb. 1998.

[42] Yury V. Kissin, "Chemical mechanisms of catalytic cracking over solid acidic catalysts: Alkanes and alkenes," *Catalysis Reviews*, vol. 43, no. 1-2, pp. 85–146, 2001.

[43] George S. Hammond, "A correlation of reaction rates," *Journal of the American Chemical Society*, vol. 77, no. 2, pp. 334–338, Jan. 1955.

[44] T. Demuth, X. Rozanska, L. Benco, J. Hafner, R. A. van Santen, and H. Toulhoat, "Catalytic isomerization of 2-pentene in H-ZSM-22 — A DFT investigation," *Journal of Catalysis*, vol. 214, no. 1, pp. 68–77, Feb. 2003.

[45] J.S. Buchanan, J.G. Santiesteban, and W.O. Haag, "Mechanistic considerations in acid-catalyzed cracking of olefins," *Journal of Catalysis*, vol. 158, no. 1, pp. 279–287, Jan. 1996.

[46] A. Corma and A.V. Orchillés, "Current views on the mechanism of catalytic cracking," *Microporous and Mesoporous Materials*, vol. 35–36, pp. 21–30, Apr. 2000.

[47] Richard J. Quann, Larry A. Green, Samuel A. Tabak, and Frederick J. Krambeck, "Chemistry of olefin oligomerization over ZSM-5 catalyst," *Industrial & Engineering Chemistry Research*, vol. 27, no. 4, pp. 565–570, Apr. 1988.

[48] Jérôme P. G. Pater, Pierre A. Jacobs, and Johan A. Martens, "Oligomerization of hex-1-ene over acidic aluminosilicate zeolites, MCM-41, and silica-alumina co-gel catalysts: A comparative study," *Journal of Catalysis*, vol. 184, no. 1, pp. 262–267, 1999.

[49] A. K. Nowak, A. E. Wilson, K. Roberts, and K. P. Datema, "Hexane cracking in ZSM-5: in Situ ^{13}C cross-polarization magic-angle-spinning NMR and flow Reactor/GC experiments," *Journal of Catalysis*, vol. 144, no. 2, pp. 495–505, Dec. 1993.

[50] G. R. Bamwenda, Y. X. Zhao, and B. W. Wojciechowski, "The influence of reaction temperature on the cracking mechanism of 2-methylhexane," *Journal of Catalysis*, vol. 148, no. 2, pp. 595–606, Aug. 1994.

[51] W. O. Haag, R. M. Lago, and P. B. Weisz, "The active site of acidic aluminosilicate catalysts," *Nature*, vol. 309, no. 5969, pp. 589–591, June 1984.

[52] J. Abbot, A. Corma, and B. W. Wojciechowski, "The catalytic isomerization of 1-hexene on H-ZSM-5 zeolite: The effects of a shape-selective catalyst," *Journal of Catalysis*, vol. 92, no. 2, pp. 398–408, Apr. 1985.

[53] M. Guisnet and P. Magnoux, "Deactivation by coking of zeolite catalysts. prevention of deactivation. optimal conditions for regeneration," *Catalysis Today*, vol. 36, no. 4, pp. 477–483, June 1997.

[54] M. Guisnet and P. Magnoux, "Coking and deactivation of zeolites: Influence of the pore structure," *Applied Catalysis*, vol. 54, no. 1, pp. 1–27, Sept. 1989.

[55] Ying-Xin Sun, Jing Yang, Li-Feng Zhao, Jian-Xing Dai, and Huai Sun, "A two-layer ONIOM study on initial reactions of catalytic cracking of 1-butene to produce propene and ethene over H-ZSM-5 and H-FAU zeolites," *The Journal of Physical Chemistry C*, vol. 114, no. 13, pp. 5975–5984, Apr. 2010.

[56] John B. Nicholas and James F. Haw, "The prediction of persistent carbenium ions in zeolites," *Journal of the American Chemical Society*, vol. 120, no. 45, pp. 11804–11805, Nov. 1998.

[57] Werner O. Haag, Rudolph M. Lago, and Paul B. Weisz, "Transport and reactivity of hydrocarbon molecules in a shape-selective zeolite," *Faraday Discussions of the Chemical Society*, vol. 72, no. 0, pp. 317–330, Jan. 1981.

[58] Xiangxue Zhu, Shenglin Liu, Yueqin Song, Sujuan Xie, and Longya Xu, "Catalytic cracking of 1-butene to propene and ethene on MCM-22 zeolite," *Applied Catalysis A: General*, vol. 290, no. 1–2, pp. 191–199, 2005.

[59] Yury V. Kissin, "Chemical mechanism of hydrocarbon cracking over solid acidic catalysts," *Journal of Catalysis*, vol. 163, no. 1, pp. 50–62, Sept. 1996.

[60] Li Li, Jinsen Gao, Chunming Xu, and Xianghai Meng, "Reaction behaviors and mechanisms of catalytic pyrolysis of C_4 hydrocarbons," *Chemical Engineering Journal*, vol. 116, no. 3, pp. 155–161, 2006.

[61] Yu-Hua Guo, Min Pu, Ling-Yan Liu, Hua-Feng Li, and Biao-Hua Chen, "Theoretical study of two pathways of double-bond isomerization of pentene catalyzed by zeolites," *Computational Materials Science*, vol. 42, no. 2, pp. 179–185, Apr. 2008.

[62] M. Guisnet, P. Andy, N. S. Gnep, E. Benazzi, and C. Travers, "Skeletal isomerization of n-butenes: I. mechanism of n-butene transformation on a nondeactivated H-Ferrierite catalyst," *Journal of Catalysis*, vol. 158, no. 2, pp. 551–560, 1996.

[63] D. Rutenbeck, H. Papp, D. Freude, and W. Schwieger, "Investigations on the reaction mechanism of the skeletal isomerization of n-butenes to isobutene: Part I. reaction mechanism on H-ZSM-5 zeolites," *Applied Catalysis A: General*, vol. 206, no. 1, pp. 57–66, Jan. 2001.

[64] Guoliang Xu, Xiangxue Zhu, Sujuan Xie, Xiujie Li, Shenglin Liu, and Longya Xu, "1-butene cracking to propene on high silica H-MCM-22: relations between product distribution and feed conversion under various temperatures," *Catalysis Letters*, vol. 130, no. 1-2, pp. 204–210, June 2009.

[65] Oleg Bortnovsky, Petr Sazama, and Blanka Wichterlova, "Cracking of pentenes to C_2–C_4 light olefins over zeolites and zeotypes: Role of topology and acid site strength and concentration," *Applied Catalysis A: General*, vol. 287, no. 2, pp. 203–213, June 2005.

[66] Stian Svelle, Stein Kolboe, and Ole Swang, "Theoretical investigation of the dimerization of linear alkenes catalyzed by acidic zeolites," *The Journal of Physical Chemistry B*, vol. 108, no. 9, pp. 2953–2962, 2004.

[67] Matthias Vandichel, David Lesthaeghe, Jeroen Van der Mynsbrugge, Michel Waroquier, and Veronique Van Speybroeck, "Assembly of cyclic hydrocarbons from ethene and propene in acid zeolite catalysis to produce active catalytic sites for MTO conversion," *Journal of Catalysis*, vol. 271, no. 1, pp. 67–78, Apr. 2010.

[68] Yu-Hua Guo, Min Pu, Jing-Yi Wu, Jia-Ying Zhang, and Biao-Hua Chen, "Theoretical study of the cracking mechanisms of linear α-olefins catalyzed by zeolites," *Applied Surface Science*, vol. 254, no. 2, pp. 604–609, Nov. 2007.

[69] P. Jeffrey Hay, Antonio Redondo, and Yuejin Guo, "Theoretical studies of pentene cracking on zeolites: C–C -scission processes," *Catalysis Today*, vol. 50, no. 3–4, pp. 517–523, 1999.

[70] Mark N. Mazar, Saleh Al-Hashimi, Matteo Cococcioni, and Aditya Bhan, "β-scission of olefins on acidic zeolites: A periodic PBE-D study in H-ZSM-5," *The Journal of Physical Chemistry C*, vol. 117, no. 45, pp. 23609–23620, 2013.

[71] Yu-Hua Guo, Min Pu, Biao-Hua Chen, and Feng Cao, "Theoretical study on the cracking reaction catalyzed by a solid acid with zeolitic structure: The catalytic cracking of 1-hexene on the surface of h-ZSM-5," *Applied Catalysis A: General*, vol. 455, pp. 65–70, 2013.

[72] Shenglin Liu, Xiangxue Zhu, Yueqin Song, and Longya Xu, "Catalytic cracking of C_4 alkenes to propene and ethene: Influences of zeolites pore structures and Si/Al_2 ratios," *Applied Catalysis A: General*, vol. 288, no. 1–2, pp. 134–142, July 2005.

[73] Vasant R. Choudhary, Devadas Panjala, and Subhabrata Banerjee, "Aromatization of propene and n-butene over H-galloaluminosilicate (ZSM-5 type) zeolite," *Applied Catalysis A: General*, vol. 231, no. 1–2, pp. 243–251, 2002.

[74] Anton N. Mlinar, Paul M. Zimmerman, Fuat E. Celik, Martin Head-Gordon, and Alexis T. Bell, "Effects of brønsted-acid site proximity on the oligomerization of propene in H-MFI," *Journal of Catalysis*, vol. 288, pp. 65–73, Apr. 2012.

[75] Jiangyin Lu, Zhen Zhao, Chunming Xu, Aijun Duan, Xiaoning Wang, and Pu Zhang, "Catalytic cracking of isobutane over H-ZSM-5, FeH-ZSM-5 and CrH-ZSM-5 catalysts with different SiO_2/Al_2O_3 ratios," *Journal of Porous Materials*, vol. 15, no. 2, pp. 213–220, Apr. 2008.

[76] Yueqin Song, Hongbing Li, Zhijun Guo, Xiangxue Zhu, Shenglin Liu, Xionglei Niu, and Longya Xu, "Effect of variations in acid properties of H-ZSM-5 on the coking behavior and reaction stability in butene aromatization," *Applied Catalysis A: General*, vol. 292, pp. 162–170, Sept. 2005.

[77] James F. Haw, John B. Nicholas, Teng Xu, Larry W. Beck, and David B. Ferguson, "Physical organic chemistry of solid acids: lessons from in situ NMR and theoretical chemistry," *Accounts of Chemical Research*, vol. 29, no. 6, pp. 259–267, Jan. 1996.

[78] A. Corma, "Inorganic solid acids and their use in acid-catalyzed hydrocarbon reactions," *Chemical Reviews*, vol. 95, no. 3, pp. 559–614, 1995.

[79] Alexander G. Stepanov, Sergei S. Arzumanov, Mikhail V. Luzgin, Horst Ernst, and Dieter Freude, "In situ monitoring of n-butene conversion on H-ferrierite by ^1H, ^2H, and ^{13}C MAS NMR: kinetics of a double-bond-shift reaction, hydrogen exchange, and the ^{13}C-label scrambling," *Journal of Catalysis*, vol. 229, no. 1, pp. 243–251, Jan. 2005.

[80] Mercè Boronat, Claudio M. Zicovich-Wilson, Pedro Viruela, and Avelino Corma, "Influence of the local geometry of zeolite active sites and olefin size on the stability of alkoxide intermediates," *The Journal of Physical Chemistry B*, vol. 105, no. 45, pp. 11169–11177, Nov. 2001.

[81] V. B. Kazansky, "Adsorbed carbocations as transition states in heterogeneous acid catalyzed transformations of hydrocarbons," *Catalysis Today*, vol. 51, no. 3–4, pp. 419–434, July 1999.

[82] Nilton Rosenbach Jr., Alex P. A. dos Santos, Marcelo Franco, and Claudio J. A. Mota, "The tert-butyl cation on zeolite Y: A theoretical and experimental study," *Chemical Physics Letters*, vol. 485, no. 1–3, pp. 124–128, Jan. 2010.

[83] Abdelkarim Sani Souna Sido, Stéphane Walspurger, Jérémy Barbiche, and Jean Sommer, "Room-temperature alkane reactivity in zeolites: An H/D exchange study," *Chemistry – A European Journal*, vol. 16, no. 10, pp. 3215–3221, 2010.

[84] Xavier Rozanska, Rutger A. van Santen, Thomas Demuth, François Hutschka, and Juergen Hafner, "A periodic DFT study of isobutene chemisorption in proton-exchanged zeolites: Dependence of reactivity on the zeolite framework structure," *The Journal of Physical Chemistry B*, vol. 107, no. 6, pp. 1309–1315, Feb. 2003.

[85] L. Benco, J. Hafner, F. Hutschka, and H. Toulhoat, "Physisorption and chemisorption of some n-hydrocarbons at the brønsted acid site in zeolites 12-membered ring main channels: ab initio study of the gmelinite structure," *The Journal of Physical Chemistry B*, vol. 107, no. 36, pp. 9756–9762, Sept. 2003.

[86] Hanjun Fang, Anmin Zheng, Jun Xu, Shenhui Li, Yueying Chu, Lei Chen, and Feng Deng, "Theoretical investigation of the effects of the zeolite framework on the stability of carbenium ions," *The Journal of Physical Chemistry C*, vol. 115, no. 15, pp. 7429–7439, Apr. 2011.

[87] Ville Nieminen, Marek Sierka, Dmitry Yu. Murzin, and Joachim Sauer, "Stabilities of C_3–C_5 alkoxide species inside H-FER zeolite: a hybrid QM/MM study," *Journal of Catalysis*, vol. 231, no. 2, pp. 393–404, Apr. 2005.

[88] Rodrigo J. Correa and Claudio J. A. Mota, "Theoretical study of protonation of butene isomers on acidic zeolite: the relative stability among primary, secondary and tertiary alkoxy intermediates," *Physical Chemistry Chemical Physics*, vol. 4, no. 2, pp. 375–380, Jan. 2002.

[89] Cuong M. Nguyen, Bart A. De Moor, Marie-Françoise Reyniers, and Guy B. Marin, "Isobutene protonation in H-FAU, H-MOR, H-ZSM-5, and H-ZSM-22," *The Journal of Physical Chemistry C*, vol. 116, no. 34, pp. 18236–18249, Aug. 2012.

[90] Christian Tuma, Torsten Kerber, and Joachim Sauer, "The tert-butyl cation in h-zeolites: Deprotonation to isobutene and conversion into surface alkoxides," *Angewandte Chemie International Edition*, vol. 49, no. 27, pp. 4678–4680, 2010.

[91] Christian Tuma and Joachim Sauer, "Protonated isobutene in zeolites: tert-butyl cation or alkoxide?," *Angewandte Chemie*, vol. 117, no. 30, pp. 4847–4849, 2005.

[92] M. Boronat, P. M. Viruela, and A. Corma, "Reaction intermediates in acid catalysis by zeolites: prediction of the relative tendency to form alkoxides or carbocations as a function of hydrocarbon nature and active site structure," *Journal of the American Chemical Society*, vol. 126, no. 10, pp. 3300–3309, 2004.

[93] V. Van Speybroeck, *Moleculaire modellering van industriële processen. Cursus gedoceerd in 1e Master of Science: Chemical Engineering*, 2012.

[94] David Lesthaeghe, *Inzicht in het reactiemechanisme van industriële processen in de zeolietkatalyse via kwantumchemische technieken*, Doctoraatsthesis, UGent, 2007.

[95] Joachim Sauer and Marek Sierka, "Combining quantum mechanics and interatomic potential functions in ab initio studies of extended systems," *Journal of Computational Chemistry*, vol. 21, no. 16, pp. 1470–1493, Dec. 2000.

[96] M J Frisch, G W Trucks, H B Schlegel, G E Scuseria, M A Robb, J R Cheeseman, G Scalmani, Vincenzo Barone, B Mennucci, George A Petersson, H Nakatsuji, M Caricato, X Li, H P Hratchian, A F Izmaylov, J Bloino, G Zheng, J L Sonnenberg, M Hada, M Ehara, K Toyota, R Fukuda, J Hasegawa, M Ishida, T Nakajima, Y Honda, O Kitao, Hiromi Nakai, T Vreven, Jr. Montgomery J. A., J E Peralta, F Ogliaro, M Bearpark, J J Heyd, E Brothers, K N Kudin, V N Staroverov, R Kobayashi, J Normand, K Raghavachari, A Rendell, J C Burant, S S Iyengar, J Tomasi, M.; Rega Cossi N., N J Millam, M Klene, J E Knox, J B Cross, V Bakken, Carlo Adamo, J Jaramillo, R Gomperts, R E Stratmann, O Yazyev, A J Austin, R Cammi, C Pomelli, Joseph W Ochterski, R L Martin, Keiji Morokuma, V G Zakrzewski, G A Voth, P Salvador, J J Dannenberg, S Dapprich, A D Daniels, Ö Farkas, J B Foresman, J V Ortiz, J Cioslowski, and D J Fox, "Gaussian 09," 2009.

[97] Stefan Dapprich, István Komáromi, K. Suzie Byun, Keiji Morokuma, and Michael J Frisch, "A new ONIOM implementation in Gaussian98. part I. the calculation of energies, gradients, vibrational frequencies and electric field derivatives," *Journal of Molecular Structure: THEOCHEM*, vol. 461–462, pp. 1–21, Apr. 1999.

[98] A. D. Becke, "Density-functional exchange-energy approximation with correct asymptotic behavior," *Physical Review A*, vol. 38, no. 6, pp. 3098–3100, Sept. 1988.

[99] Chengteh Lee, Weitao Yang, and Robert G. Parr, "Development of the colle-salvetti correlation-energy formula into a functional of the electron density," *Physical Review B*, vol. 37, no. 2, pp. 785–789, Jan. 1988.

[100] James J. P. Stewart, "Optimization of parameters for semiempirical methods i. method," *Journal of Computational Chemistry*, vol. 10, no. 2, pp. 209–220, 1989.

[101] Jeng-Da Chai and Martin Head-Gordon, "Long-range corrected hybrid density functionals with damped atom–atom dispersion corrections," *Physical Chemistry Chemical Physics*, , no. 10, pp. 6615–6620, 2008.

[102] Stefan Grimme, "Semiempirical GGA-type density functional constructed with a long-range dispersion correction," *Journal of computational chemistry*, vol. 27, no. 15, pp. 1787–1799, Nov. 2006.

[103] M.G. Evans and M. Polanyi, "Some applications of the transition state method to the calculation of reaction velocities, especially in solution," *Transactions of the Faraday Society*, , no. 31, pp. 875–894, 1935.

[104] Henry. Eyring, "The activated complex and the absolute rate of chemical reactions.," *Chemical Reviews*, vol. 17, no. 1, pp. 65–77, Aug. 1935.

[105] An Ghysels, Toon Verstraelen, Karen Hemelsoet, Michel Waroquier, and Veronique Van Speybroeck, "TAMkin: a versatile package for vibrational analysis and chemical kinetics," *Journal of Chemical Information and Modeling*, vol. 50, no. 9, pp. 1736–1750, Sept. 2010.

[106] Bart De Sterck, *Invloed van het zeolietrooster op elementaire reacties in het hydrocarbon pool model voor het MTO-proces*, Master thesis, UGent, 2006.

[107] Kenichi Fukui, "The path of chemical reactions - the IRC approach," *Accounts of Chemical Research*, vol. 14, no. 12, pp. 363–368, Dec. 1981.

[108] Stian Svelle, Bjørnar Arstad, Stein Kolboe, and Ole Swang, "A theoretical investigation of the methylation of alkenes with methanol over acidic zeolites," *The Journal of Physical Chemistry B*, vol. 107, no. 35, pp. 9281–9289, Sept. 2003.

[109] Michel Cuendet, *Molecular Dynamics Simulation: a short introduction*, 2008, http://www.ch.embnet.org/CoursEMBnet/Pages3D08/slides/MD_cours_opt.pdf.

[110] Daan Frenkel and Berend Smit, *Understanding Molecular Simulation: From Algorithms to Applications*, Academic Press, Oct. 2001.

[111] J. VandeVondele, M. Krack, F. Mohamed, M. Parrinello, T. Chassaing, and J. Hutter, "QUICKSTEP: fast and accurate density functional calculations using a mixed gaussian and plane waves approach," *Computer Physics Communications*, vol. 167, no. 2, pp. 103–128, Apr. 2005.

[112] Ke Yang, Jingjing Zheng, Yan Zhao, and Donald G. Truhlar, "Tests of the RPBE, revPBE, -HCTHhyb, B97X-D, and MOHLYP density functional approximations and 29 others against representative databases for diverse bond energies and barrier heights in catalysis," *The Journal of Chemical Physics*, vol. 132, no. 16, pp. 164117, Apr. 2010.

[113] Stefan Grimme, Jens Antony, Stephan Ehrlich, and Helge Krieg, "A consistent and accurate ab initio parametrization of density functional dispersion correction (DFT-D) for the 94 elements H-Pu," *The Journal of Chemical Physics*, vol. 132, no. 15, pp. 154104, Apr. 2010.

[114] S. Goedecker, M. Teter, and J. Hutter, "Separable dual-space gaussian pseudopotentials," *Physical Review B*, vol. 54, no. 3, pp. 1703–1710, July 1996.

[115] Gerald Lippert, Jürg Hutter, and Michele Parrinello, "The Gaussian and augmented-plane-wave density functional method for ab initio molecular dynamics simulations," *Theoretical Chemistry Accounts*, vol. 103, no. 2, pp. 124–140, Dec. 1999.

[116] H. J. C. Berendsen, J. P. M. Postma, W. F. van Gunsteren, A. Di Nola, and J. R. Haak, "Molecular dynamics with coupling to an external bath," *The Journal of Chemical Physics*, vol. 81, no. 8, pp. 3684–3690, Oct. 1984.

[117] V. Van Speybroeck, *Statistische Fysica. Cursus gedoceerd in 2e Bachelor of Science ingenieurswetenschappen: chemische technologie en materiaalkunde*, 2011.

[118] Shichi Nosé, "A molecular dynamics method for simulations in the canonical ensemble," *Molecular Physics*, vol. 52, no. 2, pp. 255–268, 1984.

[119] Giovanni Bussi, Davide Donadio, and Michele Parrinello, "Canonical sampling through velocity rescaling," *The Journal of Chemical Physics*, vol. 126, no. 1, pp. 014101, Jan. 2007.

[120] Frank H. Allen, Olga Kennard, David G. Watson, Lee Brammer, A. Guy Orpen, and Robin Taylor, "Tables of bond lengths determined by X-ray and neutron diffraction. part 1. bond lengths in organic compounds," *Journal of the Chemical Society, Perkin Transactions 2*, , no. 12, pp. S1–S19, Jan. 1987.

[121] Julius T. Su, *An electron force field for simulating large scale excited electron dynamics*, Doctoraatsthesis, California Institute of Technology, 2007.

[122] Aditya Bhan and Enrique Iglesia, "A link between reactivity and local structure in acid catalysis on zeolites," *Accounts of Chemical Research*, vol. 41, no. 4, pp. 559–567, Apr. 2008.

[123] Edward P. L. Hunter and Sharon G. Lias, "Evaluated gas phase basicities and proton affinities of molecules: An update," *Journal of Physical and Chemical Reference Data*, vol. 27, no. 3, pp. 413–656, May 1998.

[124] Veronique Van Speybroeck, Jeroen Van der Mynsbrugge, Matthias Vandichel, Karen Hemelsoet, David Lesthaeghe, An Ghysels, Guy B. Marin, and Michel Waroquier, "First principle kinetic studies of zeolite-catalyzed methylation reactions," *Journal of the American Chemical Society*, vol. 133, no. 4, pp. 888–899, Feb. 2011.

[125] Longfei Lin, Caifeng Qiu, Zuoxi Zhuo, Dawei Zhang, Shufang Zhao, Haihong Wu, Yueming Liu, and Mingyuan He, "Acid strength controlled reaction pathways for the catalytic cracking of 1-butene to propene over ZSM-5," *Journal of Catalysis*, vol. 309, pp. 136–145, Jan. 2014.

[126] Xiaoping Tang, Huaqun Zhou, Weizhong Qian, Dezheng Wang, Yong Jin, and Fei Wei, "High selectivity production of propylene from n-butene: Thermodynamic and experimental study using a shape selective zeolite catalyst," *Catalysis Letters*, vol. 125, no. 3-4, pp. 380–385, Oct. 2008.

[127] Xiangxue Zhu, Shenglin Liu, Yueqin Song, and Longya Xu, "Butene catalytic cracking to propene and ethene over potassium modified ZSM-5 catalysts," *Catalysis Letters*, vol. 103, no. 3-4, pp. 201–210, Oct. 2005.